

DOCTOR OF PHILOSOPHY

Universality of complex systems: partition function zeros analysis and complex networks

Sarkanych, Petro

Award date:
2020

Awarding institution:
Coventry University

[Link to publication](#)

General rights

Copyright and moral rights for the publications made accessible in the public portal are retained by the authors and/or other copyright owners and it is a condition of accessing publications that users recognise and abide by the legal requirements associated with these rights.

- Users may download and print one copy of this thesis for personal non-commercial research or study
- This thesis cannot be reproduced or quoted extensively from without first obtaining permission from the copyright holder(s)
- You may not further distribute the material or use it for any profit-making activity or commercial gain
- You may freely distribute the URL identifying the publication in the public portal

Take down policy

If you believe that this document breaches copyright please contact us providing details, and we will remove access to the work immediately and investigate your claim.

Universality of complex systems: partition function zeros analysis and complex networks

By

Petro Sarkanych

April 2020



*A thesis submitted in partial fulfilment of the University's requirements for the Degree
of Doctor of Philosophy*

Content removed on data protection grounds





Certificate of Ethical Approval

Applicant:

Petro Sarkanych

Project Title:

Statistical Physics of Complex Systems

This is to certify that the above named applicant has completed the Coventry University Ethical Approval process and their project has been confirmed and approved as Low Risk

Date of approval:

05 July 2018

Project Reference Number:

P72964



Certificate of Ethical Approval

Applicant:

Petro Sarkanych

Project Title:

Statistical Physics of Complex Systems

This is to certify that the above named applicant has completed the Coventry University Ethical Approval process and their project has been confirmed and approved as Low Risk

Date of approval:

05 September 2016

Project Reference Number:

P37109

CONTENTS

| | |
|---|-----------|
| Introduction | 9 |
| 1 Literature review | 16 |
| 1.1 Some models and methods to analyse complex systems | 16 |
| 1.2 Models | 17 |
| 1.2.1 Pattern formation | 17 |
| 1.2.2 Interplay between the energy and entropy: universality and marginal dimensions | 20 |
| 1.3 Methods | 22 |
| 1.3.1 Partition function zeros | 22 |
| 1.3.2 Complex networks | 26 |
| 1.4 Conclusions | 27 |
| 2 Ordering in complex spin systems: partition function zeros | 28 |
| 2.1 Two dimensional Ising model with dipole interaction | 28 |
| 2.1.1 The model | 28 |
| 2.1.2 Density of Fisher zeros | 31 |
| 2.2 One dimensional Potts model with invisible states | 33 |
| 2.2.1 Introduction. Classical phase transitions in 1D | 33 |
| 2.2.2 Potts model with invisible states on a 1D chain | 35 |
| 2.2.3 Transfer matrix | 37 |
| 2.2.4 Partition function zeros and the transfer matrix method | 38 |
| 2.2.5 Yang-Lee edge singularity exponent | 41 |
| 2.2.6 Duality relations | 43 |

| | | |
|----------|---|-----------|
| 2.2.7 | Lee-Yang zeros for models with direct physical realisability . . . | 45 |
| 2.2.8 | Phase transitions at positive temperatures | 49 |
| 2.2.9 | Fisher zeros | 55 |
| 2.3 | Conclusions | 57 |
| 3 | Universal critical behaviour of spin systems on networks | 64 |
| 3.1 | Potts model with invisible states on a graph. Mean field approximation. | 64 |
| 3.2 | Marginal dimensions of the Potts model with invisible states on a complete graph | 68 |
| 3.2.1 | The case $q = 2$ | 69 |
| 3.2.2 | The case $1 \leq q < 2$ | 72 |
| 3.3 | Ising model with invisible states on scale-free network. | 77 |
| 3.3.1 | Critical behaviour | 78 |
| 3.4 | Conclusions | 84 |
| 4 | Universal topological properties of complex social networks of nar- ratives | 86 |
| 4.1 | Bylynas | 86 |
| 4.2 | Network | 88 |
| 4.3 | Network properties | 93 |
| 4.3.1 | Vertex degree | 93 |
| 4.3.2 | Distances between characters | 95 |
| 4.3.3 | Closeness centrality | 98 |
| 4.3.4 | Betweenness centrality | 99 |
| 4.3.5 | Clustering coefficient | 100 |
| 4.3.6 | Small-worldness | 103 |
| 4.3.7 | Degree assortativity | 104 |
| 4.3.8 | Clustering assortativity | 106 |
| 4.3.9 | Pearson similarity | 107 |
| 4.3.10 | Resilience | 108 |

| | |
|--------------------------------------|------------|
| 4.3.11 Community structure | 109 |
| 4.4 Conclusion | 112 |
| Conclusions | 114 |
| References | 115 |

ABSTRACT

In recent years, the notion of complex system has come to the fore as complexity science has found applications in a variety of disciplines. This thesis spans a diversity of the applications of statistical physics from its fundamentals to pioneering applications in humanities.

The first chapter of the thesis provides the literature review. The main focus is given to the models of interest and methods used to describe them. In particular, two models are used within the thesis: the Ising model with dipole interactions and the Potts model with invisible states. The Ising model with dipole interactions is used to describe pattern formation in complex systems, and the Potts model with invisible states is used to investigate how entropy affects the universality. Among the methods used in the thesis, two are described in Chapter 1 in detail. The first method is to analyse the partition function zeros. Within this method roots of a partition function are considered in the complex plane of model parameters. Two most used cases are complex magnetic field (Lee-Yang zeros) and complex temperature (Fisher zeros). Based on the properties of these zeroes one can deduce the critical properties of the system. The second is a method of complex networks. Within this method, a many-body system under consideration is presented as a graph, where nodes of the graph serve as components of the system and edges are the interactions between them. Studying the properties of this graph allows to describe the system.

In the second chapter, the analysis of the partition function zeros is used to unveil the critical properties of two models. The first model is the Ising model with dipole interactions on a square lattice. This model is used to describe thin antiferromagnetic films. Within this model, each particle can stay in one of two discrete states, which are often referred as “up” and “down”. This binary opposition is what makes this model so appealing and widely applicable far beyond the field of statistical physics. We considered the Ising model on sites of a square lattice with ferromagnetic nearest-neighbours interaction with coupling J and long-range antiferromagnetic dipole interaction with coupling g . It is shown that the ratio of

the interaction constants $\delta = J/g$ plays a crucial role in the description of this model. In particular, it determines the structure in the anti-ferromagnetic low-temperature phase. We have shown that besides the ordered state, the ratio δ also affects the critical properties. In the region $0.89 < \delta < 1.2$ transition to the disordered phase is continuous with critical exponents depending on δ . At the same time, for $\delta = 1.3$ we observed a first-order phase transition. Overall, the obtained results prove that along with the universal characteristics like the dimensionality and the symmetries, the ratio of interaction coupling determines the universality class. The second model is the one-dimensional Potts model with invisible states. The Potts model builds upon the Ising model and extends it to any number q of discrete states. It is a well-known fact that the number of states q determines the properties of phase transitions. The recently proposed Potts model with invisible states takes this approach even further by introducing r additional “invisible” states. If a spin lies in one of the invisible states it does not interact with the other spins. In this sense, the number of invisible states does not change the interaction energy, but affects the number of configurations, or equally – entropy. Thus, this model has a controllable way to change the entropy by changing r and is useful to investigate how the energy-entropy interplay gives rise to such a phenomenon as a phase transition. Solving this model exactly on a 1D chain we observed that any positive number of invisible states cannot change the fact that 1D systems can be only ordered at absolute zero. However, by analysing partition function zeros, we managed to discover two conditions which shift the phase transition to positive temperatures. The first mechanism is to introduce a negative number of invisible states. On one hand, it can be understood as an external ordering mechanism. On the other hand, through a duality relation, negative values of r are connected with the complex values of the external magnetic field. Recent studies have shown that a complex magnetic field is not a purely mathematical concept, but might be indirectly measured by experiment.

In the third chapter, we consider the Potts model with invisible states on

graphs. The notion of the euclidean dimensionality is ill-defined for graphs. Thus, the ordinary formulation of the universality principle has to be adjusted when a spin system is considered on a graph. It is known that for spin systems on graphs critical properties are affected by the distribution of nodes degrees. To study the influence of this topological inhomogeneity on the critical properties we study the Potts model with invisible states on two types of graphs: complete graphs and scale-free networks. To do so we adopt a version of the inhomogeneous mean-field approximation. In the former case, the degree distribution is described by the Dirac δ -function. We show that in the region $q < 2$ the diagram is characterised by two marginal dimensions r_{c1} and r_{c2} separating regions with different types of criticality. Below the r_{c1} the phase transition is of second order. For $r_{c1} < r < r_{c2}$ there are two phase transitions: first-order phase transition at a lower temperature between two (partially) ordered states and a second-order phase transition at a higher temperature. And, finally, for $r > r_{c2}$ only the first-order phase transition remains. But in the limiting case $q = 2$ two marginal values coincide $r_{c1} = r_{c2}$. Another interesting finding is that in the percolation limit $q \rightarrow 1$ adding invisible states can make the phase transition discontinuous. For the scale-free networks, there is a power-law distribution of nodes degree. In this case, critical exponents are known to depend on the degree distribution exponent λ . We considered only the Ising case $q = 2$ on scale-free networks. We showed that even for $q = 2$ there is a similar behaviour with the case $q < 2$ on a complete graph. There are two λ -dependant marginal dimensions $r_{c1}(\lambda)$ and $r_{c2}(\lambda)$. We also showed that adding of invisible states doesn't change critical exponents of a second-order phase transition.

In the fourth chapter, we extended the concept of universality to the description of the social networks of narratives. In this case, universality is understood as the independence of certain properties of the system on the details of its structure. We considered the social network of characters of bylynas. For this network, we interpret each node as a character and links represent interactions between them. We distinguish two types of interaction friendly and hostile (following the binary op-

position in the Ising model). By looking on topological properties of social networks of narrative characters we, on the one hand, can quantitatively compare narratives with each other, and on the other hand, give additional pieces of evidence to support hypotheses about characters of narratives. In our case, we showed that bylynas possess a number of common universal features with other heroic epics. In addition, we express some suggestions on the origin of epic characters. Our analysis suggests that the character of Duke Volodymyr is likely to be collective. Dobrynia might actually be based on the uncle of the Grand Prince Volodymyr the Great with the same name. Furthermore, community detection algorithm discriminates communities centred around the characters of the so-called Galician-Volyn group.

Keywords: universality, marginal dimensions, critical exponents, complex networks.

INTRODUCTION

The concept of universality - the independence of the characteristic behaviour of a macroscopic system, consisting of many interacting parts, from the details of the structure of this system - is one of the underlying concepts of statistical physics. Increasingly, this concept is used beyond purely physical topics but in a general scientific or general cultural context. The purpose of the dissertation is to study the universality of both types of complex systems. By complex systems, we mean those that are characterized by collective behaviour, which is not a simple consequence of the aggregate properties of their constituent parts [1, 2]. The inherent features of complex systems are self-organization, the emergence of new functional capabilities, high sensitivity to small changes in initial conditions, and power laws distributions ("fat-tail" distribution) [3, 4]. The concept of a complex system relates to many traditional disciplines of science and is the subject of a new interdisciplinary field of knowledge - the complexity science [5]. Methods and concepts of statistical physics are among the important components of this branch as are concepts of universality that have become one of the basic concepts of the complex systems science.

Since complex systems are characterized by the collective behaviour of many interacting components, the theory of phase transitions provides a natural tool for their study. So the study of ordering in complex spin models allows us to understand at a principal level, and to quantitatively describe the formation of a universal behaviour in different physical, chemical, biological, and social systems (see, for example, [6]). In this case, the states of the spin variable correspond to the states of agents of different nature, and their configuration and interactions simulate real complex system equivalent [7]. Often, in such studies, the processes of ordering

on complex networks - random graphs, whose topological properties reproduce the structure of a complex system, are considered [8–11]. Examples of network structures are numerous. Thus modelling the critical behaviour of complex spin systems is becoming increasingly widespread.

Relevance of the topic. Research of complex systems is, without exaggeration, the main, or, at least one of the most important areas of modern science. According to Stephen Hawking, the 21st century will be a century of complexity. The same application of models and methods of statistical physics in this area is motivated by current challenges. Along with the general relevance of the research, each of our chosen tasks has its own motivation:

- Ising model with dipole interactions on a simple square lattice is used to describe a thin antiferromagnetic films. Some researchers believe that such materials can be used to manufacture high-density storage devices [12]. On the other hand, this model has a very rich phase diagram, which contains a number of low-temperature antiferromagnetic phases (Neel antiferromagnet, striped antiferromagnet with different stripe widths). The study of the phase diagram of this model is devoted to a significant number of works, but the nature of some types of ordering in it still remains unclear.

- The recently proposed Potts model with invisible states allows us to explain observed discrepancies between theoretical predictions and experimental observations of phase transitions in some compounds where Z_3 symmetry is spontaneously broken [13, 14]. The principle of universality allows us to apply this model to explain the phase transition of denaturation of DNA [15]. Mostly this model was previously considered only in the case of $q = 2$ visible states, the case of general q often has been overlooked. In addition, the number of invisible states can be interpreted as a measure of entropy in the system; therefore, the Potts model with invisible states gives a unique opportunity to study the influence of entropy on phase transitions and universality classes in particular.

- Consideration of spin models on networks has a connection with the problems

of sociophysics and, in particular, with the study of opinion formation [7]. The ordering of such models allows us to investigate the formation of consensus in society.

– The application of complex systems science methods and approaches to the study of ancient narratives is a new area of research that originated only a few years ago [16, 17]. Within this approach, social networks of links between heroes of a number of works of world literary heritage, such as Iliad, Odyssey, Beowulf, Irish and Icelandic sagas and many others have already been analysed. The conducted studies allow to classify different narratives and serve as a source of additional information about their features. For Old Slavic texts, this approach has not been used before.

Purpose and tasks of the research. The *themes* of the dissertation study involve three examples of complex systems: Ising model with dipole interaction, Potts model with invisible states and social network of characters of ancient narratives. *The subject of the study* is the change in the universality class of the two-dimensional Ising model with dipole interaction, the influence of the entropy contribution on the process of ordering in one dimensional systems, the characteristics of the critical behaviour of many particle systems on complex networks, the topological properties of social narrative networks. *The objective of the dissertation* is to explain the emergence of universality and scaling in complex systems of different natures. To achieve this, we used the following *methods*: the mean field approximation, the transfer matrix method, the Lee-Yang-Fisher’s formalism of analysing the zeros of the partition function in the complex field or temperature planes, and the methods of the complex networks science.

Novelty of the results. In the dissertation, the interval of the phase diagram of the two-dimensional Ising model with dipole interactions was analysed and it is shown that the critical exponents depend continuously on the ratio δ of the interaction constants. Our results confirm a second-order transition in the entire region of δ , where there is a transition between the striped antiferromagnetic phase with the thickness of the stripes $h = 1$ and the paramagnetic (tetragonal) phase. Instead, the transition between the phase with $h = 2$ and the paramagnetic phase

is first order [18]. The values of the critical exponents found by us from the partition function zeros density coincide well with the results of the short-time dynamics Monte Carlo simulations [19].

Using the transfer matrix method, the exact solution of the Potts model with q visible and r invisible states on a one-dimensional chain was found. We analysed conditions when this model has a phase transition at a positive temperature and explained why these results do not coincide with rigorous theorems [20, 21].

For the first time an expression was obtained for the free energy of the Potts model with invisible states on an arbitrary graph. In particular, for the full graph, we have shown that there are two marginal values of r , for which the nature of critical behaviour changes. A similar effect is also observed in the partial case $q = 2$ for the scale-free network [22, 23].

For the first time, the complex networks approach was used to analyse the social network of the Slavic texts bylynas. In particular, it has been shown that the social network of characters of bylynas possesses a number of quantitative characteristics which it shares with the corresponding networks of other narratives. This analysis also suggests certain arguments in favour of certain hypotheses concerning the link between the epic characters and historical figures [24, 25].

Practical value of the obtained results. The results obtained in the dissertation describe the properties of the phase diagram of a two-dimensional Ising model with dipole interaction. This model is often used to describe thin film materials that can be used to make high-density storage devices.

Despite a number of theorems that prohibit phase transitions in one-dimensional classical equilibrium systems with short-range interaction, our results show that there are two ways to circumvent such restrictions. The first of these is to consider external complex magnetic fields. These were thought to be non-physical. However, they have recently been indirectly measured experimentally through the decoherence times of the quantum system [26]. Thus, the consideration of external magnetic fields allows us to link classical and quantum spin models. The second

mechanism is to consider the negative number of invisible states. Since the increase in the number of invisible states leads to an increase in entropy in the system, their negative amount can be interpreted as an external ordering mechanism.

The results obtained for the Potts model with invisible states on the networks can be applied to problems of sociophysics. In particular, the concept of the invisible state is directly projected onto social problems, where an individual who does not interact with the environment can be represented as being in an invisible state.

Using the approach of complex networks to narratives, among other things, allows quantitative comparison of texts and their classification.

Personal contribution of the applicant. In works performed with co-authors, the author did:

- analysis of the density of partition function zeros of the Ising model with dipole interaction [18];
- exact solution of the Potts model with invisible states on a one-dimensional chain. Analysis of the Lee-Yang and Fisher zeros of this model [20, 21];
- consideration of the conditions under which the phase transition in a one-dimensional Potts model with invisible states occurs at positive temperatures [20, 21];
- analysis of expressions for the free energy in the mean field approximation for the Potts model with invisible states on the full graph [22] and the scale-free network [23];
- construction and analysis of the social network of characters of Bylyny and its comparison with the networks of characters of other epics [24].

Relationship with academic projects and programs. The dissertation was performed at the Institute for Condensed Matter Physics of the National Academy of Sciences of Ukraine and the Fluid and Complex Systems research centre of Coventry University with the support of the (\mathbb{L}^4) Collaboration & Doctoral College for the Statistical Physics of Complex Systems (Leipzig-Lorraine-Lviv-Coventry,

Europe), FP7 grant projects EU IRSES 269139 ‘Dynamics and Cooperative Phenomena in the Complex Physical and Biological Media’, 295302 ‘Statistical Physics in Diverse Realizations’, 612707, ‘Dynamics of Complex Systems’, 612669, ‘Structure and Evolution of Complex Systems with Applications in Physics and Life Sciences’.

Approbation of the dissertation. The results of the work were presented at such conferences: the fifth conference of young scientists "Problems of theoretical physics" (Kyiv, Ukraine, December 24-27, 2013), conference MECO-41 (Vienna, Austria, February 15-17, 2016), 16th All-Ukrainian Workshop and Award for young scientists in the field of Statistical Physics and Condensed Matter Theory (Lviv, Ukraine, June 9-10, 2016), "Workshop on current problems in physics" (Lviv, Ukraine, July 5-7, 2016), Christmas discussions - 2017 (Lviv, Ukraine, January 11-12, 2017), 17th Workshop and Award for young scientists in the field of Statistical Physics and Condensed Matter Theory (Lviv, Ukraine, June 8-9, 2017), Christmas discussions - 2018 (Lviv, Ukraine, January 11-12, 2017), conference MECO-43 (Krakow, Poland, May 1-4, 2018). And also at such seminars: workshop of the Department of Statistical Physics of the University of Henri Poincare (Nancy, France, January 15, 166); Postgraduate Research Seminar at the Fluid and Complex Systems Research Center at the Coventry University (Coventry, England, May 30, 2018, March 27, 2019); seminar of the Astronomical Observatory of the Ivan Franko National University in Lviv (Lviv, Ukraine, 08.06.15); poster presentation at the research symposium at the Faculty of Engineering, Environmental and Computer Sciences at the Coventry University (Coventry, England, 06.06.18); Seminars of the Laboratory of Statistical Physics of Complex Systems of ICMP of the National Academy of Sciences of Ukraine.

Publications. The materials of the dissertation have been published in 6 papers [18, 20–24], 2 preprints [25] (accepted) and 10 conference theses [27–36].

Structure of the thesis. The dissertation consists of four sections of the main text (literature review and three original sections), conclusions and list of

references. In Section 1 the literature review and the definition of basic concepts are given; in the next section, we use the partition function zeros analysis to the Ising model with dipole interaction and one-dimensional Potts model with invisible states; Section 3 is devoted to the analysis of the Potts model with invisible states on networks; In Chapter 4, using the approaches of the complex networks science, the analysis of the character networks of Bylyny was conducted; the conclusions summarized the results of the work and outlined further perspectives. The work is presented on 112 pages (130 pages including references); the bibliographic list contains 210 titles of publications.

CHAPTER 1

LITERATURE REVIEW

This chapter provides an overview of the main works related to the topic of the dissertation. First (in Section 1.1) we introduce the basic notions of the complex systems science. Further, in Section 1.2, we consider the Ising model with dipole interaction and the Potts model with invisible states used in the thesis, their properties and their applications. In Section 1.3 we describe partition function zeros, the associated methodologies and methods of complex networks science, which, along with more common methods, were used in the dissertation. And in Section 1.4 we will draw conclusions.

1.1. Some models and methods to analyse complex systems

The notion of a complex system appears more and more in scientific publications. From a physicist's point of view, the beginning of complex systems science can be considered as the paper of Philip Anderson *More is different* [1]. As a complex system we understand a system consisting of many interacting parts (agents) whose collective behaviour is not a simple consequence of the individual properties of each component. An important aspect is that we do not impose any restrictions on the nature of these agents and the types of their interaction. Using such a general concept, a wide variety of objects can be designated as complex systems. Purely physical examples include deterministic chaos, spin glass, or proteins [4, 37]. Non-physical examples of complex systems are stock markets, society, or even language [37].

Since the complex systems are determined by the accumulative effects, statistical physics, as a science of collective behaviour, takes one of the central roles in the complex systems science. Many concepts were borrowed (and adapted) from statistical physics, such as universality, critical behaviour, scaling, entropy, percolation, and many others [38]. Together with these concepts came the methods and toolset of statistical physics.

A particular example of complex systems is a system with adaptive interaction. For them, the macro- and micro-states of the systems are interrelated: the interactions define the macrostate or the configuration of the agents in the system, which in turn modifies the interaction [39].

The complex systems science, unlike traditional physics, is not limited to either the four fundamental interactions, or the consideration of matter alone, as an object of research. Therefore, traditional problems of statistical physics, can be considered as a part of complex systems science.

1.2. Models

1.2.1. Pattern formation

One of the important features of the behavior of complex systems is the formation of their so-called patterns - structures that are repeated in space or time. Various models are used to describe this phenomenon (see, for example, [40]). In this dissertation, for the analysis of this phenomenon, we considered one such model - the Ising model with dipole interactions [41].

Pattern formation is one of the exciting phenomena that can be caused by competing long- and short-range interactions in many-particle physical systems. Competition of short-range and long-range dipole interaction leads to a variety of experimentally observed structures in ultra-thin magnetic films on metal substrates, liquid crystals, polymer films, two-dimensional electron gases, Langmuir and lipid monolayers, etc. (see [42]). The above systems have important industrial applica-

tions, and therefore have become the subject of intense experimental research. In particular, the aforementioned ultrathin magnetic films became a subject of special interest because of their possible application in the creation of high-density storage devices [12].

The theoretical representation of the peculiarities of the formation of repetitive structures in the aforementioned systems was obtained by analysing a two-dimensional Ising model with competing ferromagnetic nearest neighbours interactions (with the interaction constant J) and antiferromagnetic long-range dipole interaction (with the interaction constant g) [41–51]. Within this model, the richness of the phase diagram is explained by frustrations caused by the competing nature of ferromagnetic and antiferromagnetic interactions. Analytical approaches supported by numerical simulations show that, depending on the values of J and g , the low-temperature phase of this model is characterized by spin configurations classified as regular and irregular Neel phases or stripes of different widths h ¹ with a spin oriented in one direction [43–47]. Some authors report the existence of modulated phases for the ratio J/g near the line separating low temperature phases of width h and $h + 1$ [50]. The above-mentioned low-temperature magnetic structures have much in common with those observed in liquid crystals, and striped, modulated, and paramagnetic phases are often referred to as smectic, nematic, and tetragonal. In the latter case, the domains with the opposite orientation are mutually perpendicular. Moreover, the mean field analysis revealed that the structure of the domain walls in such films is similar to the two-dimensional liquid crystals [41].

The above articles are generally consistent with the classification of repetitive structures observed in the two-dimensional Ising model with competing dipole and nearest neighbours interactions, but the details of the phase diagram remain unknown. In particular, the subject of a recent discussion was the area of the phase diagram in the region of low temperature T and $\delta = J/g$ (a sketch of the phase diagram in this area is shown in Fig. 1.1). In this sketch, it is known that the phase

¹Here and below, for this model h is the stripe width measured in lattice units.

transitions between the antiferromagnetic Neel phase (AF) and between the striped $h = 2$ and the tetragonal phases are transitions of the second and the first orders respectively. But the order of the phase transition between the striped $h = 1$ and the tetragonal phases remains unknown. In particular, the Monte Carlo simulation in [50] revealed a phase transition of the second order in the region $\delta < 0.8$ and the first-order transition in the region of $0.83 < \delta < 0.88$. As a result, there must be a tricritical point between the two regions. Further simulations in the work [51] did not observe the predicted tricritical point and indicate the continuous phase transition for the entire δ domain, which corresponds to the boundary between the striped $h = 1$ and the tetragonal phases (see Fig. 1.1)

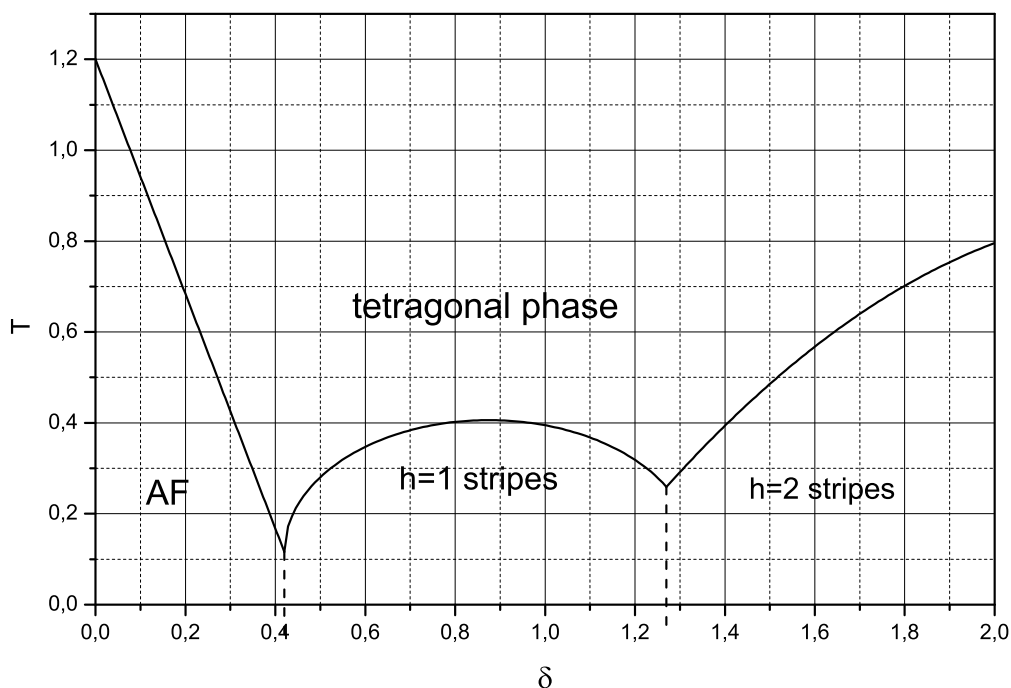


Figure 1.1. The phase diagram of a two-dimensional Ising model with competing nearest neighbours and dipole interactions (drawn from [50, 51]). AF: Neel antiferromagnet, $h = 1$, $h = 2$: striped phases.

1.2.2. Interplay between the energy and entropy: universality and marginal dimensions

The concept of universality - the independence of certain properties of the system from the details of its structure - plays a central role in understanding the physical properties of various many particle systems. Phase transitions of second order are examples of phenomena demonstrating universality [52, 53]. For systems with short-range interaction, global factors such as dimensionality of space or dimensionality and symmetry of the order parameters determine the universal properties of such a phase transition. These features are characteristic of different systems, regardless of the details of their structure. Such systems belong to the same universality class. It is usually determined by critical exponents, ratio of critical amplitudes, and scaling functions. Another value that is inherent in the critical behavior of complex systems is the marginal dimension that characterizes the number of components of the order parameter, for which the type of phase transition changes.

Examples of such systems are $O(m)$ symmetric spin models [54]. In this model, a transition of the second order is observed, provided that the dimensionality of the space exceeds the lower critical value $d > d_{lc}$ (where $d_{lc} = 1$ for the Ising case $m = 1$ and $d_{lc} = 2$ for $m \geq 2$) [55, 56]. However, when the $O(m)$ symmetry is violated by the presence of terms invariant under the cubic group (the so-called anisotropic cubic model corresponding to the calculation of crystalline anisotropy [57–59]), this results in the appearance of the boundary value of m_c . For a given dimensionality of the space d , $m_c(d)$ separates the regions where phase transitions occur under different scenarios. For example, $d = 3$ cubic crystal with three easy axes should have a first-order phase transition if m_c is less than 3 and the second order if greater. The theoretical predictions favour $m_c(d = 3) < 3$ [60, 61], supporting the first order scenario in these systems [58, 59]. Another example is the q -state Potts model with short-range interaction [62]. Since this model has a discrete symmetry group Z_q , then the lower critical dimension $d_{lc} = 1$. The marginal value $q_c(d)$ for $d > d_{lc}$ also

divides the second and first order regimes. For $d = 2$, the second-order transition is observed for $q \leq q_c = 4$ and the first order otherwise. For $d = 3$, the boundary value of q_c is lower than 3 [63]. In addition, for 3- and 4-states Potts model in two dimensions, the order of the phase transition changes with increase of the range of interactions [64]. Additional examples of marginal dimensions separating the regions with different types of phase transition are given by non-linear ordering systems [65], frustrations [66, 67], structural disorder [61, 68, 69], competing fluctuating fields [70–72] or non-linear interactions in a n -vector model with a ferromagnetic or nematic order [73]. There, the nonlinearity plays the role of the marginal dimensions.

We are interested in the marginal dimensions of the Potts model with invisible states [74]. The model was recently introduced to explain the differences between the theoretical predictions and experimental observations of the phase transition in some two-dimensional systems where the Z_3 -symmetry is spontaneously broken [13, 14, 75]. Although these systems undergo ferromagnetic phase transitions, it turns out to be of the first order, whereas the standard Potts model provides a second-order scenario for $d = 2$, $q = 3$. The model continues to attract considerable interest [76–83], although some basic questions about its behavior remain unresolved. In particular, to explain the changes in the marginal number of states (marginal dimensions) of q_c separating the regimes of the first and the second order, the model introduces r additional Potts states (so-called invisible states) that do not contribute to the interaction energy of the system, but do contribute to entropy. From now on we will use the term (q, r) -Potts model for the model with q visible and r invisible states. Consequently, for the fixed space dimension d and the number of states q , the value r_c represents the limit dividing the regions of the first and second order.

The question of the marginal dimensions of the Potts model with invisible states is one of the central issues discussed in the context of this model. A Bragg-Williams type of the mean-field analysis leads to an estimate of $3 < r_c < 4$ for $q = 2$ [74, 77, 79]. Obtained within the framework of the mean-field approach, this estimate does not have a clear dependence on the dimension of space. Another

mean-field approach using 3-regular random (thin) graphs also shows a change in the order of the phase transition, but the value of $r_c \simeq 17$ obtained for $q = 2$ [83] is much higher than in the Bragg-Williams approach. Numerical simulations of the Potts model with invisible states on a $d = 2$ lattice gave significant evidence that the model has a phase transition of the first order at $q = 2, 3, 4$ for high values of r . But for numerical methods, it remains a challenge to get the exact value of r_c [74]. Rigorous results indicate the existence of a first-order regime for any $q > 0$, provided that r is sufficiently large [81, 82]. The exact values of r_c are also known on the Bethe lattice [80]. Moreover, for the Bethe lattice with three nearest neighbors, the value r_c is the same as for a 3-regular random graph.

1.3. Methods

1.3.1. Partition function zeros

In 1952, thanks to the work of Lee and Yang, a new way to understand the critical behaviour appeared [84, 85]. The main idea was to consider the partition function Z in the plane of a complex magnetic field. The partition function is given by the formula

$$Z(h, T) = \sum_{\{s_i\}} e^{-H(\{s_i\}, h, T)/T}, \quad (1.1)$$

where h and T denote the external magnetic field and temperature, respectively, the summation is taken over all possible spin configurations, and $H(\{s_i\}, h, T)$ denotes the energy of the system in the given configuration and for the given values of temperature and field. Since, by definition, the partition function (1.1) is the sum of non-negative terms, it is obvious that all its roots are complex. Solutions h_i of the equation

$$Z(h_i, T) = 0 \quad (1.2)$$

are called the Lee-Yang zeros. In the thermodynamic limit, when the size of the system N goes to infinity, the Lee-Yang zeros approach the real axis at the critical

point.

Subsequently, Fisher proposed a similar approach. His idea was to consider the partition function in the complex temperature plane T [86]. Zeros of the partition function in the complex temperature plane are called Fisher zeros.

For a long time complex magnetic fields were considered to be completely mathematical constructs, whose roles, although important, are limited only by the fundamental theories that underlie the phase transitions. But recently it has been shown that the complex magnetic fields of the spin bath are connected with the quantum coherence times of a spin probe placed in this bath [26, 87]. The obtained results show that the times when the quantum coherence reaches zero are equivalent to the complex value of the magnetic fields in which the partition functions becomes zero (Lee-Yang zeros) [84, 85]. The zeros method is considered fundamental for understanding phase transitions and a powerful tool for analysing critical behaviour. Lee-Yang zeros directly reflect properties of the partition function, and therefore give important information about the nature of the phase transition. Recently, the exact solution for the classical Ising antiferromagnetic chain in a magnetic field showed the existence of an infinite cascade of thermal phase transitions, the origins of which were traced to the lines of Lee-Yang zeros, thus connecting them with the observed and potentially measurable quantities [88].

Zeros of the partition function, in addition to helping identify critical points, also allow us to find universal properties of phase transitions such as critical exponents or the ratio of critical amplitudes [89–94]. In this dissertation we will use two methods for analysing the zeros of the partition function, namely scaling of the closest to the real axis zero and the method of analysing the density of the zeros. The main points of these two methods are given below.

Scaling of zeros closest to the critical point

In [89], using the renormalization group approach, it was shown that finite-size scaling for the coordinates of the partition function zeros has the form

$$\operatorname{Re} z = z_c + A \cdot L^{-\Lambda} \quad (1.3)$$

$$\operatorname{Im} z = B \cdot L^{-1/\nu}, \quad (1.4)$$

where z_c denotes a critical point, ν is the correlation length critical exponent, L is a linear system size and Λ is the so-called shift exponent. Although this ansatz should hold for the entire scaling area, it is best to use it for zero closest to the critical point, since the scaling corrections have the least effect there.

Density of partition function zeros

An alternative to scaling of the zeros closest to the critical point is the density of zeros, which was introduced in Refs. [95, 96]. A particular advantage of this method is that it allows to discriminate between the first- and second-order (as well as higher order) phase transitions as well as to measure the strength of first- and second-order phase transitions in the form of the latent heat and critical exponents. Below we briefly describe the main steps of the partition function density analysis. Provided that the zeros of the partition function of the model in the complex plane are known, one can write it in the factorized form

$$Z_L(z) = A(z) \prod_j (z - z_j(L)) \quad , \quad (1.5)$$

where z stands generically for an appropriate function of complex temperature (in the Fisher case) or complex field (in the Lee-Yang case), L is the linear extent of the lattice and $A(z)$ is a smooth function that never vanishes. The free energy density follows as

$$f_L(z) = \frac{1}{L^d} \ln Z_L(z) \quad (1.6)$$

$$= \frac{1}{L^d} \left(\ln A(z) + \sum_j \ln(z - z_j(L)) \right) .$$

The first term on the right contributes only to the regular part of thermodynamic functions and will be dropped henceforth. The remainder, which will be referred to as $f_L^s(z)$, gives rise to singular behaviour.

It is suitable to parametrize the zeros by

$$z = z_c + r \exp(i\varphi) , \quad (1.7)$$

where z_c is a critical point coordinate. Let us define the density of zeros as

$$g_L(r) = L^{-d} \sum_j \delta(r - r_j(L)) , \quad (1.8)$$

with $z_j = z_c + r_j \exp(i\varphi)$. Subsequently, the free energy and the cumulative distribution function of zeros are defined as

$$f_L^s(z) = \int_0^R g_L(r) \ln(z - z_c - r e^{i\varphi}) dr + \text{c.c.} \quad , \quad (1.9)$$

$$G_L(r) = \int_0^r g_L(s) ds = \begin{cases} = \frac{j}{L^d} & r \in (r_j, r_{j+1}) \\ = \frac{2j-1}{2L^d} & r = r_j \end{cases} \quad (1.10)$$

where c.c. means complex conjugate and R is some appropriate cutoff. In the thermodynamic limit and for first order phase transitions, Lee and Yang already have shown [84, 85] that the density of zeros has to be non-zero crossing the real axis. This corresponds to the cumulative distribution of zeros

$$G_\infty(r) = g_\infty(0)r + br^{w+1} + \dots \quad , \quad (1.11)$$

where the slope at the origin is related to the latent heat (or magnetization) via

$$\Delta e \propto g_\infty(0) \quad . \quad (1.12)$$

Furthermore, it has been shown (see [90–93, 97, 98]) that the necessary and sufficient condition for the specific heat at second-order phase transitions to have the leading

critical behaviour $C \sim t^{-\alpha}$, is

$$G_{\infty}(r) \propto r^{2-\alpha} \quad . \quad (1.13)$$

The above survey leads to the conclusions that a plot of $G_L(r_j) = (2j-1)/2L^d$ against $r_j(L)$ should: (i) go through the origin, (ii) display L - and j - collapse, and (iii) reveal the order and strength of the phase transition by its slope near the origin.

1.3.2. Complex networks

The zeros method, as described above, is based on the concept of a partition function, a function that fully describes the thermodynamic behaviour of the system. It can be used for arbitrary localization of interacting agents. One of these localizations is the placing them on a complex network. From a mathematical point of view, a complex network is a graph. The graph consists of two sets: the set of vertices (nodes) and the set of edges (links) that connect these vertices [99]. The graph theory is a well-defined section of discrete mathematics. The difference lies in the fact that graph theory is interested in certain characteristics of a particular graph. Complex networks science is about the statistical properties of networks of a large size [2].

On the one hand, the representation in the form of a complex network is natural for the system of interacting agents [4, 8]. In this representation, each agent is placed on a node, and the link between the nodes corresponds to the fact of their interaction². On the other hand, many natural and anthropogenic objects have a network structure, and not a regular lattice. Examples vary from nanostructures [100] to the large-scale structure of the universe [101]; from transport networks [102, 103] to social networks [104, 105]. A separate area of research is the study of phase transitions and critical phenomena on complex networks [10, 106–110]. One of the motivations for considering such tasks is their application to the description

²It is worth noting that the word interaction here is used broadly and is not limited to four fundamental interactions.

of processes in the society [7]. Another is the study of the influence of the topology of the network on the universal properties of phase transitions. It was shown that the very existence of the phase transition and, as a consequence, critical exponents depend on the nodes degree distribution function $P(k)$ [110, 111]. For scale-free networks, where the node degree distribution function is the following $P(k) \propto k^{-\lambda}$, the critical exponents become λ -dependent [107, 110–112]. Thus, the λ parameter, along with other global parameters, determines the universal properties of the system.

1.4. Conclusions

In this chapter, we reviewed the main models and methods used in the thesis. Despite the fact that the universal properties in statistical physics have been explored for nearly half a century, but for complex systems they are still poorly understood.

In particular, for the Ising model with dipole interaction, there are contradictory data regarding the nature of the phase transition in the region $0.8 \leq \delta \leq 1.3$, and the partition function zeros analysis has not yet been applied.

The available results for the Potts model with invisible states were targeted either on the partial case $q = 2$ of visible states, or formulated as strict theorems, which made it impossible to estimate the marginal value of invisible states, which leads to a change in the order of phase transition. Moreover, this model has never been considered on networks (besides the Bethe lattice), where one can observe the interplay between the entropy contribution from the number of invisible states and the topological effect by the structure of a network. It is also worth noting that for this model, no exact solution has yet been found.

Despite the fact that the methods of complex networks have been used to analyse epic narrative social networks of a number of nations of the world, it was never applied to the Bylyny - the epic of the Eastern Slavs.

This dissertation is devoted work to the solution of these and related tasks.

CHAPTER 2

ORDERING IN COMPLEX SPIN SYSTEMS: PARTITION FUNCTION ZEROS

In this chapter, we apply the method of partition function zeros for the study of the Ising model with dipole interaction and the Potts model with invisible states. An interesting feature of both models is that the type of phase transition and the universality class of each of them depend on the values of the system parameters, such as the interaction constants ratio δ for the Ising model with dipole interaction (2.1), and the number of invisible states r for the Potts model (2.4). Applying the method of partition function zeros (Section 2.1) we analyse the phase diagram and obtain the critical exponent α for the Ising model with dipole interaction. In particular, we show that there is a second order phase transition and the value of critical exponents depend on the ratio of interaction constants. Using the transfer matrix approach, in Section 2.2 we obtain an exact solution of the Potts model with invisible states on a one-dimensional chain. The main results of this section are outlined in [18, 20, 21].

2.1. Two dimensional Ising model with dipole interaction

2.1.1. The model

The Hamiltonian of the 2d Ising model with competing ferromagnetic nearest-neighbour and antiferromagnetic dipole interactions reads

$$H = -\delta \sum_{\langle i,j \rangle} \sigma_i \sigma_j + \sum_{i < j} \frac{\sigma_i \sigma_j}{r_{ij}^3}. \quad (2.1)$$

Here, $\delta = J/g > 0$, J and g being strengths of the nearest neighbour and dipole interactions, correspondingly. The summation is performed over the sites of the $L \times L$ square lattice. The first sum in (2.1) spans all pairs of nearest-neighbour Ising spins $\sigma_i = \pm 1$, while in the second term all pairs of lattice sites are taken into account. The Ising spins are aligned out of the plane. Even though the second term in the Hamiltonian represents only a part of an actual dipole interaction potential, we will keep the name 'Ising model with dipole interaction' as it is widely used in the literature.

In the limiting cases of $J = 0$ or $g = 0$ (i.e. δ equals 0 or ∞) the Hamiltonian (2.1) presents a pure dipole interaction model or the usual Ising model, correspondingly. Both cases are characterized by a single (antiferro- or ferromagnetic) low temperature phase and by a continuous second-order phase transition to the paramagnetic state. Note, that the antiferromagnetic-to-paramagnetic phase transition belongs to the universality class of the 2d Ising model too [49, 113]. The phase behaviour of the model (2.1) is much more complicated for nonzero δ , as was briefly described in the Introduction. The part of the phase diagram of the model in the region of small δ of $T - \delta$ plane is sketched in Fig. 1.1.

Previous analyses of the phase diagram were performed either by numerical or analytical tools, based on calculation of the partition function

$$Z_L(\beta) = \text{Tr} \exp(-\beta H), \quad (2.2)$$

where $\beta = 1/T$ and the trace is performed over all spin configurations. We are going to analyse the partition function behaviour in the complex T (complex β) plane. Since the pioneering papers of Lee and Yang [84, 85] and Fisher [86] where the partition function zeros in complex field and complex temperature planes were studied, this type of analysis became a powerful tool to study phase transitions in various models. For the model under consideration (2.1) it has been recently applied in Ref. [51], where the first zero of the partition function closest to the origin has been calculated for different values of interaction ratio δ at different lattice sizes $L = 12 - 72$. The finite size scaling (FSS) analysis of the zeros' coordinates allows

| δ | $d\nu$ [51] | $\alpha = 2 - d\nu$ | α/ν [51] | $\alpha = \frac{2\alpha/\nu}{d+\alpha/\nu}$ | α_{zd} |
|----------|-------------|---------------------|-------------------|---|---------------|
| 0.89 | 1.807(70) | 0.193(70) | 0.364(20) | 0.308(17) | 0.194(17) |
| 0.91 | 1.817(68) | 0.183(68) | 0.375(19) | 0.316(16) | 0.191(14) |
| 0.93 | 1.779(61) | 0.221(61) | 0.399(20) | 0.333(17) | 0.221(16) |
| 0.95 | 1.741(53) | 0.259(53) | 0.424(20) | 0.350(17) | 0.255(14) |
| 0.97 | 1.706(46) | 0.294(46) | 0.461(19) | 0.375(16) | 0.292(14) |
| 1.00 | 1.659(37) | 0.341(37) | 0.522(17) | 0.414(14) | 0.349(13) |
| 1.10 | 1.415(25) | 0.585(25) | 0.888(21) | 0.615(15) | 0.5882(84) |
| 1.20 | 1.223(21) | 0.777(21) | 1.496(28) | 0.856(16) | 0.788(17) |
| 1.30 | 1.0093(28) | 0.9907(28) | 2.0183(66) | 1.0046(33) | 1.011(13) |

Table 2.1. Critical exponents of the 2d Ising model with competing ferromagnetic nearest-neighbour and antiferromagnetic dipole interactions for different values of the interaction ratio δ . Results of Ref. [51] obtained by FSS of the partition function zeros and of the specific heat, $d\nu$ and α/ν are shown in the second and fourth columns, respectively. The specific heat critical exponents α obtained via hyperscaling relations from these values are given in the third and in the fifth columns, correspondingly. The sixth column contains our results obtained via the partition function zeros density analysis (α_{zd}).

one to obtain the value of the correlation length critical exponent ν . The value of $d\nu$ obtained in Ref. [51] is given in Table 2.1 (second column) for different values of δ . Provided that the hyperscaling relation $\alpha = 2 - d\nu$ holds, one can use it to obtain the specific heat critical exponent α . Corresponding $\alpha(\delta)$ values recalculated from the second column are quoted in the third column of the Table 2.1. Since $\alpha = 1$ for first-order phase transitions, the obtained values of the exponents $\alpha < 1$ serve an evidence for a second-order phase transition in the considered region of δ . This result has been further supported by a FSS analysis of the specific heat, leading to the ratio α/ν that is quoted in the fourth column of Table 2.1 [51]. Again, using the hyperscaling relation and values from the fourth column one can extract the value of the α at $d = 2$ via: $\alpha = \frac{2\alpha/\nu}{d+\alpha/\nu}$. The last value is shown as a function of δ in the fifth column of the table.

We note that, although the estimates for α support a continuous phase-

transition scenario ($\alpha < 1$), they do not agree numerically. Moreover, the methods used for their determination do not deliver their direct evaluation, but rather rely on hyperscaling relations. Therefore, in the next section we will use method described in Section 1.3.1 to analyse Fisher zeros of the model with the Hamiltonian (2.1).

2.1.2. Density of Fisher zeros

As has been stated in the previous section, the input data for our analysis are provided by the coordinates of the partition function zeros calculated in [51] for different δ and L . From these, we calculate $G(r)$ dependence of the cumulative density function (1.10) for different values of δ . Obtained in this way, a typical $G(r)$ plot is shown in Fig. 2.1 for $\delta = 1$. Corresponding cumulative density functions for other values of δ show similar behaviour. Subsequently, the set of functions $G(r)$, for every value of δ , is fitted with a power-law $G(r) = ar^{2-\alpha} + b$, which gives specific heat critical exponent α . It is worth noting that for each fit obtained values of parameter b were very small, allowing us to use ansatz (1.13). The resulting values are listed in the last column of Table 2.1, α_{zd} .

There are several conclusions one can make comparing the data for the specific heat exponents from Table 2.1. First of all it is worth noting that the results obtained by three different techniques: (i) FSS of partition function zeros (third column of the table, obtained by hyperscaling relation from data of Ref. [51]), (ii) FSS of the specific heat [51] (fifth column of the table) and (iii) density of partition function zeros analysis (last column of the table, our data) give value of $\alpha < 1$ up to $\delta < 1.3$. Recalling that $\alpha = 1$ serves as evidence for a first-order phase transition (cf. Eqs. (1.11) and (1.13)) one can conclude that the transition from the striped $h = 1$ to the tetragonal phase (see the phase diagram Fig. 1.1) occurs through a continuous transition scenario. For the values of $\delta \geq 1.3$ all three approaches predict a first-order phase transition, leading to the conclusion that the tricritical point is located in region $1.2 < \delta < 1.3$.

All three approaches deliver δ -dependent values of the critical exponents, mak-

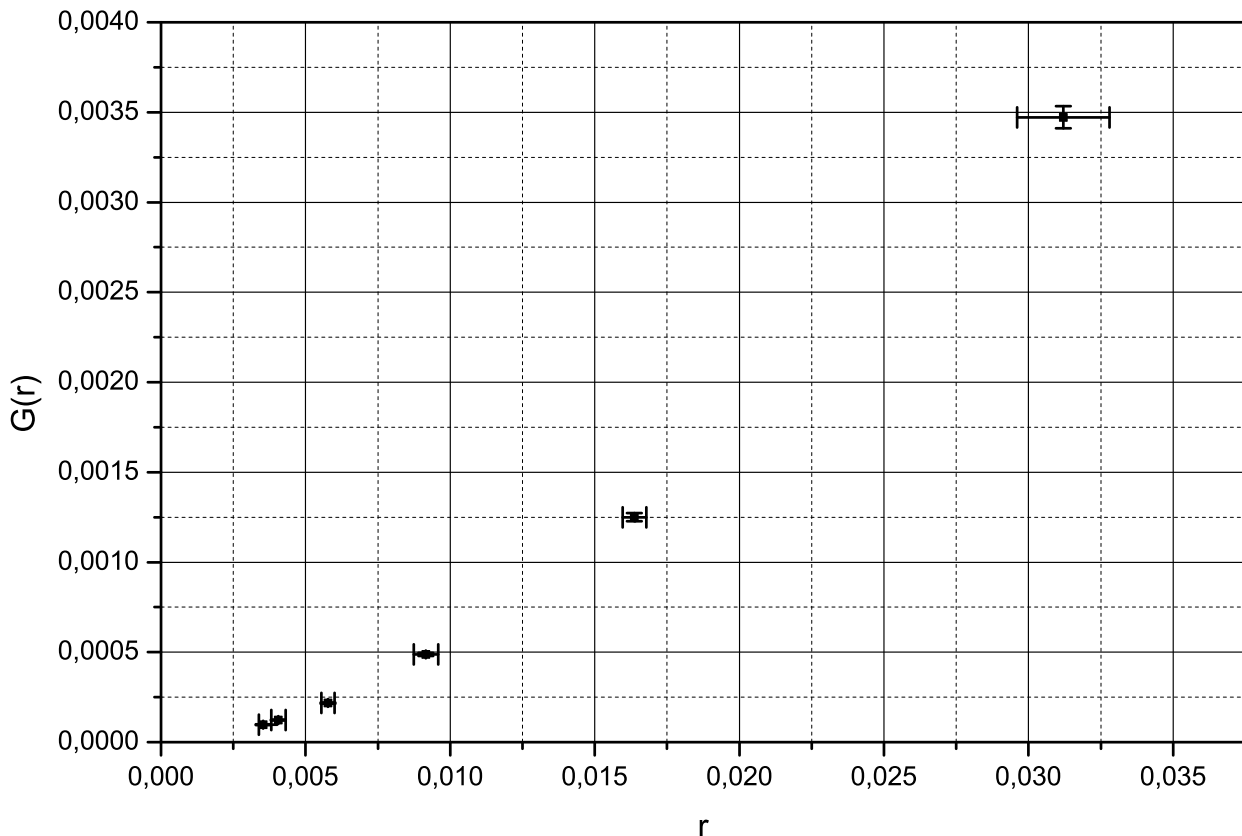


Figure 2.1. Cumulative density function $G(r)$ for $\delta = 1$.

ing δ along with the space dimension d the global variable that defines the universality class. Dependency of the critical exponent α calculated in this study (α_{zd}) on the interaction parameter δ is shown in Fig. 2.2. Let us note however, that the numerical values of the exponents obtained via different approaches differ. In particular, results of the FSS analysis of partition function zeros (third column of the table) are in good agreement with the analysis of the density of partition function zeros (sixth column of the table). But they essentially differ from the results obtained on the basis of a FSS analysis of the specific heat behaviour [51]. In addition, from the scaling of the magnetic susceptibility maxima, authors obtained questionable value $\gamma/\nu = 2.3193(82)$, while for the first order regime it is expected to be $\gamma/\nu = 2$ [114, 115]. This result calls for further investigation.

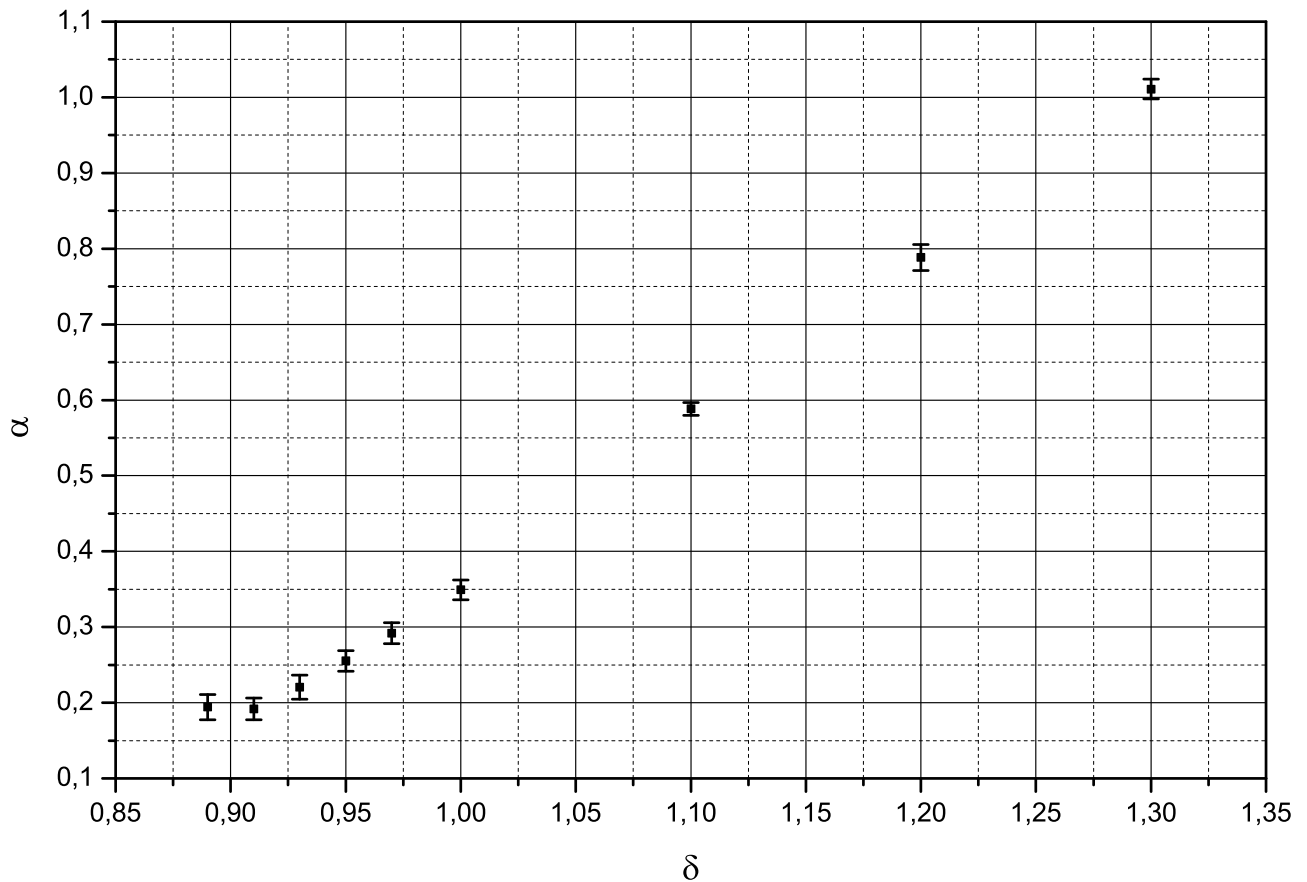


Figure 2.2. Dependency of the critical exponent α calculated in this study (α_{zd}) on the interaction parameter δ .

2.2. One dimensional Potts model with invisible states

2.2.1. Introduction. Classical phase transitions in 1D

As is widely known, in his famous 1925 paper [116], and following a suggestion by Wilhelm Lenz, Ernst Ising sought a positive-temperature phase transition in a one-dimensional (1D) classical equilibrium system with short-range interactions [117]. This was the start of a vast amount of literature on the statistical mechanics of critical phenomena, including a number of studies on why it is impossible to have a phase transition in such systems [118–121]. The lower critical dimension is now defined as that below which a phase transition cannot occur at positive temperature and at least two physical dimensions are required for many short-range classical

equilibrium models.

Landau and Lifschitz gave heuristic arguments suggesting that entropic excesses prevent phase transitions below the upper critical dimension[118]; later similar reasoning was given rigorously by Simon and Sokal [122]; van Hove’s approach was based on proofs of analyticity of the transfer matrix eigenvalues and free energy [119]; Ruelle extended this giving rigorous theorems [120] and, more recently, Cuesta and Sánchez [121] presented more general results about the non-existence of phase transitions in 1D short-ranged systems. For such classical, equilibrium models with short range interactions in 1D second-order phase-transition type phenomena can only occur at zero temperature. The essence of early no-go arguments is that there is an entropy excess in 1D systems relative to interaction energy so that the delicate balance that gives a phase transition is not achieved. The role played by domain walls was further investigated in Ref. [123].

To escape the limitations of no-go theorems, interactions with sufficiently long range can be introduced [124–128]. Another way out is provided by non-equilibrium systems [129] and further exceptions are discussed in Ref. [121]. In particular one can consider models with complex couplings [130–132]. We show, that models with a negative number of invisible states or complex fields acting on them might possess a positive temperature phase transition [20, 21].

The usual concept of universality means that critical behaviour is determined by dimensionality, the range of the interaction and the symmetries of the system. Although the number of invisible states r does not change any of these properties, it was shown to control the order of the phase transition in Refs. [22, 74, 76, 77]. For example although the two-dimensional $(2, 0)$ –state Potts model (which is the ordinary Ising model) is the archetypal example of a continuous phase transition, the model with $(2, 30)$ states undergoes a first-order transition.

Our analysis confirms that the Potts model with a positive number of invisible states adheres to the no-go theorems in one dimension in that the only possibility for a phase transition is at zero temperature. However, if external magnetic field is

allowed to be complex we obtain positive temperature phase transitions [130–132]. The same phenomenon can be achieved through introducing a negative number of invisible states. Although some of these concepts are unphysical in and of themselves, they can be linked with physicality in a number of interesting ways.

Low-dimensional models are of continued theoretical and physical interest [121]. A new combinatorial approach was used to solve Ising’s model in Ref. [133] and it was suggested that the method could be applied to the 2D problem. The first experimental verification of Onsager’s 1943 solution of the 2D Ising model [134] is also a very recent development, offering a “promising candidate for numerous applications” [135].

For these reasons, we analyse 1D models with invisible states using Lee-Yang and Fisher zeros. There have been other approaches to access phase transitions in 1D models. Following on from suggestions by Anderson [124–126], Dyson [127] proved that systems with long range order can have positive-temperature phase transitions and Fröhlich and Spencer proved the existence of a spontaneous magnetization at positive low temperature for the one-dimensional Ising model with long-range interactions. Later, Asorey and collaborators showed that in 1D short range models with complex values of the interaction constant, phase transitions at positive temperatures are possible [130–132]. Cuesta and Sánchez gave three further examples of phase transitions, both of purely academic interest and with importance for phenomena such as surface growth and DNA denaturation [121]. For quantum phase transitions the critical dimensionality is also reduced relative to the corresponding classical transition [136]. Some chemical compounds are well described by quasi one dimensional models [80, 137–141]. Here we are interested in pure 1D equilibrium models which are both classical and short-range.

2.2.2. Potts model with invisible states on a 1D chain

We consider the Potts model with invisible states [the (q, r) –Potts model] with nearest-neighbour interactions on a 1D chain of N spins with periodic boundary

conditions. The partition function is

$$Z = \sum_s \exp(-\beta H_{(q,r)}), \quad (2.3)$$

where \sum_s denotes the sum over all possible spin configurations. With periodic boundary conditions $s_{N+1} = s_1$ the Hamiltonian can be rewritten as a sum of terms representing one bond each, namely

$$H_{(q,r)} = \sum_i H_i, \quad \text{where} \quad H_i = -\delta_{s_i, s_{i+1}} \sum_{\alpha=1}^q \delta_{s_i, \alpha} - h_1 \delta_{s_i, 1} - h_2 \delta_{s_i, q+1}, \quad (2.4)$$

where the variable i spans the N sites of the chain, $s_i = 1, \dots, q, q+1, \dots, q+r$ is a Potts variable and h_1 and h_2 are two ordering fields acting on the first visible and first invisible states respectively, so that

$$Z = \sum_s \prod_i \exp(-\beta H_i). \quad (2.5)$$

The final term in Eq. (2.4) selects only one of the r invisible states as interacting with the external field h_2 . As such, it contributes to the energy if $h_2 \neq 0$. The $r-1$ remaining identical invisible states contribute only to the entropy, as do all invisible states if h_2 vanishes. This means that different microscopic configurations could be understood as the same macroscopic configuration. In terms of the partition function the effect is to multiply some of the terms by $(r-1)$. Similarly, as was done in Ref. [74], we can collect all invisible states into a single one with appropriate weight and consider the equivalent Hamiltonian of a diluted Potts model:

$$H_{(q,r)}^{eq} = - \sum_i \delta_{\sigma_i, \sigma_{i+1}} \sum_{\alpha=1}^q \delta_{\sigma_i, \alpha} - h_1 \sum_i \delta_{\sigma_i, 1} - h_2 \sum_i \delta_{\sigma_i, q+1} - T \ln(r-1) \sum_i \delta_{\sigma_i, q+2}, \quad (2.6)$$

where $\sigma_i = 1, \dots, q, q+1, q+2$ is a new Potts variable and all (except the one along the field h_2) the invisible states are gathered into one with the appropriate weight. The Hamiltonian (2.6) is, of course, different to that in Eq. (2.4). But the corresponding partition functions are the same.

2.2.3. Transfer matrix

To develop the formalism to solve the model (2.4) exactly, we define the transfer matrix $\mathbf{T} = \mathbf{T}(s_i, s_j)$ as [142–145]

$$\mathbf{T}(s_i, s_j) = \exp \left[\beta(\delta_{s_i, s_j} \sum_{\alpha=1}^q \delta_{s_i, \alpha} + h_1 \delta_{s_i, 1} + h_2 \delta_{s_i, q+1}) \right], \quad (2.7)$$

so that, in the explicit form of a $(q+r) \times (q+r)$ matrix,

$$\mathbf{T} = \begin{pmatrix} yz_1 & 1 & 1 & \cdots & 1 & z_2 & 1 & \cdots & 1 \\ z_1 & y & 1 & \cdots & 1 & z_2 & 1 & \cdots & 1 \\ z_1 & 1 & y & \cdots & 1 & z_2 & 1 & \cdots & 1 \\ \vdots & \vdots & \vdots & \ddots & \vdots & \vdots & \vdots & \ddots & \vdots \\ z_1 & 1 & 1 & \cdots & y & z_2 & 1 & \cdots & 1 \\ z_1 & 1 & 1 & \cdots & 1 & z_2 & 1 & \cdots & 1 \\ \vdots & \vdots & \vdots & \ddots & \vdots & \vdots & \vdots & \ddots & \vdots \\ z_1 & 1 & 1 & \cdots & 1 & z_2 & 1 & \cdots & 1 \end{pmatrix} \quad (2.8)$$

where the columns are given by the values of s_i , the rows are given by the values of s_{i+1} and where temperature and field dependencies have been absorbed into the variables

$$y = e^\beta, \quad z_1 = e^{\beta h_1}, \quad z_2 = e^{\beta h_2}. \quad (2.9)$$

Along with the temperature variable y we use another variable $t = y^{-1} = e^{-\beta}$ to map the infinite range $0 \leq T < \infty$ to the finite region $0 \leq t \leq 1$.

The partition function can then be recast as

$$Z = \prod_{i=1}^{i=N} \sum_{\{s_i\}} \mathbf{T}(s_i, s_{i+1}) = \text{Sp } \mathbf{T}^N = \sum_i \lambda_i^N, \quad (2.10)$$

where λ_i are the eigenvalues of \mathbf{T} .

Some of the eigenvalues can be found using the symmetry of the transfer matrix. It is easy to show that matrix (2.8) has five different eigenvalues. On the one hand, because the final r columns of the matrix are proportional, one eigenvalue is zero and is $r - 1$ times degenerate. On the other hand, because $(q - 1)$ elements of the main diagonal are equal to y , choosing $\lambda = y - 1$ leads to $q - 2$ linearly

independent eigenvectors. This leaves only three unknown eigenvalues. They can be found using invariant permutations. This approach leads to the equation for the three remaining eigenvalues:

$$(r-1-\lambda+z_2)(yz_1-\lambda-z_1)(y-\lambda-1)-\lambda z_1(y-\lambda-1)-(q-1)(yz_1-\lambda-z_1)\lambda=0. \quad (2.11)$$

This is an equation of third power and can, therefore, be solved exactly. Since the partition function (2.10) is defined by eigenvalues and all the λ 's have been found, the problem is solved exactly [20].

2.2.4. Partition function zeros and the transfer matrix method

Critical behaviour of equilibrium systems can be extracted from the partition function. In our case, the latter is described by the eigenvalues of the transfer matrix (2.10) and, since we have shown that they can all be found explicitly, the critical properties of the Potts model with invisible states can, in principle, also be found explicitly. This allows us to access the Lee-Yang zeros [84, 85] and the Fisher zeros [86] in Sections 2.2.7, 2.2.8, 2.2.9.

The standard approach is to label the eigenvalues of the transfer matrix in such a way that they are ordered in magnitudes; $|\lambda_1| \geq |\lambda_2| \geq |\lambda_3| \geq \dots$. The partition function zeros are then found using the condition that (at least) two eigenvalues are largest by modulus [146]

$$|\lambda_1| = |\lambda_2|. \quad (2.12)$$

Since the partition function is analysed in the complex (T or h) plane, the eigenvalues are complex as well. Therefore condition (2.12) can be written as

$$\lambda_2 = \lambda_1 e^{i\phi}. \quad (2.13)$$

From Eq. (2.10), the partition function is a sum of eigenvalues to the power N . In our case the eigenvalue $\lambda = 0$ makes no contribution so that the partition function takes the form $Z = \lambda_1^N + \lambda_2^N + \lambda_3^N + \lambda_4^N$. Of these four eigenvalues, three

are roots of the polynomial (2.11) and the fourth equals $y - 1$. Taking into account the orders of magnitude of the eigenvalues, the partition function may be rewritten in such a way as to single out the main terms:

$$Z = \lambda_1^N \left[1 + e^{iN\phi} + \left(\frac{\lambda_3}{\lambda_1} \right)^N + \left(\frac{\lambda_4}{\lambda_1} \right)^N \right]. \quad (2.14)$$

In the limit of large N only the leading two terms in the expression in parentheses on the right-hand side of Eq. (2.14) contribute so that we obtain the phase ϕ given by

$$1 + e^{iN\phi} = 0 \quad \text{or} \quad \phi = \frac{2k - 1}{N} \pi, \quad k = 1 \dots N. \quad (2.15)$$

In the thermodynamic limit values of the phase ϕ span the whole region $0 \leq \phi \leq 2\pi$. Therefore the coordinates of the partition function zeros are found solving Eq. (2.13) with the phase given by Eq. (2.15). This method is appropriate when all the eigenvalues are given explicitly. However, when they are given as the roots of the polynomial, one can use the method suggested in Ref. [147] for models with three non-zero eigenvalues or that put forward in Ref. [141] adapted for models with four non-zero eigenvalues.

Following this method, the four eigenvalues of the transfer matrix are presented as the roots of the polynomial of fourth order¹. In the most general case it has the form

$$\lambda^4 + a_3\lambda^3 + a_2\lambda^2 + a_1\lambda + a_0 = 0. \quad (2.16)$$

For the Potts model with invisible states Eq. (2.16) is obtained by multiplying Eq. (2.11) by $[\lambda - (y - 1)]$. The corresponding coefficients have the form

$$\begin{aligned} a_0 &= (y - 1)^3 z_1 (r + z_2 - 1); \\ a_1 &= -(y - 1)^2 (z_1 (q + y - 1) + (2z_1 + 1)(r + z_2 - 1)); \\ a_2 &= (y - 1) ((z_1 + 1)(q + y - 1) + (z_1 + 2)(r + z_2 - 1) + yz_1 - 1); \\ a_3 &= -q - r - yz_1 - 2y - z_2 + 4. \end{aligned} \quad (2.17)$$

¹Since one does not know in advance which eigenvalue is the maximum one, all four eigenvalues have to be considered.

The goal of the method is to obtain a λ -independent equation linking together temperature, fields and other model parameters. To derive this we use four equations from Vieta's theorem together with the condition (2.13). Excluding all eigenvalues from these five equations we obtain

$$F(q, r, z_1, z_2, y) = F_1 F_2 (f_1 + f_2 + f_3 + f_4), \quad (2.18)$$

where

$$F_1 = 8a_2 \cos^2 \left(\frac{\phi}{2} \right) \cos(\phi) - a_3^2 [2 \cos(\phi) + 1];$$

$$F_2 = 4a_1 [2 \cos(\phi) + 1] \left[\cos \left(\frac{\phi}{2} \right) + \cos \left(\frac{3\phi}{2} \right) \right]^2 - 32a_2 a_3 \cos^4 \left(\frac{\phi}{2} \right) \cos \phi + a_3^3 [2 \cos(\phi) + 1]^2;$$

and

$$f_1 = 16a_0^3 \left[\cos \left(\frac{\phi}{2} \right) + \cos \left(\frac{3\phi}{2} \right) \right]^4;$$

$$f_2 = a_1^2 \left[a_2^2 (a_3^2 - 2a_2(\cos(\phi) + 1)) - a_1^2 (1 + 2 \cos(\phi))^3 + 2a_1 a_3 \left(a_2 (5 \cos(\phi) + \cos(2\phi) + 3) - a_3^2 (1 + \cos(\phi)) \right) \right];$$

$$f_3 = -2a_0 \left[a_2^3 \left(8a_2 \cos^4 \left(\frac{\phi}{2} \right) - a_3^2 (\cos(\phi) + 1) \right) + a_1^2 \left(4a_2 \cos^2 \left(\frac{\phi}{2} \right) (7 \cos(\phi) + 5 \cos(2\phi) + \cos(3\phi) + 5) - a_3^2 (2 \cos(\phi) + \cos(2\phi)) \right) + a_1 a_2 a_3 \left(-4a_2 \cos^2 \left(\frac{\phi}{2} \right) (6 \cos(\phi) + \cos(2\phi) + 3) + a_3^2 (5 \cos(\phi) + \cos(2\phi) + 3) \right) \right];$$

$$f_4 = a_0^2 \left[128a_2^2 \cos^4 \left(\frac{\phi}{2} \right) \cos^2(\phi) + a_3^4 (2 \cos(\phi) + 1)^3 - 8a_2 a_3^2 \cos^2 \left(\frac{\phi}{2} \right) \left(7 \cos(\phi) + 5 \cos(2\phi) + \cos(3\phi) + 5 \right) + 8a_1 a_3 \left(\cos \left(\frac{\phi}{2} \right) + \cos \left(\frac{3\phi}{2} \right) \right)^2 (2 \cos(\phi) + \cos(2\phi) + 3) \right].$$

For each value of ϕ given by Eq. (2.15) all the roots of Eq. (2.18) provide the values of parameters when two eigenvalues are equal by modulus, but not all of them are actual partition function zeros. Actual zeros are characterised by the condition that two largest eigenvalues are equal by modulus.

We analyse the zeros of the partition function in the plane of complex magnetic field and complex temperature. According to the Lee-Yang theorem, for the ferromagnetic Ising model on a d -dimensional regular lattice, magnetic zeros are purely imaginary [84, 85]. This statement can be generalised to many other models [94]. Transforming to the complex $z = e^{-\beta h}$ -plane, the counterpart zeros lie on an arc of the unit circle. Lee-Yang zeros have been called “protocritical points” [146] because they have the potential to become actual critical points. The protocritical point at an end of the arc which lies closest to the positive real axis is referred to as the “Yang-Lee edge” (henceforth also referred to as the “edge”) [148]. If the temperature is higher than the critical one, the circular arc is open, i.e. it does not cross the positive real axis. As the temperature is lowered, the arc becomes a circle and the edge pinches the real axis when the critical temperature is reached, precipitating the phase transition. For temperatures lower than the critical value, the arc is closed into a full circle so that zeros cross the real z axis.

In Eq. (2.18), ϕ takes discrete values for finite systems according to Eq. (2.15). Having these data, we used finite-size scaling to determine the critical exponents (see Section 2.2.9). To establish whether the phase transition occurs at positive or negative temperature, we determine the critical temperature by enabling the Lee-Yang zeros to pinch the real axis. This only occurs for infinite volume and we achieve this simply by setting $\phi = 0$ in Eq. (2.18). Alternatively, one can directly access zeros in the thermodynamic limit and the true (infinite N) Lee-Yang edge by using the Beraha-Kahane-Weiss (BKW) theorem [149–151].

2.2.5. Yang-Lee edge singularity exponent

In this section we show that the Yang-Lee edge singularity exponent $\sigma = \frac{1}{2}$ remain unchanged by introducing invisible states. To do so we closely follow the method developed in Refs. [141, 147].

With increase of system size, Lee-Yang zeros $z_1 = |z_1|e^{i\theta}$ terminate in the complex plane at the Yang-Lee edge $z_1^e = |z_1^e|e^{i\theta_e}$. Their density $g(z_1)$ in the vicinity

of z_1^e is governed by the edge singularity exponent σ [152]:

$$g(\theta) \propto |\theta - \theta_e|^\sigma. \quad (2.19)$$

In circumstances where, for a given value of T , the zeros are located on curves (the so-called singular line [95] as opposed to two dimensional regions [96]), the function g can be written for a fixed $|z_1|$ keeping dependency of the phase θ only. The exponent σ , like the other critical exponents, is characteristic of a given universality class. For the 1D Ising and q -state Potts models its exact value is $\sigma = -\frac{1}{2}$ [84, 85, 147, 152]. Another known exact value for the σ -exponent has been obtained for the spherical model, where $\sigma = \frac{1}{2}$ independently of the type of interaction (short- or long-range) and space dimensionality [153].

The density of the partition function zeros in the region $(\phi, \phi + \Delta\phi)$ is proportional to the number of zeros in this region divided by the length of the part of the cord these zeros occupy. Since for each ϕ there is a certain zero, than the number of zeros in the region $(\phi, \phi + \Delta\phi)$ is proportional to $\Delta\phi$. Therefore, the density can be written as

$$\tilde{g}(\phi, \phi + \Delta\phi) \propto \frac{\Delta\phi}{\int_{\phi}^{\phi+\Delta\phi} \sqrt{\left(\frac{\partial \text{Re}z_1}{\partial \phi}\right)^2 + \left(\frac{\partial \text{Im}z_1}{\partial \phi}\right)^2} d\phi}. \quad (2.20)$$

In the thermodynamic limit zeros form continuous curve with density at the point ϕ given by

$$\tilde{g}(\phi, \phi + d\phi) = g(\phi) \propto \frac{1}{\sqrt{\left(\frac{\partial \text{Re}z_1}{\partial \phi}\right)^2 + \left(\frac{\partial \text{Im}z_1}{\partial \phi}\right)^2}}. \quad (2.21)$$

In the vicinity of the edge θ_e (which corresponds to $\phi = 0$) coordinates of zeros can be expanded into the Taylor series

$$z_1(\phi) \approx z_1^e + \frac{\partial^2 z_1(0)}{\partial \phi^2} \phi^2 + \dots, \quad (2.22)$$

The linear term is absent since Eq. (2.18) is an even function of ϕ . Substituting the expansion (2.22) into Eq. (2.21) we obtain a simple relation between the density

function $g(\phi)$ and the phase ϕ :

$$g(\phi) \propto |\phi|^{-1}. \quad (2.23)$$

In the thermodynamic limit, close to the edge point, the phase and coordinates of zeros are connected through

$$\theta - \theta_e \propto |z_1 - z_1^e|. \quad (2.24)$$

Using expansion (2.22) in the right-hand side of the Eq. (2.24) we arrive at

$$\phi^2 \propto (\theta - \theta_e). \quad (2.25)$$

Relation (2.23) together with Eq. (2.25) lead to the power-law behaviour of the density of zeros as a function of their phase close to the edge point

$$g(\theta) \propto |\theta - \theta_e|^{-1/2}. \quad (2.26)$$

Thus the Yang-Lee edge singularity exponent is $\sigma = -\frac{1}{2}$. This value follows immediately from the symmetry of zeros under the substitution $\phi \rightarrow -\phi$, which is observed for the models considered in Refs. [80, 141, 147, 154].

2.2.6. Duality relations

To facilitate the analysis of the partition function zeros, we first discuss some properties of the eigenvalues, which will be used later in the text.

In Eq. (2.11), the quantities r and z_2 appear only in one term together as a sum. We conclude that the magnetic field acting on the invisible states plays the same role as additional invisible states. In this way $r + z_2 - 1$ can be treated as a temperature-dependent number of invisible states. For this reason, in this section z_2 is included in r and is never shown explicitly.

Duality means that under a certain unitary transformation \mathbf{S} , the transfer matrix changes according to the rule [155]

$$\mathbf{S}\mathbf{T}(y, z_1)\mathbf{S}^{-1} = \alpha\mathbf{T}^T(y^D, z_1^D), \quad (2.27)$$

where $y^D = y^D(y, z_1)$, $z_1^D = z_1^D(y, z_1)$ denote variables dual to y, z_1 , and \mathbf{T}^T is the transposed transfer matrix. Eq. (2.27) can be rewritten in terms of the eigenvalues

$$\lambda(y^D, z_1^D) = \frac{1}{\alpha(y, z_1)} \lambda(y, z_1). \quad (2.28)$$

Eq. (2.28) is useful when explicit expressions for the eigenvalues are known. But in our case solving the third-order equation (2.11) results in having cumbersome expressions for each λ and thus Eq. (2.28) will be hard to handle. Instead, let us derive relations for the coefficients in the third-order polynomial in the left hand side of Eq. (2.11). In the most general case the equation reads

$$\lambda^3 + A_1(y, z_1)\lambda^2 + A_2(y, z_1)\lambda + A_3(y, z_1) = 0. \quad (2.29)$$

Eq. (2.29) holds for both ordinary and dual variables. Substituting (2.28) into (2.29) we get the following transformation rules for the coefficients A_1, A_2, A_3 :

$$\begin{aligned} A_1(y^D, z_1^D) &= \frac{1}{\alpha} A_1(y, z_1), \\ A_2(y^D, z_1^D) &= \frac{1}{\alpha^2} A_2(y, z_1), \\ A_3(y^D, z_1^D) &= \frac{1}{\alpha^3} A_3(y, z_1). \end{aligned} \quad (2.30)$$

Using the first two equations of (2.30) and Eq. (2.28) with $\lambda = y - 1$ one recovers expressions for the dual variables:

$$\begin{aligned} \alpha &= \frac{(y-1)(q(z_1-1) + (r-1)z_1 + 1)}{q^2 + q(2r-1) + (r-2)r}, \\ y^D &= \frac{(q+r-1)(q+r+z_1-1)}{q(z_1-1) + (r-1)z_1 + 1}, \\ z_1^D &= \frac{q^2 + q(2r+y-2) + r^2 - 2r - y + 1}{(y-1)(q+r-1)}. \end{aligned} \quad (2.31)$$

These expressions allow us to substitute temperature by field and vice versa without changing the behaviour of the system. Substituting $r = 0$ into (2.31) one recovers the duality relations for the ordinary 1D Potts model obtained in [154].

2.2.7. Lee-Yang zeros for models with direct physical realisability

Lee-Yang zeros for the ordinary Potts model

We first consider the ordinary q -state Potts model when the number of invisible states and, correspondingly, the second magnetic field are set to zero ($r = 0$ and $h_2 = 0$). This ordinary Potts model is thoroughly investigated so our results can be compared to those previously obtained [154]. In this case one of the roots of Eq. (2.11) becomes $\lambda = y - 1$, reducing the number of different eigenvalues to three. The remaining two eigenvalues are found as the roots of Eq. (2.11) and fully recover results obtained in Ref. [154]. The three eigenvalues are

$$\lambda_{1,2} = \frac{1}{2} \left[(y(z_1 + 1) + q - 2) \pm \sqrt{(y(1 - z_1) + q - 2)^2 + (q - 1)4z_1} \right], \quad \lambda_3 = y - 1. \quad (2.32)$$

In Ref. [146] it was shown that the edge can be recovered from the condition that the largest eigenvalues of the transfer matrix are degenerate. Two of these eigenvalues in Eq. (2.32) are degenerate when the expression under the square root sign vanishes.

We plot the resulting loci of Lee-Yang zeros of the 1D Ising model ($q = 2$) in Fig. 2.3. The $T > 0$ case is illustrated in the left panel. There the edge is strictly complex meaning there is no phase transition in the symmetric phase. As the temperature decreases, the edge approaches the real axis. The limiting case of $T = 0$ is represented in the right panel, albeit for a finite-size system (the circle is complete for an infinite chain of sites). In the thermodynamic limit the approach of the edge to the critical point ($h = 0$ or $z = 1$) triggers the zero-temperature spontaneous (zero-field) phase transition. Fig. 2.3 illustrates the $q = 2$ case only, for which the Lee-Yang unit-circle theorem is obeyed. Altering the number of Potts states alters the loci of zeros (not shown in the plot); while they remain circular, their radii are q -dependent for positive temperature. If $q < 2$ the radii of these circles are less than 1 and if $q > 2$ the radii exceed 1. However, at $T = 0$ all Lee-Yang arcs close into circles and cross the real axis at $\text{Re } z_1 = 1$.

To more compactly illustrate the dependencies of zeros on the both temperat-

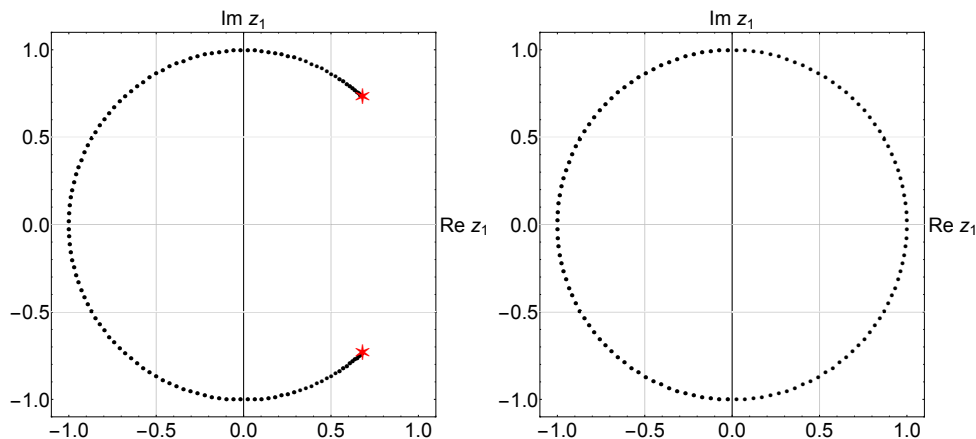


Figure 2.3. Lee-Yang zeros in the complex $z_1 = e^{-\beta h_1}$ -plane of the 1D Ising model ($q = 2, r = 0$) for fixed values of T . The plots are for finite N but the curves become continuous in the thermodynamic limit. The left panel displays Lee-Yang zeros with a positive value of the temperature ($T = 1.091$). The Yang-Lee edges, represented as large red stars, do not reach the positive real axis indicating no phase transition. The right panel displays zeros with vanishing temperature ($T = 0$). The approach of the zeros to the real axis at $z_1 = 1$ at infinite N indicates a zero-field ($h_1 = 0$) phase transition.

ure and on the number of states, instead of plotting the loci of the full sets of zeros as in Fig. 2.3, we plot the coordinates of the edges for different values of T and q in Fig. 2.4. We call these “edge loci”. Such plots allow us to capture a greater span of q and T values while keeping the essential information because where the edge loci cross the real axis is where a phase transition can happen. For different given values of q the edge loci form different closed curves. But in each case the real axis is crossed at $T = 0$ confirming that the only possibility is for a phase transition at zero temperature, as observed nearly a hundred years ago by Ising (in the $q = 2$ case) [116].

To summarise, in this subsection we have recovered known results, supporting the viability of the approach.

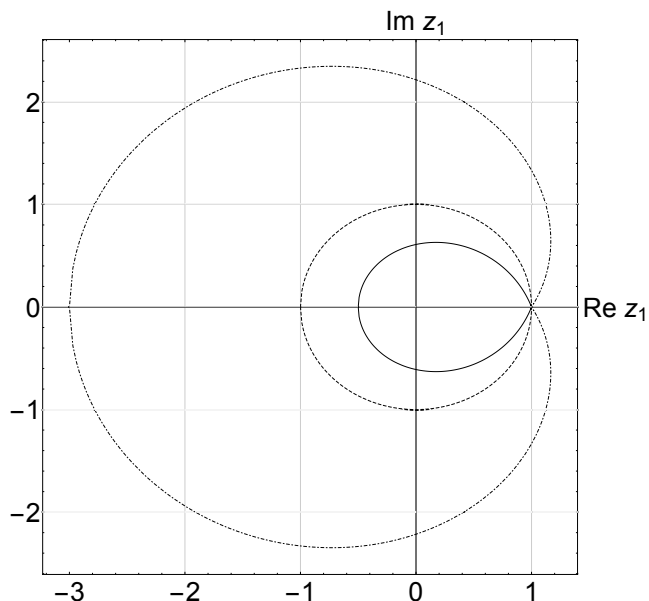


Figure 2.4. Edge loci in the complex z_1 -plane for three Potts models ($q = 1.5, q = 2, q = 4$, moving inside out) without invisible states ($r = 0$). Each locus spans the full range of temperature values ($0 \leq T \leq \infty$) and intersects the $\text{Re } z_1$ axis at $T = 0$.

Lee-Yang zeros for the Potts model with invisible states

Having recovered well-known results for the ordinary Ising model in Fig. 2.3 and the ordinary Potts model in Fig. 2.4, and illustrated how the loci depend on q , we turn our attention to the Potts model with invisible states. As follows from Eq. (2.11) an external field acting on invisible states effectively works as an additional number of such states. We elaborate on this duality in Section 2.2.6 where we present a similar relationship between field and temperature. Therefore, without loss of generality, we can set $h_2 = 0$ (or $z_2 = e^{-\beta h_2} = 1$) in Eq. (2.11) arriving at

$$(r - \lambda)(yz_1 - \lambda - z_1)(y - \lambda - 1) - \lambda z_1(y - \lambda - 1) - (q - 1)(yz_1 - \lambda - z_1)\lambda = 0. \quad (2.33)$$

Setting $z_2 = 1$ in Eq. (2.18), and using the method described earlier, we extract the Lee-Yang zeros in the complex z_1 -plane for any value of T at fixed values of q and r . As a counterpart of Fig. 2.3 for the ordinary Potts model we plot Lee-Yang zeros of the (2, 2)-state Potts model for different temperatures in Fig. 2.5.

As seen from the plot, zeros form circular arcs, but their radii are not unity

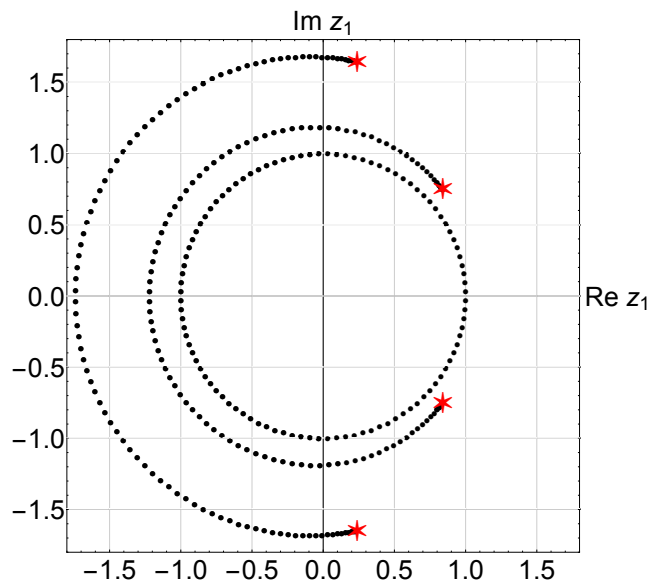


Figure 2.5. Lee-Yang zeros for the $(2, 2)$ -state Potts model in the complex $z_1 = e^{-\beta h_1}$ -plane at $y = e^\beta = 2$ (outer locus), $y = 4$ and $y \rightarrow \infty$ (inner, closed circle, representing $T = 0$) for systems of size $N = 100$. The inner circle is identical to the right panel of Fig. 2.3 for the Ising model. As in the left panel of Fig. 2.3, the outer two loci indicate there is no transition at non-zero temperature. The Yang-Lee edges are highlighted in red.

and increase with increasing temperature (lower y -values) as the system is driven further away from the (zero-temperature) phase transition. The same behaviour was observed even in the ordinary Potts model (Fig. 2.4). The difference is that even in the Ising case ($q = 2$) the presence of the invisible states changes the radius of the circle. It is only at $T = 0$ that zeros lay on the closed circle of unit radius.

To find the Yang-Lee edge one has to identify when the two largest eigenvalues of the transfer matrix are equal. This means that the polynomial (2.11) also has degenerate roots. This condition is equivalent to the discriminant $\mathbb{D}(y, z_1, z_2, q, r)$ of Eq.(2.11) vanishing [156]:

$$\mathbb{D}(y, z_1, z_2, q, r) = 0. \quad (2.34)$$

The discriminant \mathbb{D} is a polynomial function of its arguments y , z_1 , z_2 , q and r . By setting $z_2 = 1$ and fixing the numbers of visible and invisible states (q and r , respectively) we can scan values of the temperature ($y = e^\beta$) to determine the co-

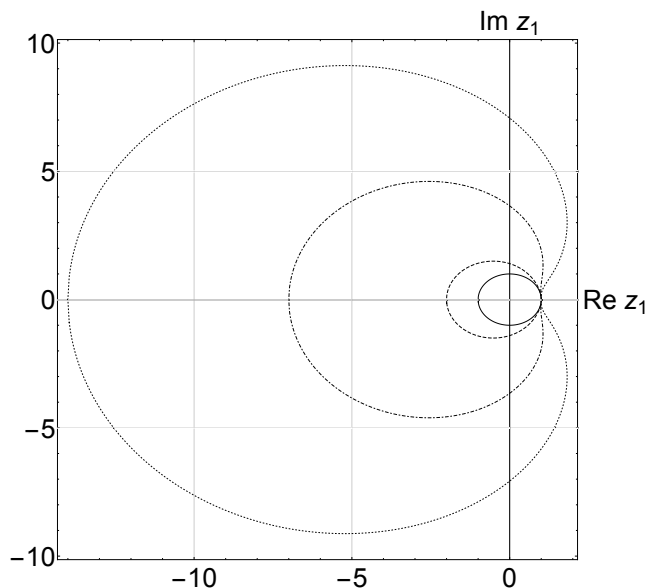


Figure 2.6. The edge loci in the complex z_1 -plane for $q = 2$ and $r = 0, 1, 6, 13$ moving inside out. All plots cross at the real axis at $z_1 = 1$ indicating only zero temperature phase transitions. This is the invisible-states counterpart of Fig. 2.4.

ordinates of the edge points. Finding these coordinates for all possible temperatures $0 \leq T < \infty$ (or $1 \leq y < \infty$) we obtain the edge loci as shown in Fig. 2.6. This is the counterpart of Fig. 2.4 (it is the Ising model with invisible states). Comparison between the two figures illustrates that invisible states are manifest in Lee-Yang-zero terms by widening the edge loci. But the behaviour of Lee-Yang zeros discussed above signals that the presence of invisible states does not change the fact that there is only a zero-temperature phase transition.

To summarise, in this subsection we have shown that systems with a positive number of invisible states also fail to manifest a positive-temperature phase transition in 1D.

2.2.8. Phase transitions at positive temperatures

In this section we introduce new ways to instigate positive-temperature phase transitions in a one-dimensional classical model with short-range interactions.

We start with analysing Lee-Yang zeros in the complex z_2 -plane. This will

give us an insight into what is needed to shift the phase transition to positive temperatures. Earlier we have already mentioned that r and z_2 contribute only as a sum. It appears that having a negative value of this sum is key to achieving a positive-temperature phase transition in the current context. While mathematically identical, this mechanism can be interpreted physically in two different ways. Negative values of z_2 lead to complex values of the external magnetic field h_2 . The effect of complex model parameters on the phase transition in 1D was already discussed in Refs. [130–132]. In our case similar behaviour is achieved by tuning h_2 . Alternatively, negative values of invisible states $r < 0$, based on the duality discussed in Section 2.2.6, have the same effect. Although both of these conditions are exotic, they either have connections to physical systems or have potential to be manifested physically in the future [26, 87, 157].

Zeros in complex z_2 for $h_1 = 0$

To begin our investigations we take inspiration from the analysis of so-called Potts zeros. In the ordinary Potts model, these are studied by an extended Fortuin-Kasteleyn representation [158] by promoting the Potts variable q to a complex number. Zeros in the complex q -plane are used to find the critical number of states for a given temperature [159–161]. While values of q below 2 are unphysical in terms of spin models, they can have physical manifestations — for example $q = 1$ describes percolation, $q = 0$ spanning trees and Abelian sandpile model for self-organised criticality [162–165].

We have seen earlier that r acts similarly to an external magnetic field h_2 . One can therefore interpret zeros in the complex r -plane as Lee-Yang-type zeros in the complex plane of z_2 . We obtain partition function zeros in the complex z_2 -plane by substituting values of q , r , h_1 into Eq. (2.18) in a similar manner as in the previous section. On the other hand, we can analyse the behaviour of the edge coordinates directly by solving Eq. (2.34). The corresponding plot is given in Fig. 2.7 for the particular case $q = 2$.

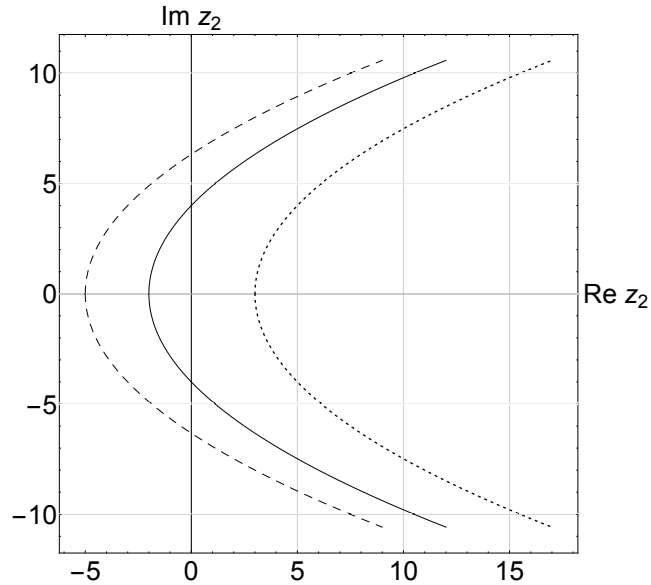


Figure 2.7. Yang-Lee edge locus corresponding to complex z_2 for $q = 2$, $h_1 = 0$ and $r = 4$ (dashed line), $r = 1$ (solid line) and $r = -4$ (dotted line). Each point of the lines represent a certain temperature in the region $0 \leq t \leq 1$.

For positive values of r , the only crossing point with the real z_2 axis is located on the negative part. This is illustrated in Fig. 2.7. The middle edge locus in Fig. 2.7 was obtained for $r = 1$. Increasing r serves to shift the locus to the left; but its shape remains the same. This confirms our interpretation of Fig. 2.6 that increasing the value of r pushes the loci further away from a physical phase transition. One may infer that the converse also holds; decreasing r to a negative number of invisible states may shift the real edge locus from the negative real semi-axis to its positive counterpart. This is supported in the rightmost locus of Fig. 2.7 where $r = -4$.

To summarise this section, we have observed that zeros in complex h_2 cross the real axis at negative values of z_2 when r is positive, or vice versa, when $r < 0$, $z_2 \geq 0$. Of course, the figure refers to the complex z_2 -plane, corresponding to a field acting on entropic (invisible) states only. To connect with previous studies of Lee-Yang zeros we have to examine the complex h_1 or z_1 -plane.

Lee-Yang zeros in the complex z_1 -plane with a complex field acting on invisible states: The case $z_2 < 0$ ($h_2 \in \mathbb{C}$).

Following on from the above considerations, we extend our search for positive-temperature phase transitions in one dimension to an analysis of the effects of negative values of z_2 (meaning a complex external magnetic field h_2) through Lee-Yang zeros in the complex h_1 -plane. Using the same method as previously deployed, we substitute into Eq. (2.18) negative value of z_2 and obtain Lee-Yang zeros for various values of q , r and temperatures t . Results are represented in Fig. 2.8, which is the positive- r and negative- z_2 counterpart of Fig. 2.3 (which has vanishing values of r and h_2). At small temperatures these zeros lay close to the unit circle of Fig. 2.3, but increasing the temperature does not leave the Lee-Yang zeros on the unit circle. Instead they assume rather moon-like shapes. Moreover, although the locus of Lee-Yang zeros opens with increasing temperatures as in Fig. 2.3, the orientation of the arcs is reversed. It is worth noting here, that in order to obtain plots shown in Fig. 2.8 we fixed z_2 and not h_2 , meaning that with the change of temperature t the external magnetic field is changed.

To further analyse the complex values of h_2 that shift the phase transition to positive temperatures, we set $h_1 = 0$ and use the condition (2.34) for the discriminant to find when two eigenvalues are equal and largest by modulus. This leads to a relation between the critical temperature and field h_2 , namely

$$z_2 = y - q - r \pm 2i\sqrt{q(y-1)}. \quad (2.35)$$

In this equation both y and $z_2 = y^{h_2}$ are temperature dependent. Fixing q , r and sweeping through the region $1 \leq y < \infty$ (meaning a temperature range $0 \leq t \leq 1$), we solve numerically Eq. (2.35) and obtain complex values for h_2 . In Fig. 2.9 we plot these values for the (2, 3)-state Potts model in the form $e^{-\beta h_2}$. The curve forms two lines, each point of which corresponds to a certain positive critical temperature. The upper and lower branches correspond to complex conjugate values of the field.

To summarise this subsection, we have observed that a complex field acting

purely on invisible states can induce a positive-temperature phase transition in 1D. Although this appears exotic, 60 years after their introduction [84, 85], it has recently been established that complex external magnetic fields h_1 can be mapped into physically accessible quantum coherence times [87]. Similarly, tuning complex values of the external field h_2 may one day be accessible, perhaps by changing the “invisible” part of a system’s behaviour from classical to quantum.

Zeros in the complex z_1 -plane for $h_2 = 0$ and $r < 0$

We build upon the observation in Fig. 2.7 that the edges in the complex z_2 -plane are horizontally shifted to the right by reducing r to negative values. Moreover, taking into account results of the previous subsection, where the transition is observed for negative values of z_2 and the duality relation between r and z_2 , we expect to obtain a phase transition for $r < 0$ as well. Using an extended Fortuin-Kasteleyn representation we relax the condition of positivity on the number of invisible states r . In Fig. 2.10, we plot the Lee-Yang zeros in complex z_1 for the $(2, -5)$ -state Potts model for different values of temperature. Fig. 2.10 is a negative- r counterpart of Figs. 2.3 and 2.5. Our principal result in this subsection is that loci of zeros cross the real axis at positive temperatures for negative values of r . In particular, the left plot in the second line shows that, in the absence of field h_1 (i.e., when $z_1 = 1$), the zeros cross the real axis at a positive value of t (namely $t = 0.25$). This is the sought-after spontaneous, zero-field, positive-temperature phase transition in 1D. The correlation length is infinite at the critical temperature but the entropy has discontinuity. Therefore the phase transition can be interpreted as of first order. However, small part of the entropy dependency on the temperature has an unphysical region. This can be as a consequence of unphysical values of the model parameters. Similar behaviour was earlier established in the models with complex interactions [130–132]. This connection is obvious, since we showed earlier that negative values of r have the same effect on the system as complex external magnetic field.

Each of the loci in Fig. 2.10 crosses the real axis, corresponding to a critical point. Negative values of z_1 represent complex values of physical field h_1 . Values $z_1 > 1$ represent $h_1 > 0$ — a positive field acting on the first state $s = 1$. Positive values in the range $0 < z_1 < 1$ correspond to negative values of h_1 . Such negative values of the external magnetic field are effectively the same as positive external fields acting on the other ($s \neq 1$) states. For the ordinary Ising case ($q = 2, r = 0$) negative values of the external magnetic field acting on the first state ($s = 1$), say, effectively represent the same physics as a positive external field acting on the other ($s = 2$) state. For the ordinary Potts model with $q > 2, r = 0$, negative external fields disfavour one of the states reducing the symmetry from Z_q to Z_{q-1} . In three dimensional three state Potts model this affects the phase diagram; weak magnetic fields do not change the order of the phase transition, while strong negative magnetic field changes it to the three-dimensional (3D) Ising universality class [166].

The figure also illustrates that, as for the ordinary Potts model, the Lee-Yang circle theorem is violated for the Ising model with a negative number of invisible states; the loci of zeros are not circular.

The set of crossing points for various temperatures in the range $0 \leq t \leq 1$ can be interpreted as a phase diagram and is shown for the $(2, -5)$ -state model as solid black line in Fig. 2.11. The spontaneous transition is identified at $t = 0.25$, $z_1 = 1$. The counterpart for the ordinary Ising model is at $t = 0$, $z_1 = 1$ — i.e., at vanishing instead of positive temperature. To further illustrate this representation, in Fig. 2.11 we divide the (t, z_1) -plane into regions. The different colours represent different eigenvalues which are maximal by absolute values. Where they coincide is where criticality occurs.

A curious phenomenon in Fig. 2.10 is the flipping with increasing T of the edges of the loci (illustrated as large stars) from the positive to negative half planes. This happens not at the zero-field critical point but at a lower value of T . The reason for this is that the edges in Fig. 2.10 are each away from the real axis and are pseudocritical points with $\text{Im } z_1 \neq 0$ — not zero-temperature critical points. The

phase diagram of Fig. 2.11 has vanishing imaginary field $\text{Im } z_1 = 0$. To access the LY edges, and their flipping, requires non-zero values of $\text{Im } z_1$ and three examples of this are depicted in Fig. 2.12. Different colours in the plot represent different eigenvalues. These are basically three slices through of a 3D plot with axes t (temperature), $\text{Re } z_1$ and $\text{Im } z_1$. These plots are given for the fixed temperature, when flipping occurs and coordinates of the edge. Three eigenvalues are equal by modulus exactly at the point where flipping occurs. Such a behaviour signals existence of a point with unusual Lee-Yang edge singularity exponent [167].

To summarise this section, while positive values of r do not change the order and temperature of the phase transition, negative numbers of invisible states shift it to positive temperatures. In addition, there is a curious phenomenon involving the flipping of the locations of the edges relative to the other Lee-Yang zeros. This occurs at a value of temperature below the critical one and is explained by complex fields.

2.2.9. Fisher zeros

Fisher zeros are usually considered at the critical value of the external field. For the spontaneous phase transition the critical value of the field is $h_1 = 0$ corresponding to $z_1 = 1$. In this case one of the roots of the polynomial (2.11) becomes $\lambda = y - 1$ so that the polynomial (2.11) has only three different eigenvalues. Fisher zeros can be obtained from the condition that (at least) two eigenvalues of the transfer matrix are largest by modulus [146]. This approach allows to obtain zeros of the finite-size system and thus use the finite-size scaling technique (FSS) for the Fisher zeros coordinates. In the thermodynamic limit the line of zeros crosses the real axis at the transition point.

Critical temperature

Fixing $z_1 = z_2 = 1$ in Eq. (2.18) we arrive at the equation for the coordinates of the partition function zeros in the complex y -plane at given pair of (q, r) . It is most

convenient to display Fisher zeros in the complex $t = y^{-1}$ -plane. In this case they form closed curves around the origin $t = 0$ (rather than the “run-away” behaviour at $y \rightarrow \infty$). The infinite region $0 \leq T < \infty$ corresponds to the section $0 \leq t \leq 1$. In Fig. 2.13(a) we plot coordinates of the zeros for $q = 2$ and $r = 0, 1, 2, 5$ at fixed $N = 128$. The case $r = 0$ recovers results for the 1D Ising model. For $q = 2, r = 0$ zeros lie on the imaginary axis. With increasing N , the zero closest to the real axis closes in and with $N \rightarrow \infty$ it crosses the real axis at $t = 0$ ($T = 0$), implying again that there is only a zero temperature phase transition for the 1D systems [118, 168].

As one can see from Fig. 2.13(a), the presence of invisible states changes the locus of Fisher zeros. Now the zeros have both real and imaginary parts and in addition one more crossing point of the real t -axis appears. However this crossing point is located in the unphysical region $t < 0$ (complex values of T). $t = 0$ remains the point where the Fisher zeros approach the real axis and this confirms that the phase transition in the 1D Potts model is not changed by the presence of the invisible states. The critical exponents of this transition are discussed later.

We extend these considerations and show in Fig. 2.13(b) the locus of zeros for the $(2, r)$ -state Potts model with negative values of r .²

As we can see from the figure, the locus of Fisher zeros in case $r = -5, -7$ intersect the real axis at the value $t_c = -\frac{1}{q+r-1}$. This means that besides the ordinary zero temperature phase transition we observe finite temperature phase transition in 1D model. The equivalent representation of the Potts model with invisible states through Eq. (2.6) indicates that the chemical potential is $\mu = -T \log r$. Therefore the negative number of invisible states is equivalent to a model with complex chemical potential. Again, via the aforementioned relation between the complex external field and decoherence time [87], this gives a connection to the behaviour of quantum systems.

²We do not show in the plot some points in the region $t > 1$ that correspond to negative temperatures.

Critical exponents

With the coordinates of the Fisher zeros to hand it is possible to obtain values of critical exponents. We will use the methods described in Subsections 1.3.1, 1.3.1. The first method to use is the scaling of the zero closest to the critical point. This will provide us with correlation length critical exponent ν . Another approach to analyse the partition function zeros is to use partition function zeros density [95, 96]. This method allows to use not only coordinate of the closest zero but consider zeros density function. Scaling of the density function is determined by the specific heat critical exponent α .

We have used both techniques to extract the critical exponents from the coordinates of the zeros. Using system sizes from $N = 500$ to $N = 1000$ with increment $\Delta N = 20$ $q = 2$ and $r = 6$ we obtained $\nu = 0.9998(2)$, $\Lambda = 1.9997(2)$ and $\alpha = 1.002(2)$, which are in a good agreement with the hyperscaling relation $\alpha = 2 - d\nu$. Moreover these values remain close to the values $\nu = 1, \alpha = 1, \Lambda = 2$ with q and r changing.

It is worth mentioning that in the absence of magnetic field exact solution can be obtained and critical exponents are the same as in 1D Ising model ($\nu = 1, \alpha = 1, \eta = 1, \gamma = 1, \mu = 0, \beta = 0, \delta = \infty$).

2.3. Conclusions

In this chapter we used the approach of partition function zeros to analyse universal properties of two different classical spin systems. For the Ising model with dipole interactions we showed that the very nature of critical behaviour depends of the strength of dipole interaction. It is triggered by parameter δ - a ratio of the nearest neighbours ferromagnetic interaction constant to the dipole antiferromagnetic coupling. The phase diagram of the model is characterised by low temperature antiferromagnetic (both checkerboard-like and striped with the width h) and high temperature tetragonal (paramagnetic) phases. We analysed the Fisher zeros

density to obtain specific heat critical exponent α . We showed that in the range $0.89 \leq \delta \leq 1.2$ the phase transition between $h = 1$ striped antiferromagnetic ground state and tetragonal phase is of the second order, with δ -dependent critical exponents. Even though change in δ affects neither space dimensionality nor symmetries, it is shown to define universality class. For larger values the phase transition becomes discontinuous. As we shown at $\delta = 1.3$ transition from $h = 2$ striped phase into the tetragonal one is of first order. This suggests, that tricritical point exists for the marginal value of δ separating $h = 1$ and $h = 2$ striped antiferromagnetic ground states. More about marginal values of model parameters we will discuss in the following chapter.

For the one dimensional Potts model with invisible states we obtain the exact solution. This also allowed for analytical treatment of partition function zeros. Fisher and Lee-Yang zeros were analysed to show that there are two possible ways to shift phase transition to positive temperatures, despite the no-go theorems [118, 120]. The negative amount of invisible states r or complex external field h_2 acting on the invisible subsystem both lead to similar effects. This statement is further supported by the duality relation proving both of these mechanisms to have the same mathematical manifestation. On the other hand, we also show that for any positive r and real magnetic fields the phase transition belongs to the universality class of the one dimensional Ising model. Again, changing r allows to shift the phase transition in one dimension to the physically accessible temperatures. We will expand upon the universal properties of the Potts model with invisible states in the next chapter.

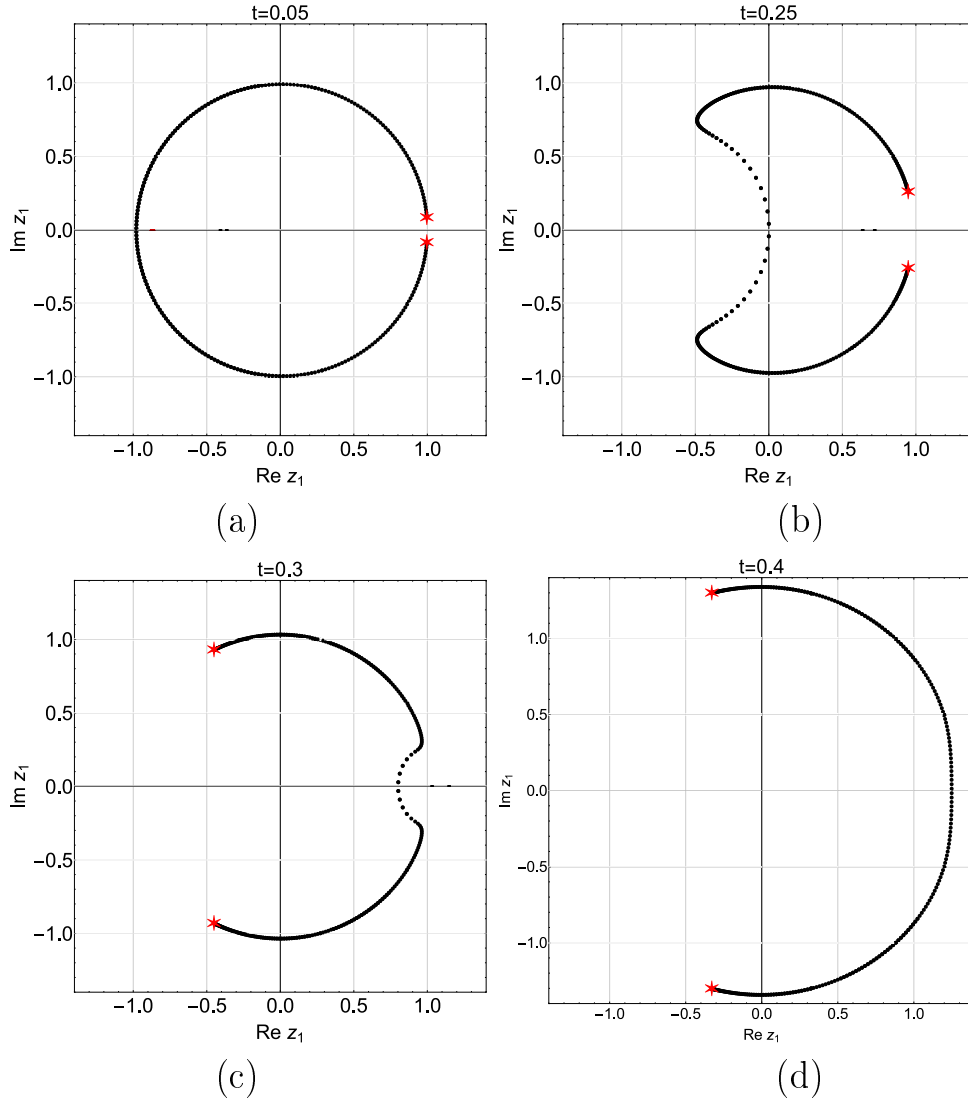


Figure 2.8. Lee-Yang zeros in the complex z_1 -plane for the $(2, 2)$ -state Potts model with $z_2 = -5$ for different temperatures (a) $t = 0.05$, (b) $t = 0.25$, (c) $t = 0.3$ and (d) $t = 0.4$. Large red stars correspond to the edges. Overall behaviour of zeros is similar to that described in the previous subsection.

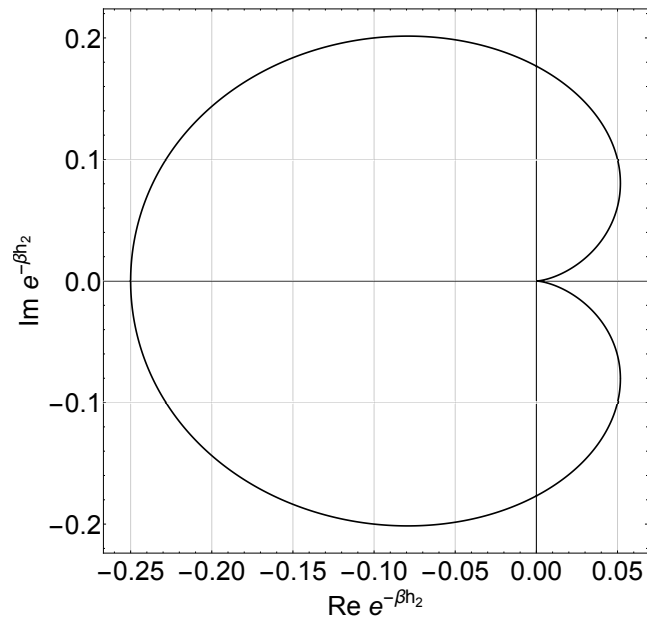


Figure 2.9. Values of $e^{-\beta h_2}$, for which the phase transition in the (2,3)-state Potts model occurs at positive temperature. Each point of the plot corresponds to a certain physically accessible critical temperature.

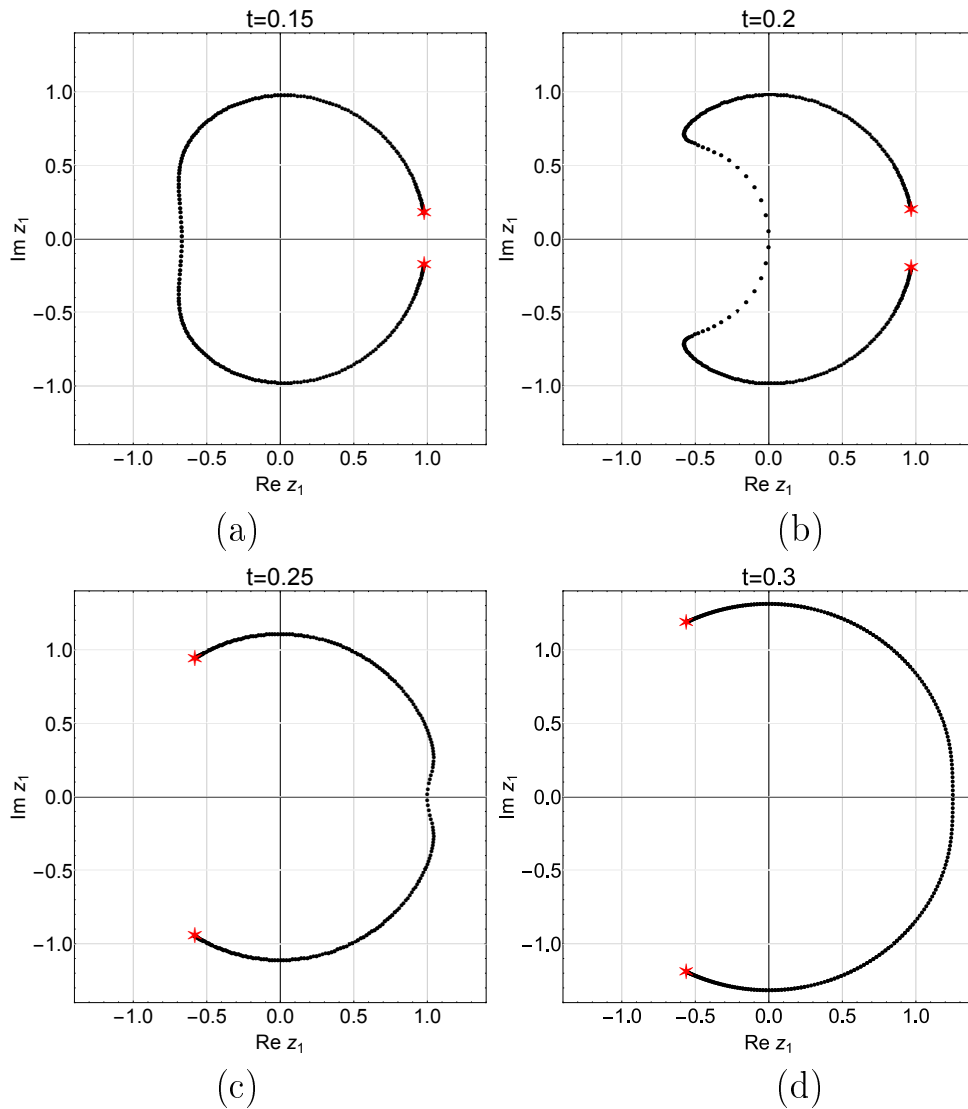


Figure 2.10. Lee-Yang zeros of the $(2, -5)$ -state Potts model at different values of temperature (a) $t = 0.15$, (b) $t = 0.2$, (c) $t = 0.25$, (d) $t = 0.3$ in the complex z_1 -plane for the system size $N = 256$. Panels (a) and (b) illustrate zeros below the zero-field critical temperature $t_c = 0.25$, panel (c) and (d) illustrate zeros at and above t_c . Large red stars show edges and black dots ordinary Lee-Yang zeros. For small temperatures the edge is located in the positive semi plane $\text{Re } z_1 > 0$, while at higher temperature it jumps to the region $\text{Re } z_1 < 0$. This jump occurs below the critical temperature t_c .

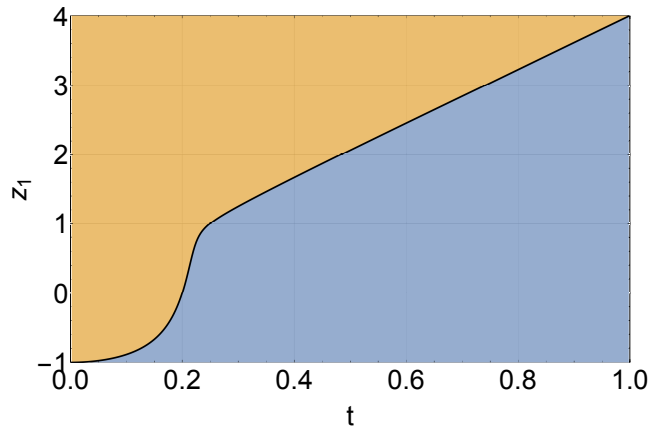


Figure 2.11. Phase diagram of the $(2, -5)$ -state Potts model. (t, z_1) -plane is divided into regions according to the maximal eigenvalue. Values $z_1 < 0$ correspond to the complex values of magnetic field h_1 , while $0 < z_1 < 1$ corresponds to negative values of physical field h_1 .

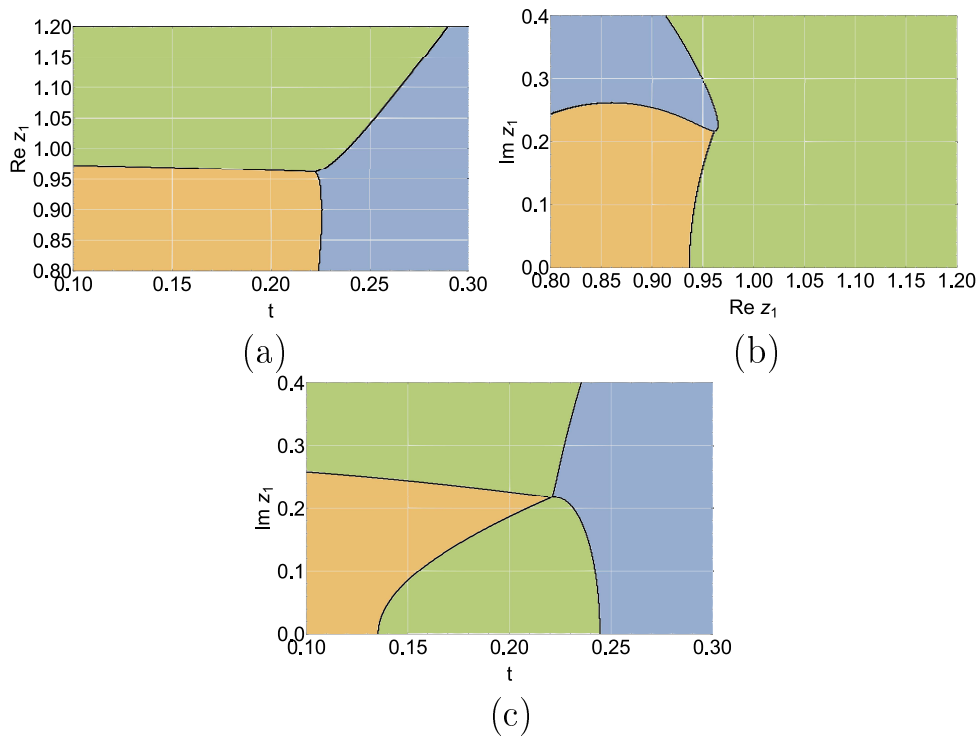


Figure 2.12. Three cross-sections of the 3D phase diagram. Each section is given at the fixed values of parameters when flipping of the edge occurs: (a) - fixed $\text{Im } z_1$, (b) - fixed t , (c) - fixed $\text{Re } z_1$. Colour of the region represent the eigenvalue, which is the largest by modulus inside this region. When three colours meet is the point where flipping of the edge occurs.

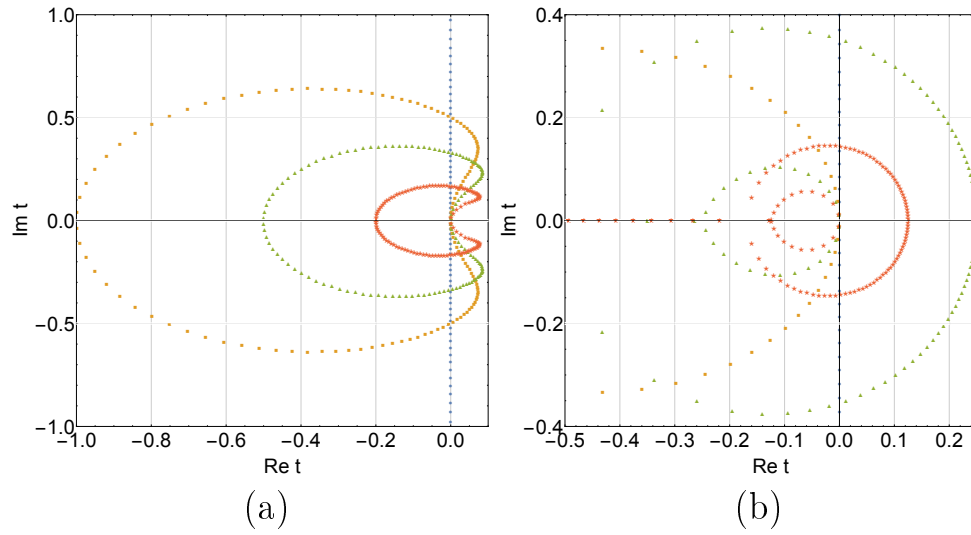


Figure 2.13. Fisher zeros of the $(2, r)$ -state Potts model in $t = y^{-1} = e^{-\beta}$ -plane for system size $N = 128$ with a) $r = 0$ (blue), 1(yellow), 2(green), 5(red) and b) $r = 0$ (blue), -2 (yellow), -5 (green), -7 (red).

CHAPTER 3

UNIVERSAL CRITICAL BEHAVIOUR OF SPIN SYSTEMS ON NETWORKS

In the previous chapter, among other things, we showed that the type of ordering, and hence the universality class, of the Ising model with dipole interaction depends on the value of the relation between the interaction constants δ . There are marginal values of δ that separate the different parts of the phase diagram. In this chapter we are interested in the marginal values of parameters of the Potts model with invisible states. In particular, we consider this model on networks of different topologies. We are interested in a complete graph and a scale-free network. Euclidean dimensionality is ill-defined for a graph, therefore the principle of universality in these two cases requires generalization. For both these types of networks, the effect of invisible states on critical behaviour will be analysed and the existence of two marginal values of the number of invisible states r_{c1} and r_{c2} that divide the regions with different criticality is shown. The main results of this chapter are outlined in [22, 23].

3.1. Potts model with invisible states on a graph. Mean field approximation.

The question of the marginal dimensionality of the Potts model with invisible states is one of the central issues discussed within the context of this model. In this section we address this question for the model on a graph described by adjacency matrix \mathbf{A} : with matrix elements $A_{ij} = 1$ if there is an edge between nodes i and j , $A_{ij} = 0$ - otherwise. A_{ij} is symmetric matrix of size $N \times N$, where N is the number

of nodes in the network.

The Hamiltonian of the $(q+r)$ -state Potts model with r invisible states reads [74] (see also Eq. 2.4)

$$\mathcal{H} = - \sum_{\langle i,j \rangle} J_{ij} \sum_{\alpha=1}^q \delta_{S_i,\alpha} \delta_{\alpha,S_j} - h \sum_i \delta_{S_i,1}, \quad (3.1)$$

where, $J_{ij} = JA_{ij}$ is coupling matrix with a coupling constant $J > 0$, $S_i = 1, \dots, q, (q+1), \dots, (q+r)$ is a Potts spin variable on a site $i = 1, \dots, N$, $\delta_{a,b}$ are Kronecker deltas and h is a magnetic field acting on the first visible state. The first sum in the first term spans all distinct pairs of spins. Only states with $S_i = 1, \dots, q$ contribute to the interaction term in the Hamiltonian. The remaining r states do not contribute to the interaction energy but they increase the number of configurations available, and hence they contribute to the entropy (as well as to the free energy).

To proceed with the mean-field analysis, let us introduce local thermodynamic averages on a given node i :

$$\langle \delta_{S_i,\alpha} \rangle = \begin{cases} \mu_i, & \alpha = 1, \\ \nu_{1i}, & \alpha = 2, \dots, q, \\ \nu_{2i}, & \alpha = q+1, \dots, r. \end{cases} \quad (3.2)$$

Here, the averaging is performed with respect to the Hamiltonian (3.1)

$$\langle \dots \rangle = \frac{1}{\mathcal{Z}} \text{Tr} (\dots) e^{-\beta \mathcal{H}}, \quad \text{with} \quad \mathcal{Z} = \text{Tr} e^{-\beta \mathcal{H}}, \quad (3.3)$$

where β is the inverse temperature and the trace is taken over all possible spin configurations.

Note, that three different averages μ_i , ν_{1i} , and ν_{2i} are necessary to take into account the state favoured by the magnetic field and to discriminate between visible and invisible states. Their high- and low- temperature asymptotics are given in Table 3.1. At high temperatures all states are equally probable, whereas at low temperatures the direction of symmetry breaking is determined by the direction of the magnetic field.

This asymptotic behaviour together with an obvious normalization condition:

$$\mu_i + (q - 1)\nu_{1i} + r\nu_{2i} = 1 \quad (3.4)$$

allows one to define the local order parameters:

$$\begin{aligned} m_{1i} &= \mu_i - \nu_{1i}, \\ m_{2i} &= \mu_i - \nu_{2i}. \end{aligned} \quad (3.5)$$

Both m_{1i} and m_{2i} exhibit standard temperature asymptotics in that they vanish for $\beta \rightarrow 0$ and are equal to one for $\beta \rightarrow \infty$, see Table 3.1. It is easy to show that also the following conditions are satisfied:

$$\begin{aligned} \mu_i &= \frac{m_{2i}r + m_{1i}q + 1 - m_{1i}}{q + r}, \\ \nu_{1i} &= \frac{(m_{2i} - m_{1i})r + 1 - m_{1i}}{q + r}, \\ \nu_{2i} &= \frac{(m_{1i} - m_{2i})q + 1 - m_{1i}}{q + r}. \end{aligned} \quad (3.6)$$

To obtain the mean-field Hamiltonian, we represent each Kronecker-delta term as a sum of its mean value and deviation from that mean. Neglecting terms comprising a product of two such deviations,

$$\mathcal{H} = - \sum_{\langle i,j \rangle} J_{ij} [\mu_i(2\delta_{1,S_j} - \mu_j) + \sum_{\alpha=2}^q (2\delta_{\alpha,S_i} - \nu_{1i})\nu_{1j}] - h \sum_i \delta_{S_i,1}. \quad (3.7)$$

For the partition function (3.3) we then get

$$\mathcal{Z} = \prod_{i=1}^N e^{\beta \sum_j J_{ij} (\mu_i \mu_j + (q-1)\nu_{1i}\nu_{1j})} \left(e^{\beta(h+2 \sum_j J_{ij} \mu_j)} + (q-1)e^{2\beta \sum_j J_{ij} \nu_{1j}} + r \right). \quad (3.8)$$

Table 3.1. Low and high temperature asymptotics of the thermodynamic averages, Eq. (3.2), and for the order parameters, Eq. (3.5).

| | | | | | |
|----------------------------|-------------------------|----------------------------|----------------------------|-----------|-----------|
| $\beta \rightarrow \infty$ | $\mu_i = 1$ | $\nu_{1i} = 0$ | $\nu_{2i} = 0$ | $m_1 = 1$ | $m_2 = 1$ |
| $\beta \rightarrow 0$ | $\mu_i = \frac{1}{q+r}$ | $\nu_{1i} = \frac{1}{q+r}$ | $\nu_{2i} = \frac{1}{q+r}$ | $m_1 = 0$ | $m_2 = 0$ |

We consequently derive the free energy as

$$F = \sum_{\langle i,j \rangle} J_{ij}(\mu_i \mu_j + (q-1)\nu_{1i}\nu_{1j}) - \frac{1}{\beta} \sum_i \ln \left(e^{\beta(h+2\sum_j J_{ij}\mu_j)} + (q-1)e^{2\beta\sum_j J_{ij}\nu_{1j}} + r \right) \quad (3.9)$$

In the spirit of the mean-field approximation, we assume that the coupling matrix is proportional to the probability of two vertices to be connected

$$J_{ij} = \frac{Jk_i k_j}{N\bar{k}}, \quad (3.10)$$

where k_i and k_j are degrees of nodes i and j correspondingly and $\bar{k} = \frac{\sum_i k_i}{N}$ is the average node degree over the network.

As for the next step we introduce global weighted order parameters m_1 and m_2 according to the rules

$$m_1 = \frac{\sum_i k_i m_{1i}}{\sum_i k_i}, \quad m_2 = \frac{\sum_i k_i m_{2i}}{\sum_i k_i}. \quad (3.11)$$

In terms of global order parameters free energy is the following

$$F(m_1, m_2) = \frac{JN\bar{k}}{(q+r)^2} \left((rm_2 + 1 + (q-1)m_1)^2 + (q-1)(rm_2 + 1 - (r+1)m_1)^2 \right) - \frac{1}{\beta} \sum_i \ln \left(e^{\beta(h + \frac{k_i J}{q+r}(m_1(q-1)+1+rm_2))} + (q-1)e^{\frac{\beta J k_i}{q+r}(m_2 r + 1 - (r+1)m_1)} + r \right). \quad (3.12)$$

In the thermodynamic limit, when the size of the network grows to infinity $N \rightarrow \infty$, summation over node degree transforms into integration

$$\frac{F(m_1, m_2)}{N} = \frac{J\bar{k}}{(q+r)^2} \left((rm_2 + 1 + (q-1)m_1)^2 + (q-1)(rm_2 + 1 - (r+1)m_1)^2 \right) - \frac{1}{\beta} \int_2^\infty dk P(k) \ln \left(e^{\beta(h + \frac{k J}{q+r}(m_1(q-1)+1+rm_2))} + (q-1)e^{\frac{\beta J k}{q+r}(m_2 r + 1 - (r+1)m_1)} + r \right). \quad (3.13)$$

In Eq. (3.13) we introduced vertex degree distribution function $P(k)$. We have also set the lower integration boundary to $k_{min} = 2$. This is necessary and sufficient condition for the network to have a giant connected component [169]. From now and onward we will set $J = 1$ as an energy measurement scale. In the following two Sections we will apply this general result for two cases: complete graph, which is described by δ -function degree distribution exponent, and scale-free network with power-law distribution of node degree.

3.2. Marginal dimensions of the Potts model with invisible states on a complete graph

Here we consider Potts model with invisible states on a complete graph. To do so in Eq. (3.12) we substitute degree distribution function with $P(k) = \delta(k - z)$, where z is the number of nearest neighbours of each spin and $\delta(x)$ is Dirac δ -function. With this substitution free energy per spin reads

$$\begin{aligned} \frac{F(m_1, m_2)}{N} = & \frac{z}{2} \left(\frac{(m_1 q - m_1 + m_2 r + 1)^2}{(q + r)^2} + \right. \\ & \left. \frac{(q - 1)(-m_1 r - m_1 + m_2 r + 1)^2}{(q + r)^2} \right) - \\ & \frac{1}{\beta} \log \left\{ \left(\exp \left[\beta \left(h + \frac{z(m_1 q - m_1 + m_2 r + 1)}{q + r} \right) \right] + \right. \right. \\ & \left. \left. (q - 1) \exp \left[\frac{\beta z(-m_1 r - m_1 + m_2 r + 1)}{q + r} \right] + r \right) \right\}. \quad (3.14) \end{aligned}$$

For $r = 0$ one recovers the free energy of the standard Potts model as a function of a single order parameter m_1 in the mean-field approximation. Of course, m_2 does not arise in the standard Potts model. There the transition is of second order only if $q \leq 2$. In the following, we are interested how the presence of invisible states changes the order of this transition.

With the expression (3.14) to hand, the thermodynamics of the model are obtained via minimization of the free energy with respect to the two parameters

m_1 and m_2 . In particular, the system of equations that determines the free energy extrema, $\partial f/\partial m_1 = \partial f/\partial m_2 = 0$, reads

$$\frac{(q+r) [e^{\beta(h+m_1z)} - r - 1]}{e^{\beta(h+m_1z)} + r e^{\frac{\beta z(m_1r+m_1-m_2r-1)}{q+r}} + q - 1} = m_1[q + r(r+2)] - r(m_2r + 1), \quad (3.15)$$

$$\frac{(q+r) [e^{\beta(h+m_1z)} + q - 1]}{e^{\beta(h+m_1z)} + r e^{\frac{\beta z(m_1r+m_1-m_2r-1)}{q+r}} + q - 1} = -m_1r(q-1) + m_2qr + q. \quad (3.16)$$

The solutions of these equations, $m_1(T, h)$, $m_2(T, h)$ are further analysed to ensure they meet the condition of stability, i.e that they correspond to the free energy minimum, or to local minima in the case of a first-order transition. From these considerations, and numerically solving the system of non-linear equations (3.15), (3.16), we find two types of solutions at zero external magnetic field and finite temperature, namely (i) $m_1(T, 0) = 0$, $m_2(T, 0) \neq 0$ and (ii) $m_1(T, 0) \neq 0$, $m_2(T, 0) \neq 0$. Note that $m_2(T, 0)$ never vanishes at finite temperature. Therefore only $m_1(T, 0)$ is a proper order parameter, delivering a spontaneous magnetization that signals the occurrence of a phase transition. For fixed q , the transition from solution (i) to (ii) occurs at a finite r -dependent temperature $T_c(r)$.

3.2.1. The case $q = 2$

First let us consider the extension of the Ising model with invisible states. Refs. [74, 77, 79] determined that $3 < r_c < 4$ for the mean-field version of the model, valid above the upper critical dimension. Our objective here is to deliver a more precise estimate for r_c in this case. In Fig. 3.1 we plot the transition temperature for $q = 2$ as a function of r for $z = 4$. The critical temperature is a smooth function of r and tends to zero as $r \rightarrow \infty$. In this limit the system becomes one of non-interacting particles. Note that for the 2D Potts model with invisible states on a square lattice T_c vanishes for large $(q+r)$ as $T_c \approx 2/\ln(q+r)$ [81].

As has been shown in [74], $r = 4$ invisible states are sufficient to change the phase transition of the $q = 2$ Potts model from second to first order. This sets an upper bound for the marginal dimension as $r_c(q = 2) < 4$. We display

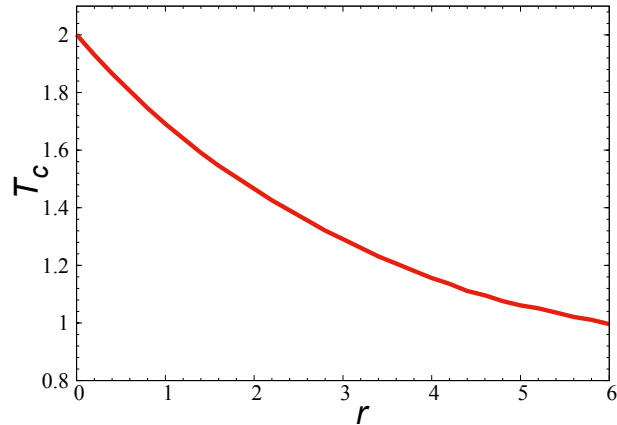


Figure 3.1. Critical temperature of the Potts model for $q = 2$, $z = 4$ as a function of the number of invisible states r . The critical temperature is a smooth function of r and tends to zero as $r \rightarrow \infty$.

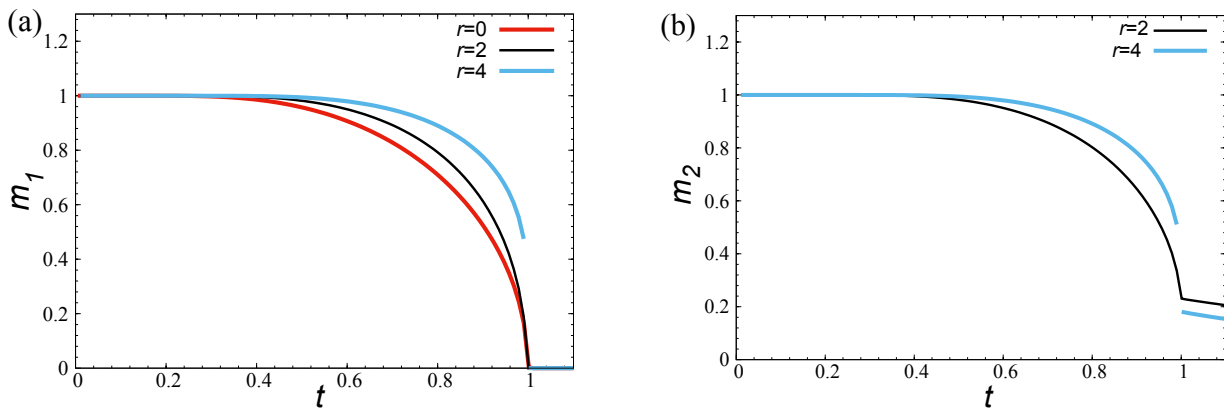


Figure 3.2. The dependency of the order parameters m_1 [Panel (a)] and m_2 [Panel (b)] on the reduced temperature $t = T/T_c$ for $r = 0, 2, 4$. For $r = 0$, we only have a single order parameter, namely m_1 . Indeed, $m_1(t)$ is a proper order parameter in that it vanishes on one side of the phase transition. In contrast, $m_2(t)$ never vanishes at finite temperature. However both m_1 and m_2 can be used to distinguish between the first and the second-order regimes as the plots demonstrate.

the temperature dependence of the order parameters in Fig. 3.2 for $r = 0, 2, 4$. Since T_c is r -dependent we use the reduced temperature $t = T/T_c$. As we have noted before, one only has $m_1(T)$ for $r = 0$. Depending on the value of r , the temperature dependency of both order parameters m_1 , m_2 is characterized by two different regimes. For $r = 0, 2$ the plots are continuous, signalling second-order phase transitions. However when $r = 4$ we observe a jump at the critical temperature. Note that both m_1 and m_2 may be used to distinguish between the first and the

second order regimes. However, it is worth re-emphasising that above the critical temperature $m_1(t) = 0$, while $m_2(t)$ vanishes only for the infinite temperature.

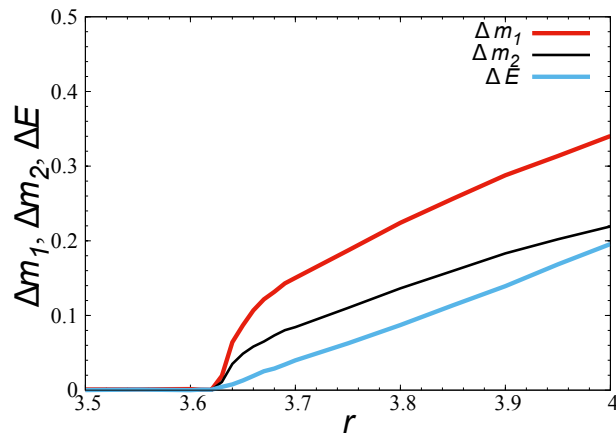


Figure 3.3. Jumps in the order parameters Δm_1 (red curve), Δm_2 (black curve) and the latent heat ΔE (blue curve) of the Potts model at $q = 2$ as functions of the number of invisible states r .

To locate the marginal value r_c , we define the jump in the order parameters by

$$\Delta m_j = \lim_{t \rightarrow 1^-} m_j(t) - \lim_{t \rightarrow 1^+} m_j(t), \quad j = 1, 2, \quad (3.17)$$

and analyse the behaviour of Δm_j as function of r . The first appearance of a non-zero value of Δm_j corresponds to the onset of the first-order phase transition. In Fig. 3.3 we plot Δm_1 and Δm_2 as functions of the number of invisible states r . Similar behaviour is observed for the latent heat $\Delta E = -\Delta S T_c$, where ΔS is the entropy jump at the phase transition point:

$$\Delta S = \lim_{t \rightarrow 1^-} S(t) - \lim_{t \rightarrow 1^+} S(t). \quad (3.18)$$

This is also plotted in Fig. 3.3. The values of r_c obtained from the vanishing of Δm_1 , Δm_2 , and ΔE are: $r_c = 3.629(1)$, $r_c = 3.627(2)$, and $r_c = 3.617(3)$, respectively. Averaging these values we get $r_c = 3.622(8)$. This estimate agrees well with the $z \rightarrow \infty$ limit of the result obtained for the Potts model with $q = 2$ visible and r invisible states on the Bethe lattice with z nearest neighbours [80]:

$$r_c = \lim_{z \rightarrow \infty} \frac{4z}{3(z-1)} \left(\frac{z-1}{z-2} \right)^2 \simeq 3.62.$$

In the vicinity of r_c , the order parameter jumps can be approximated by a power-law decay:

$$\Delta m_1 \sim (r - r_c)^{a_1}, \quad \Delta m_2 \sim (r - r_c)^{a_2}. \quad (3.19)$$

Numerical fits in the interval $r = 3.625$ to 4.0 yield estimates for the exponents: $a_1 = 0.477(10)$ and $a_2 = 0.566(15)$.

3.2.2. The case $1 \leq q < 2$

In Ref. [170], Qian *et al.* gave the fixed-points parameters of the tricritical and critical dilute Potts models in two dimensions for a range of q values. Our objective here is to do likewise for the mean-field model in the region $1 \leq q < 2$. As stated, mean-field theory provides an accurate description above the upper critical dimension which may be physically accessed when the interactions are long range. As a byproduct, we will observe a new phase transition at $t < t_c = 1$ and a new mechanism for the crossover from second to first order at $t_c = 1$.

Typical behaviour of the order parameters $m_1(t)$ and $m_2(t)$ for fixed values of q is shown in Fig. 3.4. There we plot these functions for $q = 1.2$ and $r = 4, 5, 6, 7, 8, 9$. For small values of r , $m_1(t)$ and $m_2(t)$ are smooth functions of t and the transition is second order. We observe that $m_1(t)$ vanishes linearly as t approaches $t_c = 1$ from below. This corresponds to the familiar mean-field result for the percolation critical exponent $\beta = 1$.

For larger values of r , and starting from a certain value $r = r_{c1}$, gaps in $m_1(t)$ and $m_2(t)$ appear at $\tilde{t} < t_c$. The marginal dimension r_{c1} obtained from the vanishing of these functions is $r_{c1} \simeq 6.834(11)$. The occurrence of this gap indicates a new, first-order phase transition, however it does not affect the order of the phase transition occurring at $t_c = 1$, which, for these values of r , remains second order because the order parameters remain continuous there. The gap at \tilde{t} increases with further increases of r and finally, at $r = r_{c2}$, \tilde{t} and t_c coincide. It is at this point that the transition at $t_c = 1$ becomes first order. The value r_{c2} is therefore the marginal

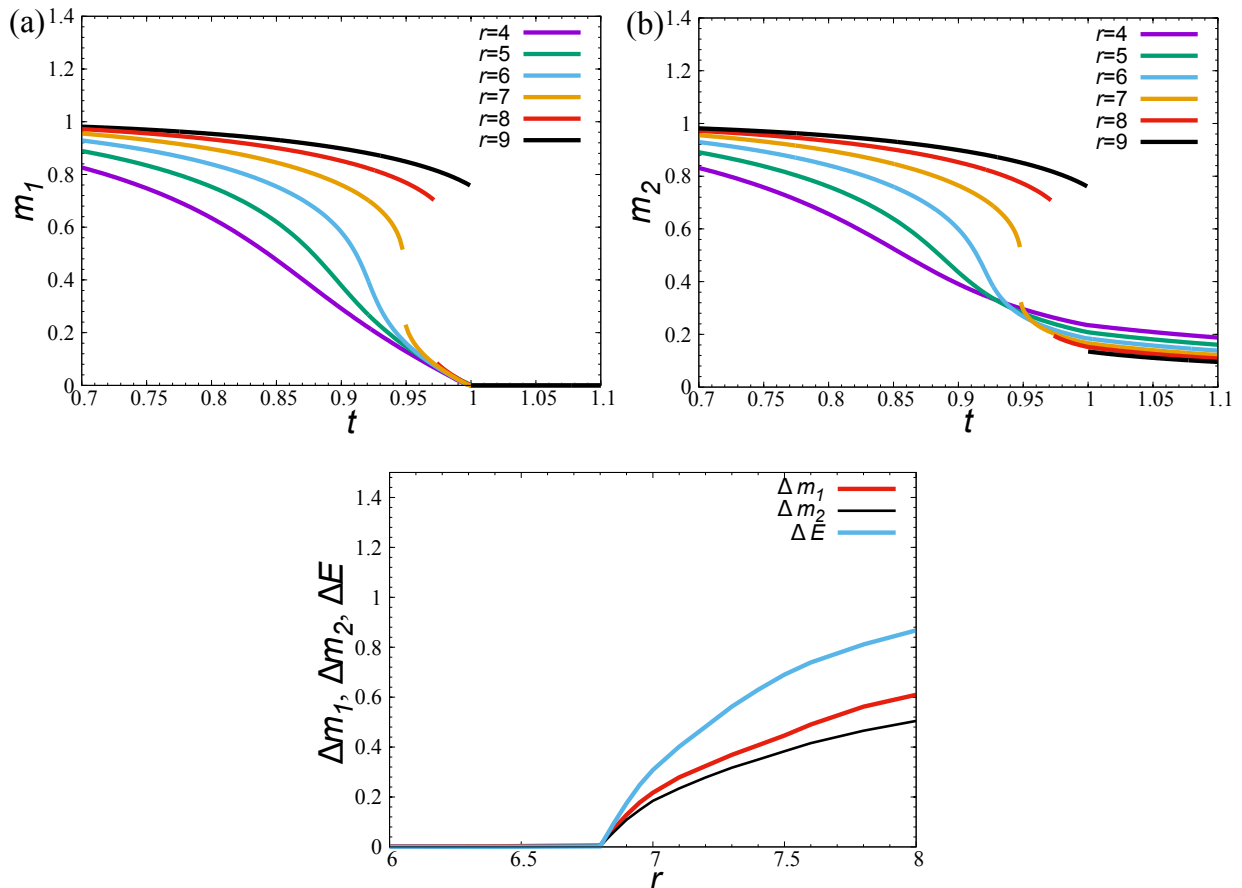


Figure 3.4. Dependencies of the first (a) and second (b) order parameters on the reduced temperature t for $r = 4, 5, 6, 7, 8, 9$ at $q = 1.2$. The second-order phase transition transforms into a first order phase transition at the value of r defined by the Eq. (3.20). Numerically solving this equation at $q = 1.2$ we get $r_{c2} \simeq 8.495(5)$. Panel (c): discontinuities in the order parameter Δm_1 (red curve), Δm_2 (black curve) and the latent heat ΔE (blue curve) as functions of r for $q = 1.2$ at $t = \tilde{t}$.

dimension (i.e., it is the value of r at which the phase transition changes its order). It is defined by the condition

$$\Delta m_1 > 0 \quad \text{at} \quad m_1(t \rightarrow t_c^+) = 0. \quad (3.20)$$

The occurrence of a gap in the order parameter at temperature $\tilde{t} < t_c$ is, to our knowledge, a new phenomenon in the theory of phase transitions.

For $r_{c1} < r < r_{c2}$, the order parameter $m_1 \neq 0$ in the temperature interval $\tilde{t} < t < t_c$. There is no new spontaneous symmetry breaking with respect to m_1 at $t = \tilde{t}$. However, its jump at $t = \tilde{t}$ is similar to that which occurs in the usual

first-order phase transition scenario. Similar behaviour is observed at $t = \tilde{t}$ for the latent heat ΔE and for Δm_2 . These functions are shown in Figs. 3.4c too.

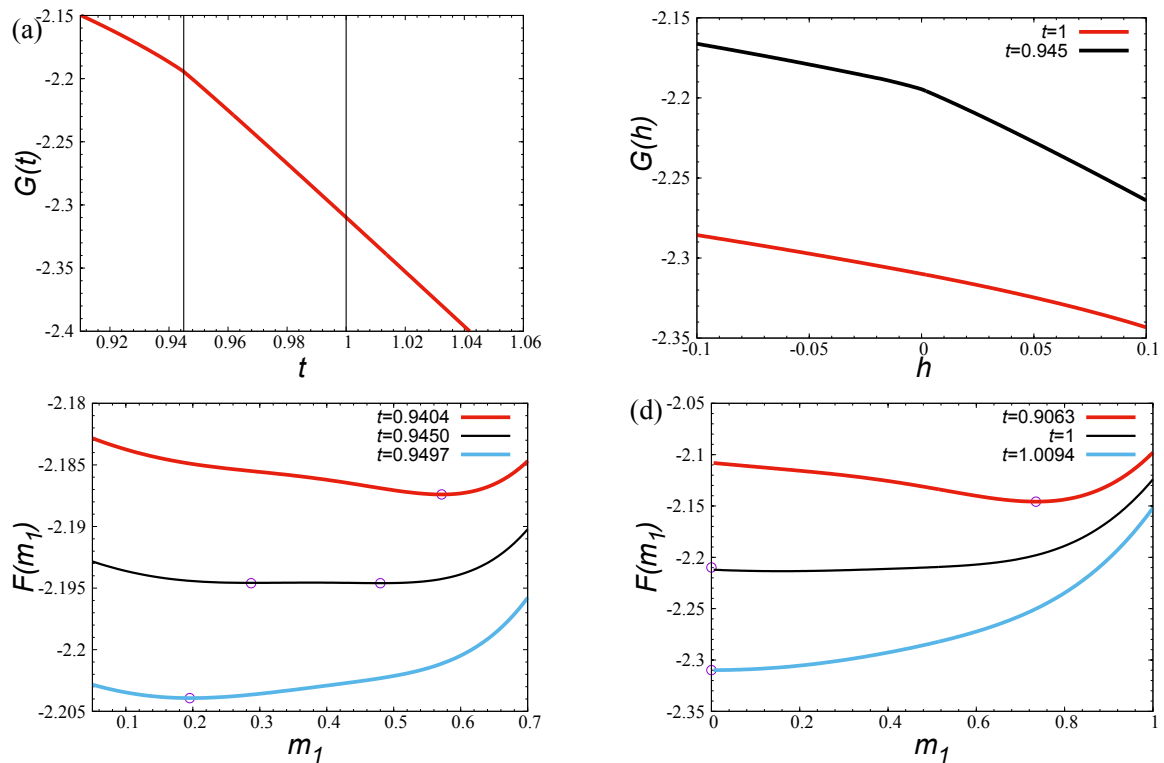


Figure 3.5. Typical behaviour of the free energy of the Potts model with invisible states at $1 \leq q < 2$ and $r_{c1} < r < r_{c2}$ ($q = 1.2$ and $r = 6.96$ for this figure); (a): Gibbs free energy $G(t)$ at $h = 0$. Temperatures \tilde{t} and t_c are shown by vertical lines. One sees a bend at \tilde{t} , it signals about the presence of a latent heat (a jump in the entropy at \tilde{t}); (b): Gibbs free energy $G(h)$ at $t = \tilde{t}$ (upper curve) and at $t = t_c$ (lower curve). A bend in the upper curve signals about a jump in the order parameter at \tilde{t} . Note that the bend is absent in lower curve: the order parameter is continuous at t_c ; (c): Mean-field free energy $F(m_1)$ at $h = 0$ and $t < \tilde{t}$, $t \simeq \tilde{t} = 0.945$, $t > \tilde{t}$ (upper, middle, and lower curves, correspondingly); (d): Mean-field free energy $F(m_1)$ at $h = 0$ and $t < t_c$, $t = t_c = 1$, $t > t_c$. The circles in Figs. (c) and (d) show global minima of the free energy.

The behaviour of the Gibbs free energy $G(t, h)$ of the Potts model with invisible states in the region $1 \leq q < 2$ and $r_{c1} < r < r_{c2}$ is elucidated in Figs. 3.5 a, b. To this end, we used conditions (3.15), (3.16) to eliminate the order-parameter

dependency of the mean-field free energy (3.14) in favour of the external field:

$$G(t, h) = f(m_1, m_2)|_{m_1^*, m_2^*}, \quad (3.21)$$

where m_1^*, m_2^* denote the coordinates of $f(m_1, m_2)$ minimum. In Fig. 3.5a we display the zero-field Gibbs free energy $G(t, h = 0)$ as a function of the reduced temperature t . The at $t = \tilde{t}$ signals the jump in the entropy, hence a first order transition. Fig. 3.5b shows the Gibbs free energy $G(h)$ at $t = \tilde{t}$ (upper curve) and at $t = t_c$ (lower curve). Again, a bend in the upper curve signals a jump in the order parameter at \tilde{t} . However, the bend is absent in the lower curve: the order parameter is continuous at t_c . The mean-field free energy $f(m_1, m_2)$ is further analysed in Figs. 3.5c, d. There we show the typical behaviour of the free energy as a function of the first-order parameter m_1 at $h = 0$ in the region of temperatures in the vicinity of $t = \tilde{t}$ (c), where the order parameter jumps between two non-zero values (characterising ordered phases), and $t = t_c$ (d). To get two-dimensional plots, parameter $m_2 = m_2(m_1)$ has been excluded from the minimum conditions (3.15), (3.16), and then substituted into $f(m_1, m_2)$:

$$F(m_1) = f(m_1, m_2(m_1)). \quad (3.22)$$

Fig. 3.5(c) demonstrates behaviour typical for the first-order phase transition: two minima exist at $t = \tilde{t} = 0.945$, see the middle curve of the figure. Different situation is observed in Fig. (d). There, the only value $m_1 = 0$ corresponds to the free energy minimum at $t = t_c = 1$.

To better understand temperature behaviour of the order parameters in the vicinity of \tilde{t} , we present, in Fig. 3.6 typical plots of the isothermal susceptibilities $\chi_1 = \partial m_1 / \partial h$ and $\chi_2 = \partial m_2 / \partial h$ for $1 < q < 2$ and $r_{c1} < r < r_{c2}$ (specifically, $q = 1.2$ and $r = 6.96$ in this figure). One observes two distinct peaks located at \tilde{t} and t_c . The values of the susceptibilities were obtained by numerical evaluation of derivatives in the limit $h \rightarrow 0$.

Values of the marginal dimensions r_{c1} and r_{c2} for different q are collected in Table 3.2. We give the average value of r_{c1} obtained numerically from the behaviour

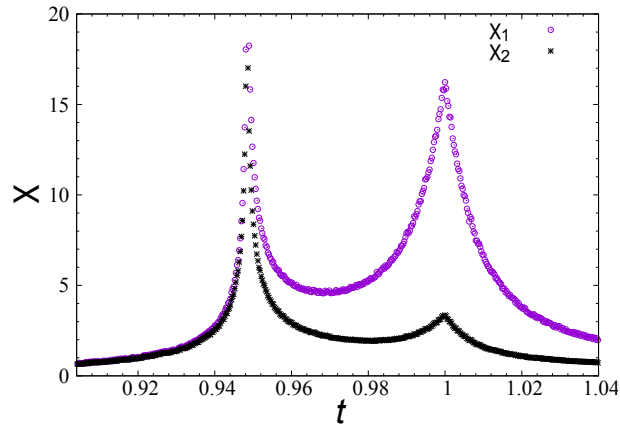


Figure 3.6. Typical behaviour of the isothermal susceptibilities χ_1 and χ_2 as functions of reduced temperature for $1 < q < 2$, $r_{c1} < r < r_{c2}$ ($q = 1.2$ and $r = 6.96$ in this figure). Distinct peaks are observed at \tilde{t} and t_c .

Table 3.2. Marginal dimensions r_{c1} , r_{c2} for different values of $1 \leq q \leq 2$.

| q | r_{c1} | r_{c2} |
|-----|-----------|----------|
| 1 | 7.334(49) | 9.55(35) |
| 1.1 | 7.132(7) | 8.995(5) |
| 1.2 | 6.834(11) | 8.495(5) |
| 1.3 | 6.577(5) | 8.025(5) |
| 1.4 | 6.268(9) | 7.535(5) |
| 1.5 | 5.980(6) | 7.025(5) |
| 1.6 | 5.658(7) | 6.525(5) |
| 1.7 | 5.315(5) | 6.025(5) |
| 1.8 | 4.914(8) | 5.505(5) |
| 1.9 | 4.447(9) | 4.825(5) |
| 2 | 3.622(8) | 3.65(5) |

of the functions Δm_1 , Δm_2 , and ΔE . The estimate for r_{c2} has been obtained from the behaviour of m_1 as the minimal value of r for which condition (3.20) holds. Fig. 3.7 shows the q -dependencies of r_{c1} and r_{c2} . For the case $q = 2$, where both marginal dimensions r_{c1} and r_{c2} have to coincide, we use the estimate $r_c = 3.65(5)$ since it includes both values quoted in the table. It is worth noting, that in the region $1 \leq q \leq 2$ the difference in the marginal dimensions is nicely approximated by a linear function: $r_{c2} - r_{c1} \simeq 2(2 - q)$, although we do not yet have a simple explanation for this observation.

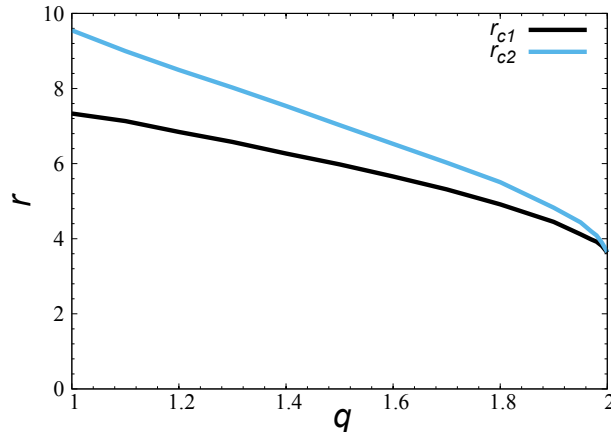


Figure 3.7. Marginal dimensions r_{c1} (lower curve) and r_{c2} (upper curve) for the Potts model at $1 \leq q \leq 2$. At $q = 2$ both r_{c1} and r_{c2} coincide within the fidelity interval: $r_{c1} = r_{c2} \simeq 3.65(5)$.

In the limiting case $q \rightarrow 1$, Eq. (3.14) gives the free energy that depends on the second-order parameter m_2 only:

$$\lim_{q \rightarrow 1} f(m_1, m_2) = \frac{z(m_2 r + 1)^2}{2(r + 1)^2} - T \log \left(e^{\frac{h + \frac{z(m_2 r + 1)}{r + 1}}{T}} + r \right). \quad (3.23)$$

Minimizing the free energy with respect to m_2 one gets the temperature behaviour $m_2(T)$. In turn, the appearance of a gap in this dependence can be used as a condition to determine the marginal dimension $r = r_{c1}$. We estimate numerically the marginal dimension r_{c2} from the limit $\lim_{q \rightarrow 1^+} r_{c2}(q)$.

3.3. Ising model with invisible states on scale-free networks.

In this Section we consider Ising model with invisible states on a scale-free network. This problem is of special interest from two points of view. On one side, scale-free networks, as an environment provide with opportunity to examine how topology affects phase transition. On the other side, invisible states have their effect on the criticality through changing entropy of the system. Thus combining this two mechanisms allows to study within the unique approach an interplay of different forms of disorder: one arising from the number of configurations of the internal degrees of freedom (number of invisible states r) and another one arising

from structural inhomogeneities 'hubs' (node degree distribution exponent λ).

To proceed further we substitute in Eq. (3.12) degree distribution function with power-law $P(k) = \frac{C}{k^\lambda}$, where $C = 2^{\lambda-1}(\lambda - 1)$ is normalisation constant and $q = 2$. This leads to the expression for the free energy:

$$f(m_1, m_2) = \frac{\bar{k}}{(2+r)^2} \left((rm_2 + 1 + m_1)^2 + (rm_2 + 1 - (r+1)m_1)^2 \right) - \frac{2^{\lambda-1}}{\beta} \int_2^\infty \frac{dk}{k^\lambda} \ln \left(e^{\beta(h + \frac{kJ}{2+r}(m_1+1+rm_2))} + e^{\frac{\beta Jk}{2+r}(m_2r+1-(r+1)m_1)} + r \right), \quad (3.24)$$

with average node degree $\bar{k} = \frac{2(\lambda-1)}{\lambda-2}$.

Eq. (3.24) gives free energy as a function of two order parameters m_1 and m_2 with a set of parameters q, r, β, λ . Usually in such a case, the next step is to present the free energy as a power series over order parameters (Landau free energy). In our case two order parameters make this expansion too cumbersome for a direct analytic treatment, thus we switch to numerical analysis of the free energy. For this purpose we adopt simplex method [171]. Its' advantage is that it does not require to know the derivatives of the function and only needs a way to evaluate it. With this numerical technique at hand in the following Section we proceed according to the plan: for fixed values of q, r and λ we sweep through a certain region of temperatures and calculate the values of m_1 and m_2 which minimise the free energy; based on the temperature behaviour of order parameters we can make conclusions about the order of the phase transition, critical temperature and critical exponents.

3.3.1. Critical behaviour

In this section we will investigate the Ising model $q = 2$ with an arbitrary number of invisible states r near the spontaneous phase transition point ($h = 0$) on a scale-free network. All our results we will compare with the analytic results known in the limit $r = 0$ [110–112]. This particular case of the Ising model on a scale-free

network hereafter is called the genuine Ising model. We will mostly be interested in the region $3 \leq \lambda \leq 5$, where λ dependent critical exponents were observed

For the invisible states Ising model on a scale-free network, one would expect that node degree distribution exponent has similar effect as for the genuine Ising model. Indeed, our analysis supports this conjecture. In particular, for low values of $\lambda \leq 3$ the system remains ordered at any finite temperature. However, region $\lambda \geq 3$ appears to exhibit some not-trivial features we will discuss in more details below.

Let us start with analysis of the critical temperature T_c . As critical we will define the temperature, at which the first order parameter m_1 vanishes. Earlier it was shown, that on a complete graph m_2 vanishes only at infinite temperature, thus only the first order parameter can be used to determine the order of the phase transitions and the critical temperature.

In Fig. 3.8 critical temperature of the Ising model with invisible states on a scale free network is given as a function of λ for various numbers of invisible states r ranging from 0 to 60. Critical temperatures obtained with our numerical technique are in a good agreement with analytical results for genuine Ising model (see upper solid and dashed line in Fig. 3.8) [110].

Another conclusion, that one can make based on the plot, is that critical temperature decreases with an increase of λ . When λ decreases below the marginal value $\lambda = 3$, no finite temperature can break spontaneous ordering: the system remains ordered at any T . This reflects the fact, that for small λ there are many nodes with high degree (hubs), making the network strongly connected. Taking this into account, in the limit $\lambda \rightarrow 3 + 0$, critical temperature rises to $T_c \rightarrow \infty$.

On the other hand, from Fig. 3.8 one can also say, that the critical temperature decreases with an increase in the number of invisible states. This is because r regulates the entropy of the system, meaning larger r - larger entropy, which leads to easier breaking of ordering. Limit $r \rightarrow \infty$ will reproduce results for non-interacting system, i.e. $T_c = 0$ [22].

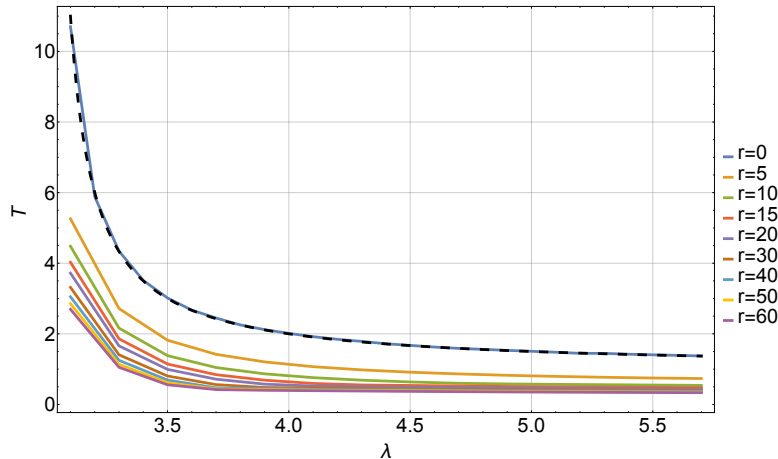


Figure 3.8. Critical temperature of the Ising model with invisible states on a scale free network as a function of the degree distribution exponent λ for different values of r : $r = 0, 5, 10, 15, 20, 30, 40, 50, 60$ going down the plot. Dashed line represents analytical results for the genuine Ising case [110–112].

The next step is to analyse the order parameters behaviour. Continuous phase transitions are described by continuous dependencies of order parameters on temperature. Alternatively, if function $m_1(T)$ has a gap, this signals that there is a jump between two different states of the system, which we will associate with the first order phase transition. As an example, in Fig. 3.9 we present order parameter dependencies on reduced temperature $\tau = T/T_c$ for fixed value $\lambda = 3.8$ and various values of r . Hereafter we are using the value $\lambda = 3.8$ to illustrate typical properties of the system, which remain qualitatively the same throughout the region $3 < \lambda < 5$.

Qualitatively similar behaviour is observed in the whole region $3 < \lambda < 5$. It is worth noting, that in case $r = 0$ there is only one order parameter, as in the genuine Ising model. As one can see from these plots, m_2 does not vanish at criticality and slowly decays as temperature is rising. The same behaviour was observed on the complete graph [22].

The system undergoes the second order phase transition for small amounts of invisible states. On the contrary, large numbers of invisible states make the phase transition discontinuous. However, there is a region, where two transitions occur at different temperatures: at lower temperature T^* there is a jump in the order

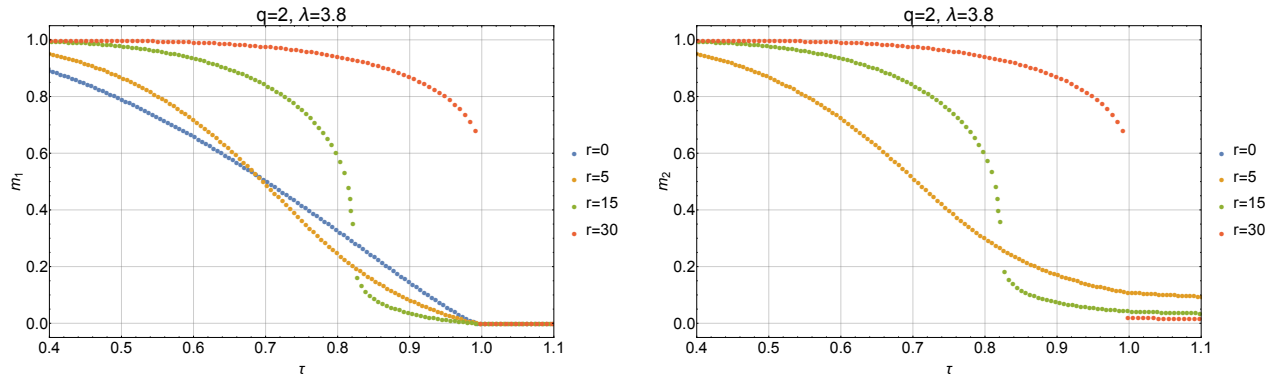


Figure 3.9. Order parameters as functions of reduced temperature $\tau = T/T_c$ for various values of r and fixed $\lambda = 3.8$. Different values of r lead to different critical regimes.

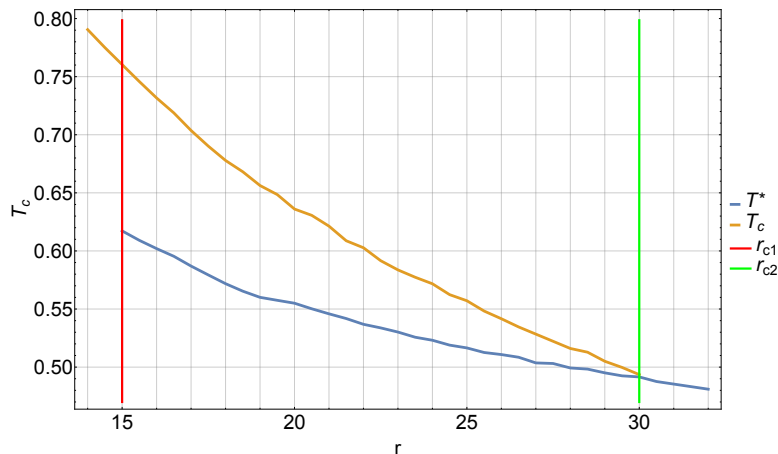


Figure 3.10. Phase transition temperatures T^* and T_c as a function r for fixed $\lambda = 3.8$. Two solid lines represent first and second order phase transition temperatures; two dashed vertical lines shows marginal values of r and limit the region of the coexistence of two phase transitions.

parameter (which we associate with the first order phase transition), and, later, at higher temperature remaining ordering completely vanishes. Similar behaviour was previously observed in Ref. [22] for the complete graph, but in the region $1 \leq q < 2$ only, while limiting case $q = 2$ showed sharp distinction between different orders regimes. At the presence of topological disorder as in the scale-free network, critical behaviour is changed. Even in the Ising case, it is characterised by two marginal values r_{c1} and r_{c2} . In Fig. 3.10 we show phase diagram in (T, r) -plane for the fixed value $\lambda = 3.8$. Lower (blue) and upper (yellow) lines represent first and second order phase transition lines respectively.

Second order phase transition line with the first order phase transition line divide (T, r) -plane into three regions. Below the lower (blue) line, system is in ordered state, while above the upper (yellow) line - the state is fully disordered. In the region between the lines, the system is characterised by residual ordering. Therefore, at r_{c2} and T_c these three phases coincide, making this point tricritical. Two vertical lines mark marginal values r_{c1} and r_{c1} , or equivalently the region, where two phase transitions coexist. For each λ value there are two marginal values $r_{c1}(\lambda)$ and $r_{c2}(\lambda)$. These two values divide the (r, λ) -plane into three regions with different critical behaviour.

Next step is to analyse properties of the second order phase transition. With order parameters as function of temperature, it is easy to find critical exponent β , which is given by:

$$m_1 \sim \left(\frac{T_c - T}{T_c} \right)^\beta. \quad (3.25)$$

Since we are minimising free energy numerically, the only way for us to proceed with the definition (3.25) is to fit obtained values $m_1(T)$. Because critical exponents are only defined at the critical temperature, from the fit we will only obtain effective value β_{eff} . In Fig 3.11 we show critical exponent β_{eff} for different values of r . For the genuine Ising case in the region we are interested in, critical exponents are λ -dependent. Analytical results yield [110–112]:

$$\beta(\lambda) = 1/(\lambda - 3). \quad (3.26)$$

In the plot we consider $\lambda = 3.8$, thus theoretical prediction is $\beta(3.8) = 1.25$. This value is shown by solid horizontal line. We can see that regardless of r , second order phase transition is characterised by the same critical exponent. Slight tendency to increase can be explained, because effective value of critical exponent is strongly dependent on the region we use for fitting: the smaller region, the better fit. However, with the increase of r , the region has to become even smaller, making it much harder to perform numerical calculations very close to the critical temperature.

In Fig. 3.12 phase diagram in (r, λ) -plane is shown. It is characterised by

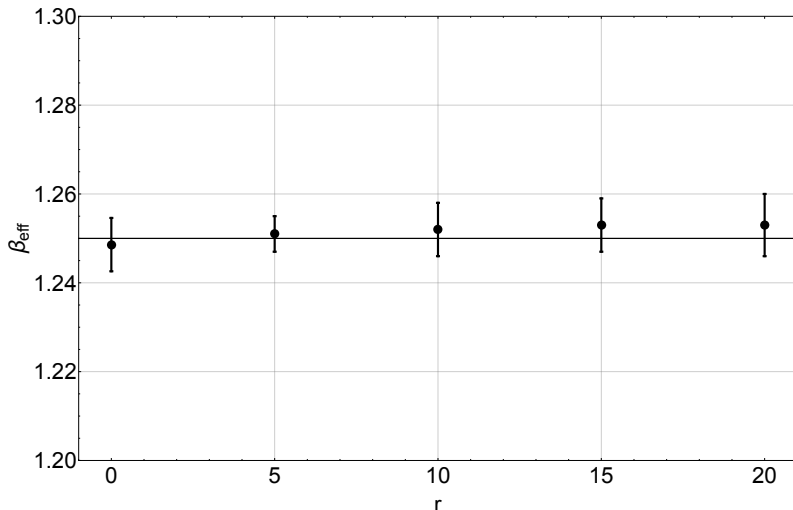


Figure 3.11. Critical exponent β as a function of number of invisible states r for fixed $\lambda = 3.8$. Solid line shows the exact result for the genuine Ising model $\beta = \frac{1}{\lambda-3}|_{\lambda=3.8} = 1.25$, Eq. (3.26).

two lines $r_{c1}(\lambda)$ and $r_{c2}(\lambda)$. Below the first one, with temperature raising, the order parameter continuously changes until it vanishes. Above the $r_{c2}(\lambda)$ line, only the first order phase transition occurs, meaning that as temperature increases, the order parameter decreases, and at T_c it abruptly drops to zero (see Fig. 3.9 for $r = 30$ case). The system undergoes two phase transitions in the region between the lines. At $T^* < T_c$ first order phase transition occur, and there is a jump between two non-zero values of m_1 . Then, at the second order phase transition temperature T_c first order parameter vanishes.

For fixed value of λ when r increases, m_1 depends on temperature continuously until $r_{c1}(\lambda)$ line is reached. Then the jump in the order parameter appears. In the region $r_{c1}(\lambda) < r \leq r_{c2}(\lambda)$ discontinuity grows with r and first order phase transition approaches second order phase transition $T^* \rightarrow T_c$. When $r_{c2}(\lambda)$ line is crossed, two critical temperatures coincide and only first order phase transition remains, while residual order parameter value is zero. Note that in the region $\lambda > 4$ order parameter behaviour close to the second order phase transition temperature is superlinear ($1/\beta = (\lambda - 3)$ is larger than one), which makes distinguishing between first and second order phase transitions even harder. Being evaluated numerically, $r_{c1}(\lambda)$ and $r_{c2}(\lambda)$ do not cross at $r \simeq 3.62$, $\lambda = 5$, as expected from the analysis of

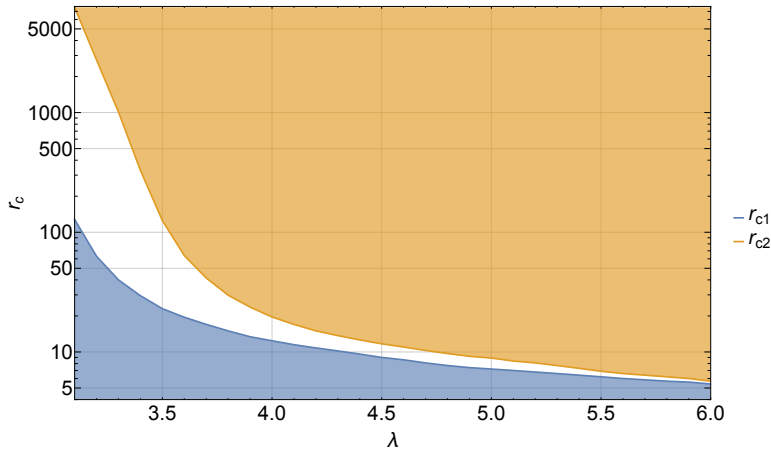


Figure 3.12. Phase diagram of the Ising model with invisible states. Three regions, presented here, differ in critical behaviour. In the lower (blue) region system possesses only second order phase transition; in the region in-between the lines there are both first and second order phase transitions at different temperatures; in upper region (yellow) only the first order phase transition occurs.

the Ising model with invisible states on the complete graph [22].

3.4. Conclusions

The main goal of the analysis presented in this chapter was to consider the Potts model with invisible states on different kinds of graphs (networks). There were several reasons to motivate the study. Firstly, euclidean dimensionality is ill-defined for graphs. This makes usual formulation of universality principle invalid. It was shown that for networks, the distribution of the vertex degree is crucial for any universality class. For instance, the Ising model on a scale-free network, where vertex degree distribution is governed by a power law $P(k) \propto k^{-\lambda}$, is described by λ -dependent critical exponents [110–112]. Secondly, some objects are better described by the topology of a network than a lattice. Examples range from nano clusters [100] to social networks [7]. In the next chapter we analyse one of the social networks.

We found an exact solution of the Potts model with invisible states on a graph within a mean field approach. This model is characterised by two order parameters.

Only one of them vanishes at critical temperature. We applied general formula for two cases - complete graph and scale-free network.

On the complete graph we showed that in the region $1 \leq q < 2$ the phase diagram is characterised by two marginal values r_{c1} and r_{c2} . Below r_{c1} the system undergoes only a second order phase transition. Above r_{c2} the phase transition is only of first order. While in the region $r_{c1} < r < r_{c2}$ there are two phase transition: first order at lower temperature and second order at higher temperature. For values of parameters where second order phase transition exists we observe mean field critical exponents, *i.e.* $\beta = 1/2$. For the Ising case $q = 2$ on the complete graph two marginal values coincide at $r_c \approx 3.62$.

On a scale-free network we considered only $q = 2$. Contrary to the complete graph case, where only one marginal values exists, we obtained λ -dependant values of marginal $r_{c1}(\lambda)$ and $r_{c2}(\lambda)$. These values have the same meaning as in the previous case of complete graph. We have also shown that everywhere where second order phase transition exist, critical exponents remain λ -dependent but uninfluenced by r .

Taking all these results into account one can state that adding invisible states changes the entropy of a system, making the phase transition sharper. However, in the region of r where the second order phase transition exists, its universal exponents remain constant. In addition, the mechanism we describe in this chapter is rather unique, and we have never seen it before.

CHAPTER 4

UNIVERSAL TOPOLOGICAL PROPERTIES OF COMPLEX SOCIAL NETWORKS OF NARRATIVES

In the previous section, we considered the behaviour of spin systems on networks. Spin models on networks are often considered as models of opinion formation [7]. In this chapter, we will be interested in the universal characteristics of such networks, however not in the sense of the universality of critical behaviour, but rather the independence of some of their properties from the details of the structure. Following recent works [16, 17], we will use the approach of complex networks to analyse the relationships between the characters of ancient narratives. The subject of research, we chose bylynas, as the only epic on the territory of the eastern Slavic lands sufficiently long for statistical analysis. We show that the social network of links between the characters of the bylynas, as well as similar works of many European cultures, [172] has a number of distinctive features. Also, within the limits of our method, we will try to elucidate arguments concerning several relevant issues relating to the relationship of the epic with the historical reality. The main results of this section are published in [24, 25].

4.1. Bylynas

Bylynas (or as they are sometimes called starynas) is a heroic epic of the Eastern Slavs. They comprise small melodic recitative songs. They have been categorised as social and proper heroic epic. Also tales can be grouped by place of

action in Kyiv, Novgorod and Moscow. Bylynas of the Moscow and Novgorod cycles are more social than heroic. Bylynas of the Moscow cycle are more concentrated on noble people and are related to later time periods. In contrast, bylynas of Novgorod cycle are centred around ordinary people - merchants, moneylenders, harpists, etc. Novgorod has always been a major trading hub and it was not subject to Tatar invasion. This is reflected in the topics of bylynas. Bylynas of the Novgorod or the Moscow cycles are far from the Kyiv cycle both by the place and time. Therefore there is no sense to analyse the whole corpus of bylynas, and the consideration can be limited to analyse of the social structure of each cycle separately. Here we investigate only Kyiv cycle of bylynas, which cover short period of the heyday of the Kyivan Rus (end 9 - mid 11 c.). Texts for the analysis were taken from [173]. This part of the epic also includes skomoroh (minstrel) songs and tales of courtship. Because these stories are not heroic, they omitted from our analysis. In total, the focus of our study was 39 bylynas of this collection. Bylynas of the Kyiv cycle include stories about the most famous heroes: Illia Muromets, Dobrynia and Oleksiy Popovych.

Bylynas were passed down from generation to generation orally. The first written record dates back to 1619 and was found in the diary of the Englishman Richard James [174]. These were the stories from the Moscow cycle. It is believed that the first dedicated collection of bylynas was made by Kirscha Danilov in the early 18th century. But this collection was published only in 1804 [175]. Most of the bylynas were collected and recorded in the northern regions of Russia in 18th-19th centuries. Researcher of the field Vasyl' Avenarius [176] explains this fact that the majority of the population of Ukraine at that time was already literate, unlike residents of remote villages of the Empire, and knowledge from generation to generation was passing in writing, rather than orally. The second reason could be that the Ukrainians had more recent heroic stories about cossacks, which replaced the older bylynas [177]. It is worth mentioning that characters of bylynas in Ukraine have migrated into other genres like folk tales or songs.

Despite the fact that bylynas have been collected across very large areas they

have a lot in common. In particular stories share scenes and have many common characters. This property also allows us to consider the characters of the bylynas as a certain structure - a social network.

4.2. Network

We define the network in characters of bylynas (hereinafter - *bylynas social network* [178]) as a graph [99], in which vertices correspond to individual characters, and the edges represent connections between individual characters. The set of vertices are denoted by V , and the number of vertices by N . The set of edges and number of them are denoted by E and L correspondingly. Each edge can be defined by a pair of vertices that connects them. Graphs can be directed or undirected. In a directed graph each edge has a direction, meaning that the vertices are ordered. In our analysis the social network of bylynas is considered as an undirected graph. It can be represented as the adjacency matrix A_{ij} . This is a matrix of size $N \times N$, each element A_{ij} of which is equal to one if there is a link between nodes i and j , and zero if there is no such edge. For an undirected graph the adjacency matrix is symmetric.

There are also weighted graphs - graphs in which each edge has its weight. In this case, the adjacency matrix does not simply consist of 1 and 0, but the elements will be weights of each edge [99]. Considering that the problem of weights in social interactions between separate individuals is not straightforward [178] (even more so when it comes to relationships, expressed by only within certain narratives), we continue to build social network as undirected unweighted graph, each edge of which reflects the fact that connected characters know each other. According to the methodology proposed in Refs. [16, 17, 172], we will assume two types of connections between epic characters: friends (if they talk to each other; when we can say from the text that they have met before; when characters are present together in a small group of people) or hostile (directly fighting or in a state war). This rules for linking make it harder to make text processing quasi-automatic and increase the time needed

for the database creation.

The analysis of the bylynas, allows us to create a database, consisting of 153 individual characters connected with two types of bonds - friendly and hostile. The resulting social network is shown in Fig. 4.1. Each character has its own code number. A list of the most important characters in the epics are presented in Table 4.2. Friendly connections are shown with a blue solid line, while hostile with the red dotted. In total the network includes 320 edges, 223 of which are friendly and 105 hostile. The total amount of friendly and hostile edges is larger than the total number of edges. This is because each bylyna itself is a short story of several characters. In various stories same characters can be both friends and enemies. Moreover, sometimes the connection type changes even within a single text [17].

A characteristic feature shown in Fig. 4.1 network is that it consists of several separate pieces, one of which (in the top left corner) is significantly larger than the others. It is called the largest connected component (part of the graph, in which there is a path between any two vertices). The existence of the largest connected component suggests that the different characters appears throughout the epics and together form the whole picture. It can be explained by the fact that Kyiv cycle of bylynas are united by scene, there is always hero-protagonist and Duke Volodymyr. Along with the largest connected component, there are some significantly smaller, not related to each other fragments. They correspond to individual or small groups of stories, which belong to Kyiv cycle, but they have no common characters with the largest connected component For example, one of the detached fragments (star in the second row from the bottom) corresponds to the story about Vavilo (node number 9). It tells how Vavilo overwhelms the antagonist king and takes his place. Characters in this story do not appear anywhere else and so they form isolated fragment of the total social network.

Sizes (number of vertices N and edges L) of the social network of bylynas are given in the first row of the Table. 4.1 together with other characteristics which will be described below. The table also contains characteristics of networks formed solely

| Network | N | L | $\langle k \rangle$ | k_{\max} | ℓ | ℓ_{rand} | ℓ_{\max} | C | C_{rand} | S | G_C | r_k | r_C |
|---|-----|------|---------------------|------------|--------|----------------------|---------------|------|-------------------|------|--------|---------|---------|
| Bylynas (<i>all</i>) | 153 | 320 | 4.18 | 52 | 2.9 | 3.61 | 6 | 0.57 | 0.03 | 23.7 | 76.5 % | -0.15 | 0.04 |
| Bylynas (<i>hostile</i>) | 98 | 102 | 2.14 | 17 | 3.63 | 5.76 | 8 | 0.06 | 0.022 | 4.3 | 51% | -0.11 | 0.012 |
| Bylynas (<i>friendly</i>) | 142 | 223 | 3.16 | 41 | 2.76 | 4.33 | 6 | 0.42 | 0.022 | 27.4 | 57% | -0.115 | -0.08 |
| Beowulf (<i>all</i>) [16] | 72 | 167 | 4.45 | 27 | 2.4 | 2.9 | 6 | 0.7 | 0.06 | 14.1 | 67.5% | -0.10 | -0.05 |
| Beowulf (<i>hostile</i>) [16] | 31 | 26 | 1.67 | - | 2.08 | 3.25 | 4 | 0 | 0.05 | 0 | 32.2% | -0.20 | - |
| Beowulf (<i>friendly</i>) [16] | 68 | 140 | 4.12 | - | 2.45 | 2.98 | 6 | 0.69 | 0.06 | 14.0 | 66.1% | -0.03 | - |
| Tain (<i>all</i>) [16] | 422 | 1266 | 6.10 | 168 | 2.8 | 3.3 | 7 | 0.8 | 0.02 | 47.1 | 98.5% | -0.33 | -0.30 |
| Tain (<i>hostile</i>) [16] | 144 | 168 | 2.33 | - | 2.93 | 5.88 | 7 | 0.17 | 0.02 | 17.1 | 90.9% | -0.36 | - |
| Tain (<i>friendly</i>) [16] | 385 | 1091 | 5.67 | - | 2.84 | 3.43 | 7 | 0.84 | 0.01 | 101 | 90.9% | -0.32 | - |
| Iliad (<i>all</i>) [16] | 716 | 2684 | 7.40 | 106 | 3.5 | 3.3 | 11 | 0.6 | 0.01 | 56.6 | 98.7% | -0.08 | 0.53 |
| Iliad (<i>hostile</i>) [16] | 321 | 361 | 2.25 | - | 4.10 | 7.12 | 9 | 0 | 0.01 | 0 | 89.4% | -0.39 | - |
| Iliad (<i>friendly</i>) [16] | 664 | 2317 | 6.98 | - | 3.83 | 3.34 | 12 | 0.62 | 0.01 | 54.1 | 82.3% | 0.10 | - |
| Gisli saga [17] | 103 | 254 | 4.9 | 44 | 3.4 | 2.9 | 11 | 0.6 | 0.05 | 10.8 | 98% | - | 0.01(7) |
| Saga 1 [17] | 132 | 290 | 4.4 | 31 | 3.9 | 3.3 | 10 | 0.5 | 0.03 | 12.7 | 97% | 0.15(5) | 0.00(6) |
| Egils saga [17] | 293 | 769 | 5.3 | 59 | 4.2 | 3.4 | 12 | 0.6 | 0.02 | 25.5 | 97% | 0.07(3) | 0.08(6) |
| Saga 2 [17] | 332 | 894 | 5.4 | 45 | 5.0 | 3.5 | 16 | 0.5 | 0.02 | 19.0 | 99% | - | 0.28(4) |
| Njals saga [17] | 575 | 1612 | 5.6 | 83 | 5.1 | 3.7 | 24 | 0.4 | 0.01 | 31.0 | 100% | 0.19(4) | 0.25(4) |
| Da Derga [172] | 126 | 410 | 6.51 | 71 | 2.76 | 2.77 | 7 | 0.64 | 0.05 | 12.8 | 98.4 % | 0.01(2) | 0.12(3) |
| Odyssey [172] | 301 | 1019 | 6.77 | 112 | 3.29 | 3.18 | 8 | 0.45 | 0.02 | 21.7 | 98.3 % | -0.18 | 0.31 |
| Nibelungenlied [172] | 66 | 313 | 9.48 | 43 | 2.14 | 2.11 | 5 | 0.69 | 0.14 | 4.9 | 97 % | -0.08 | 0.38 |
| Mabinogion [172] | 666 | 2427 | 7.29 | 135 | 3.83 | 3.48 | 11 | 0.48 | 0.01 | 43.6 | 76 % | -0.28 | 0.22 |
| Epic of Gilgamesh [172] | 46 | 81 | 3.52 | 19 | 2.54 | 3.08 | 5 | 0.46 | 0.08 | 7.0 | 93.5 % | 0.19 | 0.37 |
| Popol-Vuh [172] | 98 | 409 | 8.35 | 27 | 2.80 | 2.39 | 6 | 0.55 | 0.09 | 5.2 | 94.9 % | -0.34 | 0.10 |
| Navaho myths [172] | 140 | 283 | 4.04 | 32 | 3.81 | 3.62 | 9 | 0.44 | 0.03 | 14.0 | 92.1 % | -0.32 | -0.05 |
| | | | | | | | | | | | | -0.18 | 0.31 |

Table 4.1. Characteristics of social network of bylynas (our results) compared to other epics obtained in [16, 17, 172]. Here N and L indicate the number of characters and the number of edges, respectively; $\langle k \rangle$ and k_{\max} - average (4.2) and maximum (4.3) node degree; ℓ , ℓ_{rand} - average shortest path length (4.6) of the complex network and random graph (4.8) of the same size and average degree; ℓ_{\max} - network diameter (4.7); C , C_{rand} - average clustering coefficient of a complex network (4.12) and corresponding random graph (4.13); S - smallworldness (4.17); G_C - size of the largest connected component; r_k , r_C - assortativities by degree (4.23) and clustering coefficient (4.24), respectively. Notes in brackets (*all*, *hostile*, *friendly*) specify the types of edges which construct the network.

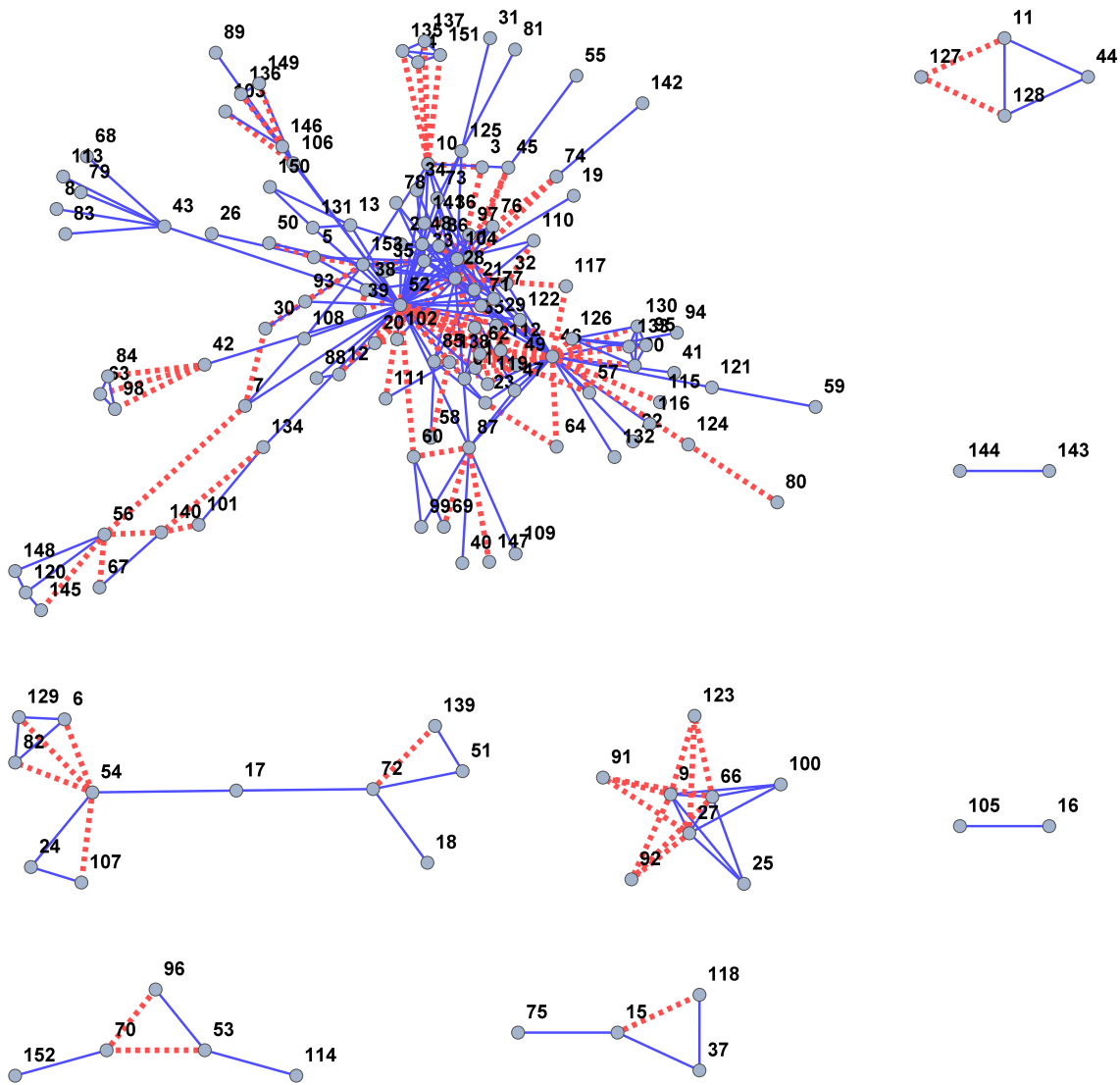


Figure 4.1. Social network of characters of Kyiv cycle bylynas. Red dashed lines corresponds to the hostile links, while blue solid to the friendly ones. Each node has its own code number. The most important characters and the corresponding numbers are listed in Tab. 4.2. The largest connected component is shown in the left top corner of the figure. Smaller subgraphs represent characters of separate stories. For example graph consisting of nodes 143 and 144 is two bulls observing troops, but do not interact with other characters. Star-like graph in the second row from the bottom describes stories about Vavilo (node number 9). Characters of this part of the epics do not appear in any other story.

by friendly (friendly network) or hostile links (hostile network). It is also worth noting that nodes which have no links are omitted in both friendly and hostile networks. Naturally, they are not taken into consideration and thus the size of

networks of a various links type will be different. Bylynas hostile network includes 98 nodes (55 isolated nodes were removed), and the largest connected component is 50 of them, representing 51 %. Size of the largest connected component of bylynas with all links taken into account is 76.5 %. This is smaller than for the epics of other nations. This can be explained by the fact that bylynas are individual stories about heroes. Different regions of Kyivan Rus had their own heroes, which are not necessarily connected to the most popular heroes. For example Vasyl' Okulovych (number 11), connected component of which is in a right upper corner of Fig. 4.1.

We will use the Table. 4.1 to compare the characteristics of social networks of bylynas with similar characteristics of other networks. Besides the above-mentioned works *Beowulf*, *Iliad*, *Táin Bó Cualinge* (*Tain*) and the Icelandic sagas *Gisli Saga*, *Vatnsdæla Saga* (we will refer to it as *Saga 1*), *Egils Saga*, *Njals Saga*, *Laxdæla Saga* (from now onwards *Saga 2*) the Table contains information on the characteristics of social networks of Irish saga *Da Derga's Hostel* (from now onwards *Da Derga*), *Odyssey*, *Nibelungenlied*, *Mabinogion*, *Epic of Gilgamesh*, *Popol Vuh* and *Navaho Myths*. In cases where appropriate information available, we present data separately for friendly, hostile and all links networks Quantitative data on these epics are taken from [172].

Comparison of the quantitative characteristics of social network of bylynas with those listed above and representing different nations serve as a the main goal set in our work: a search for universal characteristics of epic narratives. In the next section we find such characteristics of social networks of bylynas as average node degree, clustering coefficient, distance between the characters, smallworldness, correlation between nodes properties, betweenness of nodes, robustness of the network and its community structure. Each of these characteristics, we will describe below. Table. 4.1 contains all of the above characteristics for different types of networks linking for bylynas and compared to some other epics.

4.3. Network properties

4.3.1. Vertex degree

The degree k_i of a node i is the the number of connections that this node has. This is a local characteristic of the node, and in other words it is a number of vertices, which are connected to the given one. Thus this property in some sense indicates the importance of each vertex. The degree of a node i is determined by the following formula

$$k_i = \sum_j A_{ij} \quad (4.1)$$

where A_{ij} is the adjacency matrix. The whole network can be described with the average degree of nodes

$$\langle k \rangle = \frac{1}{N} \sum_i k_i, \quad (4.2)$$

and the maximum degree

$$k_{\max} = \max_i k_i. \quad (4.3)$$

Here and below, unless otherwise noted, the summation is performed over all network nodes. \max_i in (4.3) means the maximum value among all nodes. For undirected graphs

$$\langle k \rangle = \frac{2L}{N}. \quad (4.4)$$

For visualisation we show the network with vertices rescaled according to their degree. Therefore, nodes with a higher degree are shown by larger circles. The largest connected component of the network is shown in Fig. 4.2(a). As one can see from the picture, some nodes differs from the others by size. The highest degree is $k_{\max} = 52$, and it's much higher than average degree $\langle k \rangle = 4.18$, see. Table. 4.1. Although bylynas contain many characters, but they are stories about the heroes and, therefore, main attention is focused on them. Thus within the network there are several main characters - Duke Volodymyr (character 52), Illia Muromets (character 46), Dobrynia (character 28) and Oleksiy Popovych (character 1) for which the node degree strongly differs comparing to the rest of the network. The graph shown in

the Fig. 4.2(a) has a structure similar to several stars fused together: leaders are attached to a number of low degree characters and are linked directly. The character of maximum value of a node degree $k_{\max} = 52$ is connected to roughly half of all others. This is Duke Volodymyr (character 52), which is mentioned in almost every bylyna. Interestingly some researchers believe Duke Volodymyr to be a collective character [177]. We will return to this issue later in Section 4.3.6 when we will discuss the assortativity of the network.

| Character Name | No | R_k | R_c | R_b |
|--------------------|-----|-------|-------|-------|
| Duke Volodymyr | 52 | 1 | 1 | 1 |
| Illia Muromets | 46 | 2 | 2 | 2 |
| Dobrynia | 28 | 3 | 3 | 3 |
| Oleksiy Popovych | 1 | 5 | 4 | 10 |
| Mykhailo Potyk | 87 | 9 | 7 | 5 |
| Opraksiya | 104 | 4 | 5 | 13 |
| Duke | 33 | 7 | 6 | 15 |
| Vasyl' | 8 | 10 | 13 | 7 |
| Churylo | 153 | 6 | 12 | 16 |
| Soloviy the Robber | 126 | 11 | 15 | 23 |
| Tatar | 138 | 15 | 14 | 24 |
| Kudrevanko | 65 | 10 | 8 | 37 |
| Danube | 32 | 18 | 11 | 31 |
| Ivan Gostynyj Syn | 43 | 19 | 37 | 4 |
| Mykhailo | 85 | 16 | 25 | 28 |
| Kalin | 49 | 17 | 16 | 36 |
| Matviy | 77 | 12 | 9 | 49 |
| Luka | 71 | 13 | 10 | 50 |
| Hoten | 146 | 24 | 40 | 11 |
| Soloviy | 125 | 25 | 42 | 14 |

Table 4.2. Twenty main character of bylynas social network. The table shows No - code number of the character, and three ranks: R_k (according to node degree k), R_c (closeness centrality \mathcal{C}^c), R_b (betweenness centrality \mathcal{C}^b).

Let's now consider the probability that randomly selected node has a given degree k . This probability is given by the function $p(k)$ and is one of the main characteristics of a network. We know that the real social networks (see, for example, [179, 180]) are described by a power-law decreasing function $p(k) \simeq k^{-\lambda}$, $k \gg 1$.

Such networks are called scale-free [8, 178, 181–187]. Scale-free networks have a number of unique properties, related to the decreasing rate of $p(k)$. In addition to social networks, Internet, metabolism network, power grids, transport and semantic networks are also scale-free [178, 183–187]. In practice, it is more convenient to consider cumulative probability distribution function of a node degree $P(k)$, which is related to the $p(k)$ through the relation

$$P(k) = \sum_{q=k}^{k_{\max}} p(q), \quad (4.5)$$

where k_{\max} is the maximum node degree in the network. Being integral characteristic, this feature is smoother than $p(k)$ and more convenient for approximation. For the power-law like $p(k) \simeq k^{-\lambda}$ cumulative distribution function behaves like $P(k) \simeq k^{1-\lambda}$.

Fig. 4.3 shows the cumulative distribution function and its approximation with a power law. This approximation corresponds to $\lambda \simeq 2.36(7)$ with statistical criterion $\chi^2/N_{dof} = 0.041$, which means good matches between data and hypothesis. Therefore we can say that bylynas posses the scale-free social networks.

In [16, 17, 172] it has been shown that networks of epics *Beowulf*, *Tain and the Icelandic sagas* are also scale-free with values $\lambda = 2.2 - 2.9$. In particular, *Beowulf* has $\lambda = 2.4(1)$, which is very close to our value. Characteristically, the value of λ for the Icelandic sagas is higher. It is also worth mentioning that for fiction power-law distribution for a degree occurs very rarely [16].

4.3.2. Distances between characters

Real social networks, even those with large number of nodes are characterized by small average distances between them. This is so-called the *small world* effect[188] (see more in Section 4.3.6). They are known for effect of six degrees separation or six

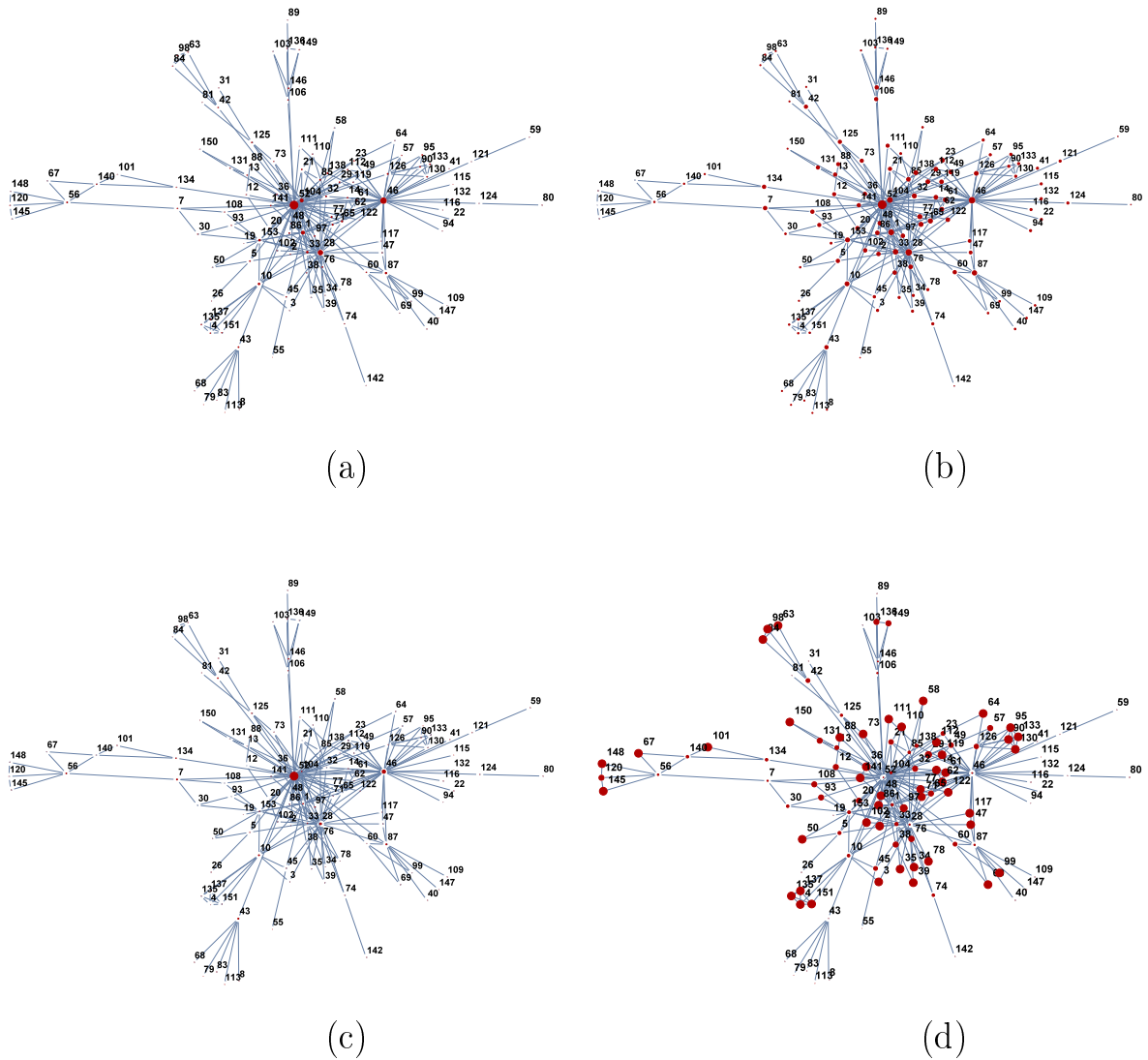


Figure 4.2. The largest connected component of the social network of bylynas (friendly and hostile links were taken into consideration). The size of each vertex is proportional to: node degree k (a), closeness centrality C^c (b) (4.9), betweenness centrality C_B (c) (4.9), clustering coefficient C (d) (4.11). As seen from a comparison of figures (a) - (d), rank (importance) of a node in different classifications is different. For example Duke Volodymyr (character 52) and Illia Muromets (character 46) have the highest degree, closeness and betweenness centralities, but their clustering coefficients are small. Or Ivan Gostynyj Syn (character 43) has a relatively high centrality values but low degree and clustering coefficient. The ranks for the most important characters are given in the Table 4.2.

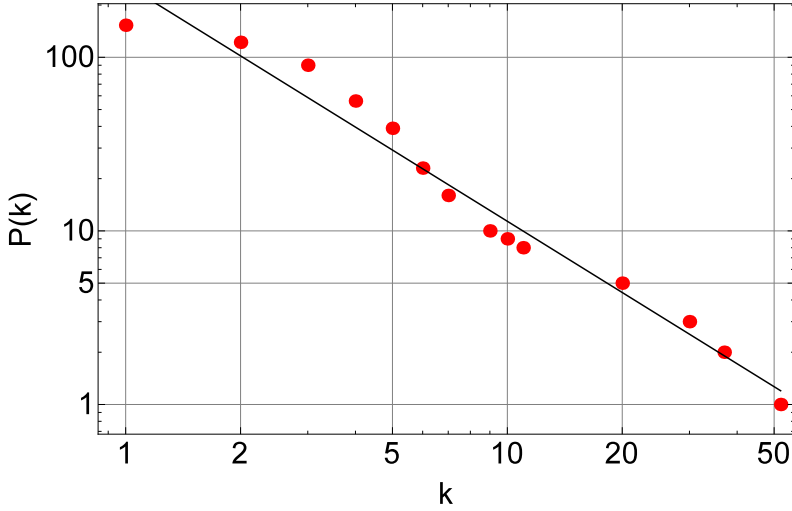


Figure 4.3. Cumulative distribution function of the node degree $P(k)$ and its power law approximation $P(k) \simeq k^{1-\lambda}$ with $\lambda \simeq 2.36(7)$ (solid line).

handshakes [189]: the average distance between two randomly selected members of society is six. We will check what are the typical distances (paths) between nodes in bylynas social network. In graph the path is the sequence of edges, which you have to walk through, to get from one node to another. The path length is determined by the number of edges traversed. The shortest path from one node to another within a consistent part of the graph is called a geodesic.

Let ℓ_{ij} denote a geodesic length between nodes i and j . Then we can define the average shortest path length

$$\ell = \frac{1}{N(N-1)} \sum_{i \neq j} \ell_{ij}, \quad (4.6)$$

and maximum shortest path length (diameter of the networks)

$$\ell_{\max} = \max_{ij} \ell_{ij}. \quad (4.7)$$

In order to find the distances (4.6) and (4.7) all geodesic in all connected components were taken into account. Corresponding values are listed in the Table. 4.1. The average pathlength for bylynas is comparable with other epics. The same can be said about the diameter of the network. Judging on the table it is also clear that these values are rather small. Particularly the maximum path length between characters

is merely 6 (for all and friendly networks). In the real-world social network where the number of people-characters is of higher orders, the distances are the same because the real world is more connected. The value $\ell_{\max} = 8$ for the hostile network of bylynas is higher, which means that this network is more "stretched". A similar feature is observed for other epics, see. Table. 4.1.

The average shortest path length ℓ is compared with the corresponding value of ℓ_{rand} calculated for classic Erdős-Rényi random graph [190] of the same size. Erdős-Rényi graph is an example of the small world network for which average pathlength grows logarithmically with the number of nodes [191]. This fact, and the lack of any correlation in nodes connectivity leads to low values of average pathlength. The latter can be estimated for a given number of nodes and their average degree [192]

$$\ell_{\text{rand}} = \frac{\log N - \gamma}{\log \langle k \rangle} + \frac{1}{2} = 3.23 \quad , \quad (4.8)$$

where $\gamma \simeq 0.5772$ is the Euler-Mascheroni constant. Obtained by this formula ℓ_{rand} for three different connection types networks of bylynas are given in the Table. 4.1. As one can be seen from the table, just as the networks of other epics, the average shortest distance in analysed networks are lower than in random graphs with relevant the number of edges and nodes.

4.3.3. Closeness centrality

Using the concept of distance between the characters one can found characteristic that is called closeness centrality [193, 194]. For each node in the graph, it is the inverse of the sum of the distances from the given node to all other nodes within connected component

$$\mathcal{C}^c(v) = \frac{1}{\sum_{t \in V} d_G(v, t)}, \quad (4.9)$$

where $d_G(v, t)$ denotes the distance between vertices v and t . Therefore, the higher closeness centrality $\mathcal{C}^c(v)$ is, the closer node v is to other nodes. In order to compare,

calculations should be done only within connected component of a network where there is a path between any two characters.

In Fig. 4.2(b) the largest connected component of bylynas social network is shown. The size of each vertex v is proportional to its closeness centrality $\mathcal{C}^c(v)$. List of the most important bylynas characters with their rank by closeness centrality (rank R_c) is given in Table 4.3. The highest values of the closeness centrality have Duke Volodymyr (character 52), Illia Muromets (character 46) Dobrynia (character 28), Oleksiy Popovich (character 1) and Duchess Opraksiya (character 104). Immediately followed by the character named Duke (character 33, do not confuse with Duke Volodymyr) and Mykhailo Potyk (character 87). Hrushevsky refers to the last two as the part of Galicia-Volyn character group [195]. According to bylynas, Duke is Galician Duke. And Mykhailo Potyk is considered to be borrowed from Western Ukraine, where he, in turn, came from Bulgaria, with a history of St. Michael from Potuka [195]. In the texts, we took into consideration, he is hero fighting on the side of Duke Volodymyr against King Lyahetskiy (character 60). According to the another version, the name came from the river Potok in Western Ukraine, from which, in turn, Potocki dynasty took the name [196]. Interesting is the fact that quantitative analysis has shown the importance of character of Galicia-Volyn region, which once was a successor of Kyivan Rus.

On the other hand it is interesting that in the network without the Volodymyr and Opraksiya the most important by closeness centrality is Dobrynia who overrank Illia Muromets. It can serve as a reflection of the fact that Illia in several texts opposes Duke Volodymyr, while Dobrynia always on the side of the ruler, and, therefore, closer to him.

4.3.4. Betweenness centrality

In addition to the above mentioned degree k_i and closeness centrality $\mathcal{C}^c(i)$, another local characteristic that can give an insight onto the importance of a node i is the betweenness centrality. This value shows how important this node is to

maintain communications between other network nodes. Let $\sigma(j, l)$ be the number of geodesic between nodes j and l , and let $\sigma_i(j, l)$ be the number of those passing through node i . Then node betweenness centrality is defined as [194]:

$$\mathcal{C}^b(i) = \frac{2}{(N-1)(N-2)} \sum_{j \neq l} \frac{\sigma_i(j, l)}{\sigma(j, l)} \quad . \quad (4.10)$$

Like the closeness centrality betweenness makes sense only within connected component. Thus N in formula (4.10) is the number of units in a connected component, and normalization is performed over all possible connections between the nodes. Accordingly, the value of $\mathcal{C}^b(i) = 1$ corresponds to the case when all the geodesic are passing through node i .

Fig. 4.2 (c) shows the largest connected component of bylynas social network, in which the size of the node is proportional to its betweenness centrality. List of main characters with their rank R_b according to the betweenness centrality is given in the Table 4.3. The main characters are Duke Volodymyr (character 52), Illia Muromets (character 46) and Dobrynia (Character 28) and the rank of Oleksiy Popovych (character 1) is significantly lower $R_b = 10$ (comparing to his rank in degree or closeness centrality: $R_k = 5, R_c = 4$). The fourth largest centrality is Ivan Gostynyi Syn (character 43). It appears just once, in story which has five unique characters. And because Ivan has a direct connection to Duke Volodymyr these five unique characters are connected to the rest of the network.

Nodes with high betweenness centrality are vital for maintaining the integrity of the network. For example, if one removes three characters of bylynas social network with the highest value of \mathcal{C}^b , network will be divided into 24 pieces, and the largest of which contains 72 nodes. Resilience of the network to removal of its individual components will be analysed in section 4.3.10.

4.3.5. Clustering coefficient

Clustering coefficient is a specific measure of correlation in the network [186]. It determines the probability that two random neighbours of a node are also inter-

connected. Clustering coefficient of a node i with a degree k_i is defined as

$$C_i = \frac{2n_i}{k_i(k_i - 1)} \quad , \quad (4.11)$$

where n_i is an umber of neighbours of node i , which are interconnected. Obviously, the $k_i(k_i - 1)/2$ is the maximum number of possible connections between k_i nodes, so the clustering coefficient of a node in fully connected graph is equal to 1. Respectively the clustering coefficient of any node in a tree (graph without loops) is 0.

Fig. 4.2(d) shows the largest connected component of bylynas social network, in which the vertex sizes are proportional to its clustering coefficient. As one can see from the figure, the importance of a node according to their clustering coefficients is significantly different from their importance according to the degree (see Fig.4.2(a) and Fig.4.2(d)). Nodes with high degree have small clustering coefficients: the larger the degree of the node, the less probable is that its neighbours are connected to each other. So each of heroes (Illia (character 46) Dobrynia (character 28), Oleksiy Popovych (character 1)) had several different independent from each other enemies, which resulted in small clustering coefficients.

As follows from the definition (4.11), clustering coefficient is a local characteristics of the node. The network as a whole can be characterized by the mean value of the clustering coefficient:

$$C = \frac{1}{N} \sum_i C_i \quad . \quad (4.12)$$

Often, to determine the extent of correlation in real networks clustering coefficients are compared with random graph of the same size C_{rand} . For a given size and average degree

$$C_{rand} = \frac{\langle k \rangle}{N - 1}. \quad (4.13)$$

By comparing clustering coefficients for the bylynas social network and corresponding random graph given in the Table. 4.1 one can quantitatively characterize the extent of the correlation in bylynas network. Networks formed with both friendly

and all edges are strongly correlated structures. Like other epics networks, their clustering coefficient is more than one order of magnitude greater than the clustering coefficient of a random graph of the same size. This is not the case for hostile network. As shown in the table for the bylynas social network its value is much less than for a friendly network and the order of magnitude is comparable with the value for the random graph. This observations may serve as the evidence of the structural balance hypothesis for epics social networks: if two characters are connected through hostile links with the third one, it is unlikely that they are also connected by hostile link.

| | friendly | hostile | all |
|--------------|----------|---------|-------|
| C^T | 0.25 | 0.08 | 0.23 |
| C_{rand}^T | 0.021 | 0.021 | 0.027 |
| R_P | 0.018 | -0.038 | 0.02 |

Table 4.3. Transitivity C^T (4.14), its estimation for a random graph C_{rand}^T and Pearson similarity r_P of bylynas social network for different types of connections. The negative value of Pearson similarity stays for structural balance hypothesis.

The alternative value that is similar to the mean clustering coefficient characterizing the presence of correlations in the network is transitivity. It is defined as [11]

$$C^T = \frac{3N_{\Delta}}{N_t} \quad , \quad (4.14)$$

where N_{Δ} is the number of closed triangles in the network (configurations with three pairs of connected nodes) and N_t is the number of connected triplets (configurations of three nodes, which is connected by only two edges). Transitivity for the random graph with N nodes can be approximately found using moments of node degree [197]

$$C_{rand}^T \approx \frac{1}{N} \frac{(\langle k^2 \rangle - \langle k \rangle)^2}{\langle k \rangle^3} \quad . \quad (4.15)$$

Table. 4.3 shows transitivity for social networks of different link types of bylynas and these values are compared with corresponding random graphs.

As noted above, transitivity is analogous to clustering but this is not always the case. An example is a wheel graph. For this graph in the limit of infinite size transitivity tends to 0, while the average clustering coefficient to 1 [198]. On the other hand, Erdős-Rényi random graph clustering coefficient and transitivity are very close [199].

From the results shown in Table. 4.3 one can reach the same conclusions as from clustering coefficient. The difference is in the areas of application. Transitivity often used for social networks[197], where it is a good representation of the structural balance hypothesis.

4.3.6. Small-worldness

As it was shown above, bylynas social networks have low value of the average shortest path ℓ and high clustering coefficient C . The former characteristic makes them similar to the classical random graph, while the latter demonstrates the essential role of correlations in the formation of these networks and this likens them to regular structures. Real social networks are extremely compact: path from one node to another lies through a small number of edges. We have already mentioned the hypothesis of six handshakes [188]. It is a clear expression of the fact that our world is small. Small-world network [186] combines the features of a random graph and regular structure: it has both small size (low value of the average shortest path ℓ) and high degree of correlation (high clustering coefficient C):

$$\ell \approx \ell_{rand}, \quad C \gg C_{rand}. \quad (4.16)$$

For numerical characteristics of small-world effect one can use so called small-worldness [200]. Its definition takes into account both of effects in (4.16):

$$S = \frac{C/C_{rand}}{\ell/\ell_{rand}}. \quad (4.17)$$

The network is called small world, if $S > 1$. Values for bylynas social networks small-worldness are given in Table. 4.1. Numerical data shown in the table indicate that

conditions (4.16) are satisfied for friendly and all links networks. Thus, bylynas social network, like other epics social networks are small worlds. As mentioned in section 4.3.5, clustering coefficient for hostile network is comparable with the corresponding random graph clustering coefficient. The second condition in (4.16) is not satisfied for this network that leads to a relatively lower value of small-worldness. Similar properties can be seen for the network of other epics presented in Table 4.1 as well.

Despite the fact that defined in (4.17) small-worldness allows quantitatively describe this effect, its usage for comparative analysis has some drawbacks. The main is that for random graph clustering coefficient scales with the system size as $C_{rand} \propto 1/N$, while for complex networks its value is considerably high. Taking into account that for both complex networks and random graphs average shortest pathlength grows logarithmically with the system size, large complex networks will always have high small-worldness. That's why this characteristic can't always answer if the network is small-world or not.

4.3.7. Degree assortativity

We know that in real social networks vertices are connected with those similar by degree [197]. Alternatively, in fictional social networks (such as Marvel universe [201]), high-degree vertices are mostly connected to low degree vertices. As we shall see below, in this respect, social networks of epic narratives occupy an intermediate position. Quantitative measure for degree correlation between neighbouring nodes is degree assortativity [197]. The probability that randomly selected edge connects nodes with degrees k and q is given by

$$\Phi(k, q) = \frac{1}{2L} \sum_{i,j} A_{ij} \delta(k_i - k) \delta(k_j - q), \quad (4.18)$$

where δ is a Kronecker delta, and coefficient $\frac{1}{2}$ allows to write the sum in symmetric way. Then the probability that at the end of randomly chosen edge node has degree

k , can be found by summing over all possible degrees on the other end of the edge

$$\phi(k) = \sum_q \Phi(k, q) \quad . \quad (4.19)$$

Let $E(k)$ be the expectation value to find a node with degree k on the end of randomly selected edge (note that this value differs from $\langle k \rangle$, as the latter is obtained by summing over nodes). It can be found using the formula

$$E(k) = \sum_k k \phi(k) = \frac{\langle k^2 \rangle}{\langle k \rangle}, \quad (4.20)$$

which links averages over edges and vertices. Similarly, we can write the expectation value to get an edge with nodes degrees k and q at the ends

$$E(kq) = \sum_{k,q} kq \Phi(k, q) \quad . \quad (4.21)$$

For uncorrelated networks $E(kq) = E(k)E(q)$. To quantify the correlation we will use Pearson correlation coefficient, which has the form

$$r_k = \frac{E(kq) - E(k)E(q)}{\sigma_k^2} \quad (4.22)$$

where $\sigma_k^2 = E(k^2) - E(k)^2$. Based on the written above, degree assortativity will have the following form

$$r_k = \frac{\sum_{i,j} A_{ij} (k_i - E(k))(k_j - E(k))}{E(k^2) - E(k)^2} \quad . \quad (4.23)$$

Degree assortativity is bounded $-1 < r_k < 1$. Negative values $r_k < 0$ indicates that the network is disassortative, i.e. that high-degree nodes are joined to nodes with a low degree. Value $r_k > 0$ characterizes assortative network, where high-degree nodes connect to each other, and nodes with a low degree are connected as well.

Assortativity for bylynas social networks are given in Table 4.1. For network of all links $r_k < 0$ which indicate that the network is disassortative. This result also is consistent with the fact that bylynas are epic tales about heroes: parts of networks are star-shaped structures (see. Fig. 4.1) where heroes associated with several less

significant characters. Completely different behaviour is typical for some Icelandic sagas. They are stories about people. And for them assortativity is positive.

The results shown in Table 4.1 indicate that most social networks of epic narratives are disassortative. It should be noted however, that this can sometimes be caused by the structure of the story itself. For example, events described in the epic *Beowulf* occur in two different places and also divided by time intervals. They are connected only through common protagonist. As shown in [16], removal of the protagonist changes the nature of network connections from disassortative to (weakly) assortative. A similar effect is present in bylynas social network. After removal of Duke Volodymyr degree assortativity increases to $r_k \approx 0.01$, which is indeed very small but positive value. This way, the network becomes more similarly to a real social network. Many researchers believe that Duke Volodymyr is a collective character [177] combining Duke Volodymyr the Great, Yaroslav the Wise and Volodymyr Monomakh [202]. Dividing Duke Volodymyr into three characters increases assortativity to $r_k \approx 0.004$. And division into four makes the network even more assortative with $r_k \approx 0.03$. Thus, we see that the distribution of Duke Volodymyr makes the network more like real social network.

4.3.8. Clustering assortativity

Besides degree assortativity there is also clustering assortativity. It is a measure of correlation between the values of clustering coefficients of neighbouring nodes. Real world social networks tend to have high clustering assortativity, which also indicates the existence of communities in the graph [203]. Since clustering is local characteristic defined for each node, then in analogy to (4.23) one can define clustering assortativity

$$r_{cl} = \frac{\sum_{i,j} A_{ij}(C_i - E(C))(C_j - E(C))}{E(C^2) - E(C)^2} . \quad (4.24)$$

Values for clustering assortativity of bylynas social networks are listed in Table 4.1. For all types of bonds it is close 0. This result indicates that the characters

in the bylynas network connect to both closely related groups and to individual characters. For network of all links resulting value r_d is close to the corresponding values for Gisli Saga and Vansdæla Saga. Overall, from the data given in the table one can not find any tendency for clustering assortativity of social network of epic narratives.

4.3.9. Pearson similarity

In the previous section we discussed the correlation between properties of individual nodes in the network, mainly clustering and degree assortativities. In this section we consider another value that describes the correlation properties of different nodes - Pearson similarity. This property shows how much common neighbours nodes i and j share in comparison with random networks [11]. It is an important feature for social networks. For example, analysing the structure of the network, a popular service *Facebook* offers a list of people each user may know. Similarly, some modern Internet search engines offer a list of pages similar to the selected one.

The Pearson similarity is normalized covariance between vectors A_i and A_j , which are i -th and j -th columns in adjacency matrix. It is calculated according to the formula

$$r_{ij} = \frac{\sum_v (A_{iv} - N^{-1}k_i)(A_{jv} - N^{-1}k_j)}{\sqrt{\sum_v (A_{iv} - N^{-1}k_i)^2} \sqrt{\sum_v (A_{jv} - N^{-1}k_j)^2}} . \quad (4.25)$$

The value of $r_{ij} < 0$ means that two nodes have less common neighbours than we would expect from a random structure, and therefore can assume that nodes are different, otherwise $r_{ij} > 0$ shows that two nodes share more common neighbours than a random connection. Averaging Pearson similarity over all pairs of vertices gives the characteristic r_P which describes the network as a whole.

The values of the average Pearson similarities are shown in Table 4.3. A small positive value, may indicate, that two connected characters have more common "friends" than on average, but the result is far from a complete graph where $r_P = 1$.

For the network of hostile links the Pearson similarity is negative, reflecting the fact that structural balance hypothesis holds in this case.

4.3.10. Resilience

More information about the structure of a complex network can be obtained by analysing the stability of the network to the removal of its individual components (the so-called attacks). This problem has much in common with the percolation on a lattice [204, 205]. An analogue to the percolation cluster in percolation problem on a network is giant connected component (see., eg, [8, 183–185] for a detailed comparison). For network of finite size the size of the largest component is analysed. The heterogeneity of networks makes the efficiency of attacks strongly dependant on the scenario (how nodes are picked for the removal). Presence of hierarchical structures in scale-free network makes them vulnerable to targeted attacks, when nodes are removed in accordance with their importance ranked by any certain property. On the other hand, these network are extremely resistant to random removal of their constituents [102, 103, 206, 207].

In Fig. 4.4 three different attacks scenarios on the bylynas social network are compared conduct: random (when nodes are removed at random) and two targeted (when nodes are removed in descending order of their degree of betweenness centrality at every step). The results presented in Fig. 4.4, were obtained for the network of all links (networks of just friendly or hostile connections are too small). As shown in the figure, random attacks are ineffective. A targeted attacks on the degree of the node, or on the betweenness are nearly equal efficient, and do much more of a damage to the network. It is enough to remove about 10 vertices, to reduce the largest connected component to about 10 % of its original size. Similar findings were made in [16, 17] for other epic narratives. In general, they are robust against random attacks, but easily destroyed by targeted removal of nodes.

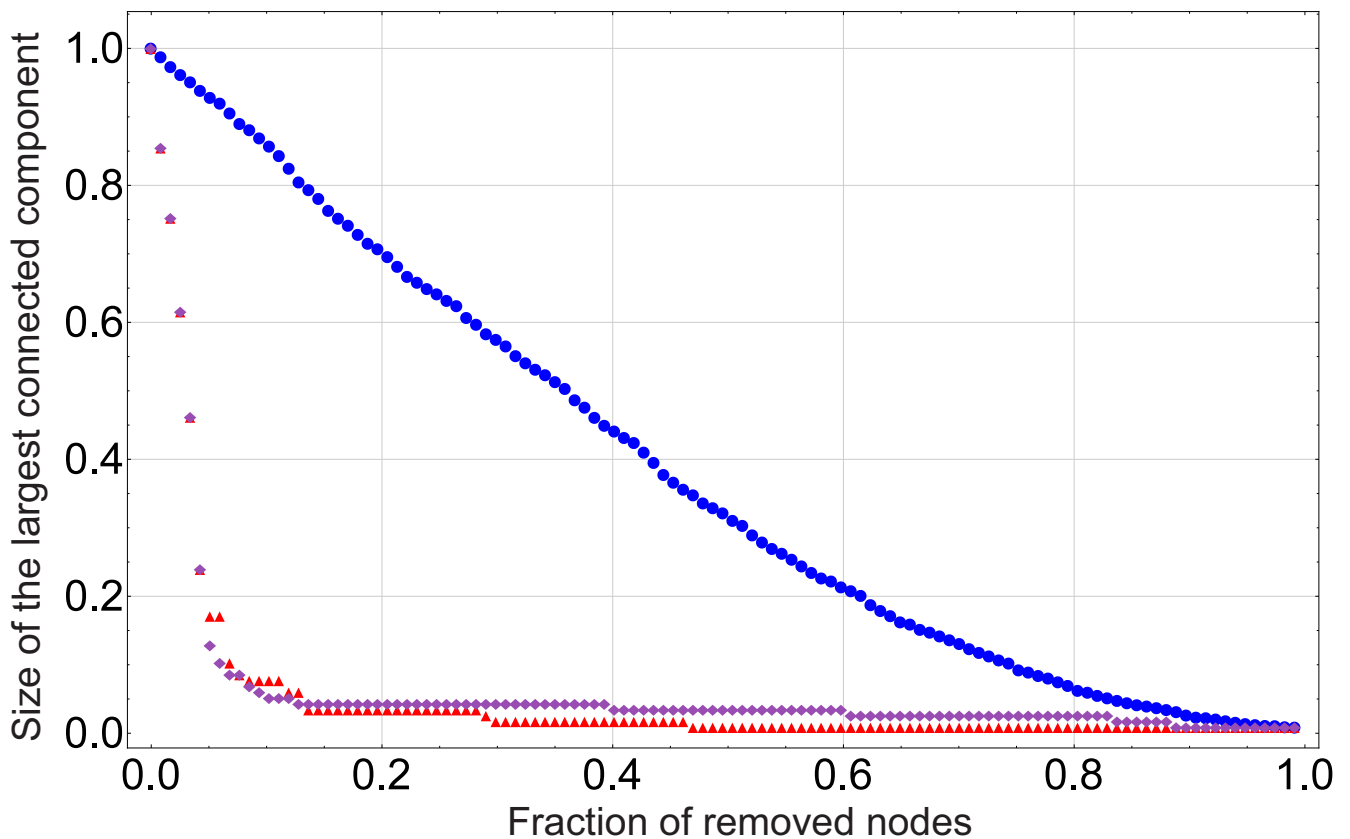


Figure 4.4. Normalized size of the largest connected component of the bylynas social network as a function of the fraction of removed nodes for three types of attacks: random (blue circles), in descending order of node degree (red triangles) and in descending order of betweenness centrality (purple diamonds). Random attacks are ineffective while targeted removal of about 10 % of nodes reduces the size of the largest connected component by the factor of 10.

4.3.11. Community structure

Sometimes in a complex network there are areas that are more connected within than with the rest of the network. Such areas are called communities. To identify these communities one can use the algorithm developed and Girvan and Newman [208]. This algorithm works as a following: an edges with the highest betweenness centrality is removed, while all the nodes remain in the network. After that betweenness centrality of all edges is recalculated and the edge with the highest value is again removed. Groups of nodes that branch out of the starting network as a result of this process form communities.

The question remains, how long this process should last. To answer this question it is necessary to calculate modularity. It is defined in the following way. For the first step the matrix \hat{E} of size $n \times n$ is constructed, where n is the number of communities at a given step this step. Element e_{st} of this matrix is the ratio between the number of connections between communities s and t the number of connections in the entire graph. It is worth noting that the element of this matrix are calculated basen on the topology of original graph, and not the one with removed edges. Then modularity can be found as follows

$$Q = \text{Sp } \hat{E} - \|\hat{E}^2\| \quad , \quad (4.26)$$

where $\|\dots\|$ means the sum of all the elements of the matrix. The optimal number of communities is one that maximizes modularity.

The application of this algorithm to the social network of bylynas (which takes into account all types of links) gives an interesting result: the largest connected component splits into 15 communities, and the value of modularity for such a distribution is $Q = 0.5$. As noted in [208], for real social networks $0.3 < Q < 0.7$, and values $Q < 0.3$ indicate that the communities in the network are hardly distinguishable. Thus, the value we receive for the modularity of the bylynas social network of is an evidence of the presence in this network of well-defined communities typical of real social networks. The largest of the communities in the network of characters has 36 nodes (red nodes in the centre of the Fig. 4.5), among which there is Duke Volodymyr (character 52) with his wife (character 104), Oleksiy Popovych (character 1) and Dobrynya (character 28). The second largest community has 22 characters - a large group of yellow nodes on the right side of Fig. 4.5, centered around Illia Muromets (character 46). This fact can serve as a demonstration of the fact that Illia Muromets to the contrast with Dobrynia and Oleksiy are representatives of various generations of heroes [173, 176]. Illia is a representative of the older heroes, while Dobrynia and Oleksiy are younger.

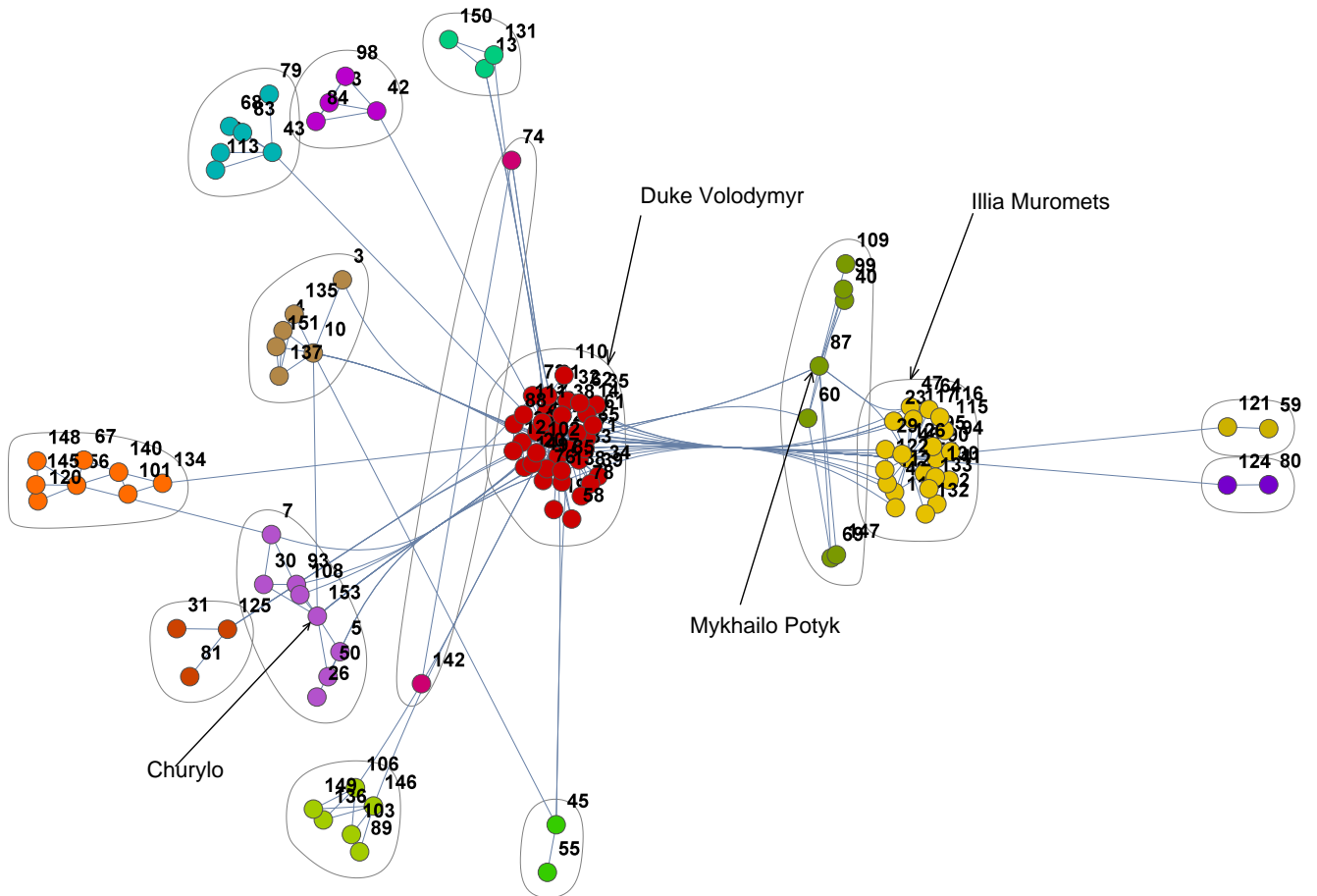


Figure 4.5. The division of the social network of bylynas into communities (all types of links are taken into account). The Newman-Girvan algorithm detects 15 communities. The largest of them are concentrated around Duke Volodymyr (character 52 in the central part of the figure) and Illia Muromets (character 46 in the right part of the figure). The next largest communities are centered around Churylo (character 153) and Mykhailo Potyk (character 87).

It is also interesting that the analysis we carried out separated communities concentrated around Churylo (character 153) and Mikhailo Potyk (character 87). Both these characters together with Duke (character 33) form a group of Galician-Volyn characters [195]. The appearance of these characters in the bylynas that describes Kyivan Rus can be explained by the fact that after the destruction of Kyiv by the Mongol-Tatars, the Rus cultural heritage moved to the west in the Galician-Volhynian kingdom. Here the bylynas have incorporated some local characters. As we can see, quantitative analysis of the social network of bylynas also highlights communities centered around these characters (see Fig. 4.5).

4.4. Conclusion

As it turned out as a result of the analysis, the social network of bylynas (see Fig. 4.1) has a number of properties that are common to social networks of other epics. These properties remain unchanged for networks characterizing epic narratives of different cultures and were created at different times. Thus, epic narratives have universal properties, which allows an additional classification, which is based on their quantitative analysis. In particular, similar to social networks of other epics, the social networks of the bylynas were strongly correlated small-world networks with the mean clustering coefficient, which far exceeds the corresponding value for the classical random Erdős-Rényi graph (the numerical values of this and other characteristics are summarized in Table 4.1). However, small-worlds are networks that take into account all or only friendly connections. The network of hostile connections has a value of the clustering coefficient and mean distances comparable with the corresponding values for the Erdős-Rényi graph, which is a quantitative manifestation of the social balance hypothesis (the enemy of my enemy is my friend) [105, 209]. Therefore, the small-world effects do not appear in it. In this sense, it is justified that we called the networks under investigation the social network of bylynas: similar effects are typical for social networks of the real world [16].

Another feature that unites networks of epic narratives is their hierarchy [16]. One of the manifestations of this property is the division of the network into communities - groups of closely connected nodes. The obtained value of modularity $Q = 0.5$ testifies the presence of well-defined communities in the network of bylynas. This property unites most of the epics mentioned in Table. 4.1. The hierarchy of the network also manifests itself in the fact that the mean value of the clustering coefficient of nodes with a certain degree k is inversely proportional to this degree $\bar{C}(k) \propto 1/k$. Insufficient sampling for social networks of bylynas does not allow to test such a relation.

Most of the social networks of epics, like real social networks, are scale-free. This statement, however, is valid with some exceptions, such as *Iliad* or *Laxdæla saga*

[16, 17]). For the network of bylynas, the scale-free property is very well observed, unlike the networks of some fictional texts [16]. Social networks of epics are similar to real social networks in their behaviour under attacks. The random removal of their components (random attacks) does not cause them significant damage, while targeted attacks quickly cluster the network. In contrast, the network of so far analysed fictional texts tend to be stable both for random and targeted attacks [16].

Social networks of bylynas is disassortative by the node degree. This property unites the majority of epics in Table 4.1. On the contrary, real social networks tend to be assortative [197]. It is interesting to note that the network of friendly connections, from which the node corresponding to Duke Volodymyr was removed, becomes weakly assortative. Thus, the removal from the network the node, which, according to some researchers, is a collective character [177] makes it more similar to social networks of the real world.

In addition to the above universal characteristics, our analysis has brought new arguments for certain hypotheses about the structure of bylynas. We have already mentioned the assumption that Duke Volodymyr is a collective image of the Kyivan prince and a quantitative confirmation of this assumption. Note also that in the network without Duke Volodymyr and the duchess the highest value of the closeness centrality belongs to Dobrynia - his distance from the rest of the characters is comparable to the Volodymyrs. This can serve as a confirmation that the uncle of Grand Prince Volodymyr Dobrynia served as a prototype for epic Dobrynia [210]. Another interesting result is that the analysis of the social network of bylynas highlights the rank of the characters Churylo, Duke and Mikhailo Potyk. Namely, these characters, Mykhailo Hrushevsky, refer to the characters of the Galician-Volyn group [195].

CONCLUSIONS

In the dissertation we considered several manifestations of cooperative behaviour of complex systems: the formation of periodically repeating patterns in the Ising model with dipole interaction, the interplay between energy and entropy, and the universal properties of ordering in the Potts model with invisible states, the universality of social networks of narratives.

Below we will briefly list the main results that were obtained in the thesis:

1. for the Ising model with dipole interaction, it was confirmed that the universality class depends on the ratio of the interaction constants δ ;
2. phase transition in the Ising model with dipole interaction undergoes second order scenario for the transition from the $h = 1$ strip phase to the tetragonal, and the transition from the $h = 2$ phase to the tetragonal is of a first order;
3. we obtained an exact solution for the Potts model with invisible states on the chain and it is shown that for external complex fields $h_2 \in \mathbb{C}$ or the negative number of invisible states $r < 0$, the transition can occur at positive temperature;
4. Potts model with invisible states on a complete graph is characterized by two marginal dimensions separating the regions with different criticality (see Fig. 3.7); item the Ising model with invisible states on scale-free networks has critical parameters dependent on the degree distribution exponent λ ;
5. social network of characters of bylynas has a number of common characteristics with networks of characters of other epics of European heritage, which evidence universality of human narrative interests.

REFERENCES

1. P. W. Anderson, “More is different,” *Science*, vol. 177, no. 4047, pp. 393–396, 1972.
2. G. Parisi, “Complex systems: a physicist’s viewpoint,” *Physica A: Statistical Mechanics and its Applications*, vol. 263, no. 1-4, pp. 557–564, 1999.
3. M. Newman, “Resource letter cs-1: Complex systems,” *American Journal of Physics*, vol. 79, no. 8, pp. 800–810, 2011.
4. Yu. Holovatch, R. Kenna, and S. Thurner, “Complex systems: physics beyond physics,” *European Journal of Physics*, vol. 38, no. 2, p. 023002, 2017.
5. S. Thurner, *43 Visions for Complexity*, vol. 3. World Scientific, 2017.
6. Yu. Holovatch ed., *Order, disorder and criticality: advanced problems of phase transition theory*, vol. 1-5. World Scientific, 2004-2018.
7. S. Galam, *Sociophysics: A Physicist’s Modeling of Psycho-political Phenomena*. Springer, 2012.
8. Yu. Holovatch et al., “Complex networks,” *Journal of Physical Studies*, vol. 10, pp. 247–289, 2006 (in Ukrainian).
9. A. Barrat, M. Barthelemy, and A. Vespignani, *Dynamical processes on complex networks*. Cambridge university press, 2008.
10. S. N. Dorogovtsev, A. V. Goltsev, and J. F. Mendes, “Critical phenomena in complex networks,” *Reviews of Modern Physics*, vol. 80, no. 4, p. 1275, 2008.
11. M. Newman, *Networks: an introduction*. Oxford university press, 2010.
12. D. Pescia and V. Pokrovsky, “Perpendicular versus in-plane magnetization in a 2d Heisenberg monolayer at finite temperatures,” *Physical Review Letters*, vol. 65, no. 20, p. 2599, 1990.

13. R. Tamura and N. Kawashima, “First-order transition to incommensurate phase with broken lattice rotation symmetry in frustrated Heisenberg model,” *Journal of the Physical Society of Japan*, vol. 77, no. 10, p. 103002, 2008.
14. E. Stoudenmire, S. Trebst, and L. Balents, “Quadrupolar correlations and spin freezing in $s=1$ triangular lattice antiferromagnets,” *Physical Review B*, vol. 79, no. 21, p. 214436, 2009.
15. A. V. Badasyan et al., “Competition for hydrogen-bond formation in the helix-coil transition and protein folding,” *Physical Review E*, vol. 83, no. 5, p. 051903, 2011.
16. P. Mac Carron and R. Kenna, “Universal properties of mythological networks,” *Europhysics Letters*, vol. 99, no. 2, p. 28002, 2012.
17. P. Mac Carron and R. Kenna, “Network analysis of the Íslendinga Sögur—the Sagas of Icelanders,” *The European Physical Journal B*, vol. 86, no. 10, p. 407, 2013.
18. P. Sarkanych, Yu. Holovatch, and R. Kenna, “On the phase diagram of the 2d Ising model with frustrating dipole interaction,” *Ukrainian Journal of Physics*, vol. 60, no. 4, p. 334, 2014.
19. C. Horowitz et al., “Phase transitions and critical phenomena in the two-dimensional Ising model with dipole interactions: A short-time dynamics study,” *Physical Review E*, vol. 92, no. 4, p. 042127, 2015.
20. P. Sarkanych, Yu. Holovatch, and R. Kenna, “Exact solution of a classical short-range spin model with a phase transition in one dimension: The Potts model with invisible states,” *Physics Letters A*, vol. 381, no. 41, pp. 3589–3593, 2017.
21. P. Sarkanych, Yu. Holovatch, and R. Kenna, “Classical phase transitions in a one-dimensional short-range spin model,” *Journal of Physics A: Mathematical and Theoretical*, vol. 51, no. 50, p. 505001, 2018.
22. M. Krasnytska et al., “Marginal dimensions of the Potts model with invisible states,” *Journal of Physics A: Mathematical and Theoretical*, vol. 49, no. 25, p. 255001, 2016.

23. P. Sarkanych and M. Krasnytska, “Ising model with invisible states on scale-free networks,” *Physics Letters A*, vol. 383, no. 27, pp. 125844, 2019.
24. P. Sarkanych et al., “Ubiversalyty and network analysis of Bylyny ,” *Journal of Physical Studies*, vol. 20, no. 4, 2016 (in Ukrainian).
25. Yu. Holovatch et al., “Math and myths - quantitative approach to comparative mythology,” accepted to *Ukraina Moderna*, 2019 (in Ukrainian).
26. X. Peng et al., “Experimental observation of Lee-Yang zeros,” *Physical Review Letters*, vol. 114, no. 1, p. 010601, 2015.
27. P. Sarkanych, Yu. Holovatch, and R. Kenna, “Partition function zeros as a measure of phase transition strength,” in *V young scientist conference Problems of theoretical physics. Program and Proceedings*, p. 101 (in Ukrainian).
28. P. Sarkanych, Yu. Holovatch, and R. Kenna, “1d Potts model with invisible states,” in *The 41st conference of the Middle European Cooperation in Statistical Physics. Book of Abstracts*, p. 72.
29. P. Sarkanych, Yu. Holovatch, and R. Kenna, “1d Potts model with invisible states,” in *16th Allukrainian young scientists school on statistical physics and condensed matter theory. Book of abstracts*, p. 43 (in Ukrainian).
30. P. Sarkanych, Yu. Holovatch, and R. Kenna, “1d Potts model with invisible states,” in *Workshop on current problems in physics. Book of abstracts*, p. 7.
31. M. Krasnytska et al., “Marginal dimensions of the Potts model with invisible states,” in *Christmass discussions – 2017. Program and proceedings*, p. 9 (in Ukrainian).
32. M. Krasnytska et al., “Marginal dimensions of the Potts model with invisible states,” in *The 42-nd Conference of the Middle European Cooperation in Statistical Physics. Book of abstracts*, p. 119.
33. P. Sarkanych et al., “Marginal dimensions of the Potts model with invisible states,” in *17th Allukrainian young scientists school on statistical physics and condensed matter theory. Book of abstracts*, p. 24 (in Ukrainian).
34. P. Sarkanych, Yu. Holovatch, and R. Kenna, “Exact solution of a 1d Potts

- model with invisible states: partition function zeros analysis,” in *Christmass discussions – 2018. Program and proceedings*, p. 9 (in Ukrainian).
35. R. Kenna, P. Sarkanych, and Yu. Holovatch, “A classical short-range spin model with phase transitions in one dimension: the Potts model with a negative number of invisible states,” in *The 43rd conference of the Middle European Cooperation in Statistical Physics. Book of Abstracts*, p. 64.
 36. P. Sarkanych et al., “Network analysis of Bylyny — traditional east slavic epic narratives,” in *The 43rd conference of the Middle European Cooperation in Statistical Physics. Book of Abstracts*, p. 95.
 37. Yu. Holovatch, “From the Ising model to statistical physics of complex systems,” *Coll. Phys. Papers of the Shevchenko Sci. Soc*, vol. 8, p. 429–449, 2011 (in Ukrainian).
 38. D. Sornette, *Critical phenomena in natural sciences: chaos, fractals, selforganization and disorder: concepts and tools*. Springer Science & Business Media, 2006.
 39. S. Thurner, R. Hanel, and P. Klimek, *Introduction to the theory of complex systems*. Oxford University Press, 2018.
 40. H. Zapolsky, “Kinetics of pattern formation: mesoscopic and atomistic modeling,” in *Order, Disorder and Criticality: Advanced Problems of Phase Transition Theory*, pp. 153–192, World Scientific, 2015.
 41. A. Kashuba and V. L. Pokrovsky, “Stripe domain structures in a thin ferromagnetic film,” *Physical Review B*, vol. 48, no. 14, p. 10335, 1993.
 42. A. Giuliani, J. L. Lebowitz, and E. H. Lieb, “Ising models with long-range antiferromagnetic and short-range ferromagnetic interactions,” *Physical Review B*, vol. 74, no. 6, p. 064420, 2006.
 43. A. MacIsaac et al., “Striped phases in two-dimensional dipolar ferromagnets,” *Physical Review B*, vol. 51, no. 22, p. 16033, 1995.
 44. A. Abanov et al., “Phase diagram of ultrathin ferromagnetic films with perpendicular anisotropy,” *Physical Review B*, vol. 51, no. 2, p. 1023, 1995.

45. I. Booth et al., “Domain structures in ultrathin magnetic films,” *Physical Review Letters*, vol. 75, no. 5, p. 950, 1995.
46. A. Vaterlaus et al., “Two-step disordering of perpendicularly magnetized ultrathin films,” *Physical Review Letters*, vol. 84, no. 10, p. 2247, 2000.
47. S. A. Cannas, D. A. Stariolo, and F. A. Tamarit, “Stripe-tetragonal first-order phase transition in ultrathin magnetic films,” *Physical review B*, vol. 69, no. 9, p. 092409, 2004.
48. P. M. Gleiser, F. A. Tamarit, and S. A. Cannas, “Metastable states in a two-dimensional Ising model with dipolar interactions,” *Physica D: Nonlinear Phenomena*, vol. 168, pp. 73–79, 2002.
49. E. Rastelli, S. Regina, and A. Tassi, “Phase transitions in a square Ising model with exchange and dipole interactions,” *Physical Review B*, vol. 73, no. 14, p. 144418, 2006.
50. E. Rastelli, S. Regina, and A. Tassi, “Phase diagram of a square Ising model with exchange and dipole interactions: Monte Carlo simulations,” *Physical Review B*, vol. 76, no. 5, p. 054438, 2007.
51. J. S. Fonseca, L. G. Rizzi, and N. A. Alves, “Stripe-tetragonal phase transition in the two-dimensional Ising model with dipole interactions: Partition function zeros approach,” *Physical Review E*, vol. 86, no. 1, p. 011103, 2012.
52. H. E. Stanley, *Introduction to Phase Transitions and Critical Phenomena*. Oxford University Press, 1987.
53. C. Domb, *The critical point: a historical introduction to the modern theory of critical phenomena*. CRC Press, 1996.
54. H. Stanley, “Exact solution for a linear chain of isotropically interacting classical spins of arbitrary dimensionality,” *Physical Review*, vol. 179, no. 2, p. 570, 1969.
55. N. D. Mermin and H. Wagner, “Absence of ferromagnetism or antiferromagnetism in one-or two-dimensional isotropic Heisenberg models,” *Physical Review Letters*, vol. 17, no. 22, p. 1133, 1966.
56. P. C. Hohenberg, “Existence of long-range order in one and two dimensions,”

- Physical Review*, vol. 158, no. 2, p. 383, 1967.
57. V. Privman, P. Hoheberg, and A. Aharony, “Dependence of universal critical behaviour on symmetry and range of interaction,” in *Phase Transitions and Critical Phenomena* (C. Domb and M. S. Green, eds.), vol. 6, p. 358, Academic Press.
 58. J. Sznajd, “Tricritical points in ferromagnets with cubic single-ion anisotropy,” *Journal of magnetism and magnetic materials*, vol. 42, no. 3, pp. 269–278, 1984.
 59. Z. Domański and J. Sznajd, “Phase diagrams of ferromagnets with cubic single-ion anisotropy,” *Physica Status Solidi (B)*, vol. 129, no. 1, pp. 135–142, 1985.
 60. R. Folk, Yu. Holovatch, and T. Yavors’kii, “Pseudo- ϵ expansion of six-loop renormalization-group functions of an anisotropic cubic model,” *Physical Review B*, vol. 62, no. 18, p. 12195, 2000.
 61. M. Dudka, Yu. Holovatch, and T. Yavors’kii, “Universality classes of the three-dimensional mn-vector model,” *Journal of Physics A: Mathematical and General*, vol. 37, no. 45, p. 10727, 2004.
 62. R. B. Potts, “Some generalized order-disorder transformations,” in *Mathematical proceedings of the Cambridge philosophical society*, vol. 48, pp. 106–109, Cambridge University Press, 1952.
 63. F.-Y. Wu, “The Potts model,” *Reviews of Modern Physics*, vol. 54, no. 1, p. 235, 1982.
 64. T. Gobron and I. Merola, “First-order phase transition in Potts models with finite-range interactions,” *Journal of Statistical Physics*, vol. 126, no. 3, pp. 507–583, 2007.
 65. Yu. Holovatch, D. Ivaneyko, and B. Delamotte, “On the criticality of frustrated spin systems with noncollinear order,” *Journal of Physics A: Mathematical and General*, vol. 37, no. 11, p. 3569, 2004.
 66. B. Delamotte, D. Mouhanna, and M. Tissier, “Nonperturbative renormalization-group approach to frustrated magnets,” *Physical Review*

- B*, vol. 69, no. 13, p. 134413, 2004.
67. P. Calabrese and P. Parruccini, “Five-loop ϵ expansion for $o(n) \times o(m)$ spin models,” *Nuclear Physics B*, vol. 679, no. 3, pp. 568–596, 2004.
 68. A. Pelissetto and E. Vicari, “Critical phenomena and renormalization-group theory,” *Physics Reports*, vol. 368, no. 6, pp. 549–727, 2002.
 69. R. Folk, Yu. Holovatch, and T. Yavorskii, “Critical exponents of a three-dimensional weakly diluted quenched Ising model,” *Physics-Uspekhi*, vol. 46, no. 2, p. 169, 2003.
 70. B. Halperin, T. Lubensky, and S.-K. Ma, “First-order phase transitions in superconductors and smectic-a liquid crystals,” *Physical Review Letters*, vol. 32, no. 6, p. 292, 1974.
 71. R. Folk and Yu. Holovatch, “On the critical fluctuations in superconductors,” *Journal of Physics A: Mathematical and General*, vol. 29, no. 13, p. 3409, 1996.
 72. M. Dudka et al., “Marginal dimensions for multicritical phase transitions,” *Condensed Matter Physics*, vol. 15, no. 4, p. 43001, 2012.
 73. A. C. van Enter and S. B. Shlosman, “First-order transitions for n -vector models in two and more dimensions: Rigorous proof,” *Physical Review Letters*, vol. 89, no. 28, p. 285702, 2002.
 74. R. Tamura, S. Tanaka, and N. Kawashima, “Phase transition in Potts model with invisible states,” *Progress of Theoretical Physics*, vol. 124, no. 2, pp. 381–388, 2010.
 75. S. Okumura et al., “Novel spin-liquid states in the frustrated Heisenberg antiferromagnet on the honeycomb lattice,” *Journal of the Physical Society of Japan*, vol. 79, no. 11, p. 114705, 2010.
 76. S. Tanaka, R. Tamura, and N. Kawashima, “Phase transition of generalized ferromagnetic Potts model-effect of invisible states,” in *Journal of Physics: Conference Series*, vol. 297, p. 012022, IOP Publishing, 2011.
 77. S. Tanaka and R. Tamura, “Dynamical properties of Potts model with invisible states,” in *Journal of Physics: Conference Series*, vol. 320, p. 012025, IOP

- Publishing, 2011.
78. T. Mori, “Microcanonical analysis of exactness of the mean-field theory in long-range interacting systems,” *Journal of Statistical Physics*, vol. 147, no. 5, pp. 1020–1040, 2012.
 79. R. Tamura, S. Tanaka, and N. Kawashima, “A method to control order of phase transition: Invisible states in discrete spin models,” in *Interface Between Quantum Information and Statistical Physics*, pp. 215–238, World Scientific, 2013.
 80. N. Ananikian et al., “Potts models with invisible states on general bethe lattices,” *Journal of Physics A: Mathematical and Theoretical*, vol. 46, no. 38, p. 385002, 2013.
 81. A. C. van Enter, G. Iacobelli, and S. Taati, “First-order transition in Potts models with "invisible" states: Rigorous proofs,” *Progress of theoretical physics*, vol. 126, no. 5, pp. 983–991, 2011.
 82. A. C. van Enter, G. Iacobelli, and S. Taati, “Potts model with invisible colors: random-cluster representation and Pirogov–Sinai analysis,” *Reviews in Mathematical Physics*, vol. 24, no. 02, p. 1250004, 2012.
 83. D. Johnston and R. Ranasinghe, “Potts models with (17) invisible states on thin graphs,” *Journal of Physics A: Mathematical and Theoretical*, vol. 46, no. 22, p. 225001, 2013.
 84. T.-D. Lee and C.-N. Yang, “Statistical theory of equations of state and phase transitions. II. lattice gas and Ising model,” *Physical Review*, vol. 87, no. 3, p. 410, 1952.
 85. C.-N. Yang and T.-D. Lee, “Statistical theory of equations of state and phase transitions. I. theory of condensation,” *Physical Review*, vol. 87, no. 3, p. 404, 1952.
 86. M. E. Fisher, *The nature of critical points*. University of Colorado Press, 1965.
 87. B.-B. Wei and R.-B. Liu, “Lee-Yang zeros and critical times in decoherence of a probe spin coupled to a bath,” *Physical Review Letters*, vol. 109, no. 18,

- p. 185701, 2012.
88. P. Timonin and G. Y. Chitov, “Infinite cascades of phase transitions in the classical Ising chain,” *Physical Review E*, vol. 96, no. 6, p. 062123, 2017.
 89. C. Itzykson, R. Pearson, and J. Zuber, “Distribution of zeros in Ising and gauge models,” *Nuclear Physics B*, vol. 220, no. 4, pp. 415–433, 1983.
 90. R. Abe, “Logarithmic singularity of specific heat near the transition point in the Ising model,” *Progress of Theoretical Physics*, vol. 37, no. 6, pp. 1070–1079, 1967.
 91. R. Abe, “Note on the critical behavior of Ising ferromagnets,” *Progress of Theoretical Physics*, vol. 38, no. 1, pp. 72–80, 1967.
 92. R. Abe, “Singularity of specific heat in the second order phase transition,” *Progress of Theoretical Physics*, vol. 38, no. 2, pp. 322–331, 1967.
 93. R. Abe, “Critical behavior of pair correlation function in Ising ferromagnets,” *Progress of Theoretical Physics*, vol. 38, no. 3, pp. 568–575, 1967.
 94. I. Bena, M. Droz, and A. Lipowski, “Statistical mechanics of equilibrium and nonequilibrium phase transitions: the Yang–Lee formalism,” *International Journal of Modern Physics B*, vol. 19, no. 29, pp. 4269–4329, 2005.
 95. W. Janke and R. Kenna, “The strength of first and second order phase transitions from partition function zeroes,” *Journal of Statistical Physics*, vol. 102, no. 5-6, pp. 1211–1227, 2001.
 96. W. Janke, D. Johnston, and R. Kenna, “Phase transition strength through densities of general distributions of zeroes,” *Nuclear Physics B*, vol. 682, no. 3, pp. 618–634, 2004.
 97. M. Suzuki, “A theory on the critical behaviour of ferromagnets,” *Progress of Theoretical Physics*, vol. 38, no. 1, pp. 289–290, 1967.
 98. M. Suzuki, “A theory of the second order phase transitions in spin systems. II: complex magnetic field,” *Progress of Theoretical Physics*, vol. 38, no. 6, pp. 1225–1242, 1967.
 99. S. Bornholdt and H. G. Schuster, *Handbook of graphs and networks: from the*

- genome to the internet*. John Wiley & Sons, 2006.
100. B. Tadić, K. Malarz, and K. Kułakowski, “Magnetization reversal in spin patterns with complex geometry,” *Physical Review Letters*, vol. 94, no. 13, p. 137204, 2005.
 101. R. de Regt et al., “Network analysis of the COSMOS galaxy field,” *Monthly Notices of the Royal Astronomical Society*, vol. 477, no. 4, pp. 4738–4748, 2018.
 102. C. von Ferber et al., “Public transport networks: empirical analysis and modeling,” *The European Physical Journal B*, vol. 68, no. 2, pp. 261–275, 2009.
 103. C. von Ferber et al., “A tale of two cities,” *Journal of Transportation Security*, vol. 5, no. 3, pp. 199–216, 2012.
 104. M. E. Newman and J. Park, “Why social networks are different from other types of networks,” *Physical review E*, vol. 68, no. 3, p. 036122, 2003.
 105. M. Szell and S. Thurner, “Measuring social dynamics in a massive multiplayer online game,” *Social networks*, vol. 32, no. 4, pp. 313–329, 2010.
 106. E. Müller-Hartmann and J. Zittartz, “New type of phase transition,” *Physical Review Letters*, vol. 33, no. 15, p. 893, 1974.
 107. M. Krasnytska, B. Berche, and Yu. Holovatch, “Phase transitions in the Potts model on complex networks,” *Condensed Matter Physics*, vol. 16, no. 2, p. 23602, 2013.
 108. M. Krasnytska et al., “Partition function zeros for the Ising model on complete graphs and on annealed scale-free networks,” *Journal of Physics A: Mathematical and Theoretical*, vol. 49, no. 13, p. 135001, 2016.
 109. G. Bianconi, “Superconductor-insulator transition on annealed complex networks,” *Physical Review E*, vol. 85, no. 6, p. 061113, 2012.
 110. S. N. Dorogovtsev, A. V. Goltsev, and J. F. F. Mendes, “Ising model on networks with an arbitrary distribution of connections,” *Physical Review E*, vol. 66, no. 1, p. 016104, 2002.
 111. M. Leone et al., “Ferromagnetic ordering in graphs with arbitrary degree distribution,” *The European Physical Journal B-Condensed Matter and Complex*

- Systems*, vol. 28, no. 2, pp. 191–197, 2002.
112. V. Palchykov et al., “Critical phenomena on scale-free networks: Logarithmic corrections and scaling functions,” *Physical Review E*, vol. 82, no. 1, p. 011145, 2010.
 113. A. MacIsaac et al., “Monte-Carlo study of two-dimensional Ising dipolar anti-ferromagnets as a model for rare-earth ordering in the R-Ba-Cu-O compounds (R= rare earth),” *Physical Review B*, vol. 46, no. 10, p. 6387, 1992.
 114. M. Fukugita et al., “Resolving the order of phase transitions in Monte-Carlo simulations,” *Journal of Physics A: Mathematical and General*, vol. 23, no. 11, p. L561, 1990.
 115. D. P. Landau and K. Binder, *A guide to Monte-Carlo simulations in statistical physics*. Cambridge university press, 2014.
 116. E. Ising, “Beitrag zur theorie des ferromagnetismus,” *Zeitschrift für Physik A Hadrons and Nuclei*, vol. 31, no. 1, pp. 253–258, 1925.
 117. T. Ising et al., “The fate of Ernst Ising and the fate of his model,” *Journal of Physical Studies*, vol. 21, 1 2017.
 118. L. Landau and E. Lifshitz, “Statistical physics, part 1: Volume 5 (course of theoretical physics, volume 5),” *Publisher: Butterworth-Heinemann*, vol. 3, 1980.
 119. L. van Hove, “Sur l’intégrale de configuration pour les systèmes de particules à une dimension,” *Physica*, vol. 16, no. 2, pp. 137–143, 1950.
 120. D. Ruelle, “Statistical mechanics of a one-dimensional lattice gas,” *Communications in Mathematical Physics*, vol. 9, no. 4, pp. 267–278, 1968.
 121. J. A. Cuesta and A. Sánchez, “General non-existence theorem for phase transitions in one-dimensional systems with short range interactions, and physical examples of such transitions,” *Journal of Statistical Physics*, vol. 115, no. 3-4, pp. 869–893, 2004.
 122. B. Simon and A. D. Sokal, “Rigorous entropy-energy arguments,” *Journal of Statistical Physics*, vol. 25, no. 4, pp. 679–694, 1981.

123. N. Theodorakopoulos, “Phase transitions in one dimension: Are they all driven by domain walls?,” *Physica D: Nonlinear Phenomena*, vol. 216, no. 1, pp. 185–190, 2006.
124. P. Anderson and G. Yuval, “Exact results in the kondo problem: equivalence to a classical one-dimensional coulomb gas,” *Physical Review Letters*, vol. 23, no. 2, p. 89, 1969.
125. G. Yuval and P. Anderson, “Exact results for the kondo problem: One-body theory and extension to finite temperature,” *Physical Review B*, vol. 1, no. 4, p. 1522, 1970.
126. P. W. Anderson, G. Yuval, and D. Hamann, “Exact results in the kondo problem. II. Scaling theory, qualitatively correct solution, and some new results on one-dimensional classical statistical models,” *Physical Review B*, vol. 1, no. 11, p. 4464, 1970.
127. F. J. Dyson, “An Ising ferromagnet with discontinuous long-range order,” *Communications in Mathematical Physics*, vol. 21, no. 4, pp. 269–283, 1971.
128. J. Fröhlich and T. Spencer, “The phase transition in the one-dimensional Ising model with $1/r^2$ interaction energy,” *Communications in Mathematical Physics*, vol. 84, no. 1, pp. 87–101, 1982.
129. M. R. Evans, “Phase transitions in one-dimensional nonequilibrium systems,” *Brazilian Journal of Physics*, vol. 30, no. 1, pp. 42–57, 2000.
130. M. Asorey and J. Esteve, “First-order transitions in one-dimensional systems with local couplings,” *Journal of Statistical Physics*, vol. 65, no. 3-4, pp. 483–494, 1991.
131. M. Asorey et al., “Rigorous analysis of renormalization-group pathologies in the 4-state clock model,” *Nuclear Physics B*, vol. 392, no. 3, pp. 593–618, 1993.
132. M. Asorey, J. Esteve, and J. Salas, “Exact renormalization-group analysis of first-order phase transitions in clock models,” *Physical Review B*, vol. 48, no. 6, p. 3626, 1993.
133. S. Seth, “Combinatorial approach to exactly solve the 1d Ising model,”

- European Journal of Physics*, vol. 38, no. 1, p. 015104, 2016.
134. L. Onsager, “Crystal statistics. I. A two-dimensional model with an order-disorder transition,” *Physical Review*, vol. 65, no. 3-4, p. 117, 1944.
 135. J.-U. Lee et al., “Ising-type magnetic ordering in atomically thin FePS₃,” *Nano Letters*, vol. 16, no. 12, pp. 7433–7438, 2016.
 136. M. Suzuki, “Relationship between d-dimensional quantal spin systems and (d+1)-dimensional Ising systems: Equivalence, critical exponents and systematic approximants of the partition function and spin correlations,” *Progress of Theoretical Physics*, vol. 56, no. 5, pp. 1454–1469, 1976.
 137. T. Rice, S. Gopalan, and M. Sigrist, “Superconductivity, spin gaps and luttinger liquids in a class of cuprates,” *Europhysics Letters*, vol. 23, no. 6, p. 445, 1993.
 138. T. Rice, “t_j ladders and cuprate ladder compounds,” *Zeitschrift für Physik B Condensed Matter*, vol. 103, no. 2, pp. 165–172, 1996.
 139. M. Azuma et al., “Observation of a spin gap in SrCu₂O₃ comprising spin-1/2 quasi-1d two-leg ladders,” *Physical Review Letters*, vol. 73, no. 25, p. 3463, 1994.
 140. M. Roger, J. Hetherington, and J. Delrieu, “Magnetism in solid He₃,” *Reviews of Modern Physics*, vol. 55, no. 1, p. 1, 1983.
 141. V. Hovhannisyanyan, R. Ghulghazaryan, and N. Ananikian, “The partition function zeros of the anisotropic Ising model with multisite interactions on a zigzag ladder,” *Physica A: Statistical Mechanics and its Applications*, vol. 388, no. 8, pp. 1479–1490, 2009.
 142. R. J. Baxter, *Exactly solved models in statistical mechanics*. Elsevier, 2016.
 143. S. Katsura and M. Ohminami, “Distribution of zeros of the partition function for the one dimensional Ising models,” *Journal of Physics A: General Physics*, vol. 5, no. 1, p. 95, 1972.
 144. S.-Y. Kim and R. J. Creswick, “Exact results for the zeros of the partition function of the Potts model on finite lattices,” *Physica A: Statistical Mechanics and its Applications*, vol. 281, no. 1-4, pp. 252–261, 2000.

145. R. Shrock and S.-H. Tsai, “Complex-temperature phase diagrams of one-dimensional spin models with next-nearest-neighbor couplings,” *Physical Review E*, vol. 55, no. 5, p. 5184, 1997.
146. M. E. Fisher, “Yang-Lee edge behavior in one-dimensional systems,” *Progress of Theoretical Physics Supplement*, vol. 69, pp. 14–29, 1980.
147. R. Ghulghazaryan, K. Sargsyan, and N. Ananikian, “Partition function zeros of the one-dimensional Blume-Capel model in transfer matrix formalism,” *Physical Review E*, vol. 76, no. 2, p. 021104, 2007.
148. M. E. Fisher, “Yang-Lee edge singularity and ϕ^3 field theory,” *Physical Review Letters*, vol. 40, no. 25, p. 1610, 1978.
149. S. Beraha, J. Kahane, and N. Weiss, “Limits of zeroes of recursively defined polynomials,” *Proceedings of the National Academy of Sciences*, vol. 72, no. 11, pp. 4209–4209, 1975.
150. S. Beraha, J. Kahane, and N. Weiss, “Limits of zeros of recursively defined families of polynomials,” *Studies in Foundations and Combinatorics*, vol. 1, pp. 213–232, 1978.
151. S. Beraha, J. Kahane, and N. Weiss, “Limits of chromatic zeros of some families of maps,” *Journal of Combinatorial Theory, Series B*, vol. 28, no. 1, pp. 52–65, 1980.
152. P. J. Kortman and R. B. Griffiths, “Density of zeros on the Lee-Yang circle for two Ising ferromagnets,” *Physical Review Letters*, vol. 27, no. 21, p. 1439, 1971.
153. D. A. Kurtze and M. E. Fisher, “The Yang-Lee edge singularity in spherical models,” *Journal of Statistical Physics*, vol. 19, no. 3, pp. 205–218, 1978.
154. Z. Glumac and K. Uzelac, “The partition function zeros in the one-dimensional q -state Potts model,” *Journal of Physics A: Mathematical and General*, vol. 27, no. 23, p. 7709, 1994.
155. H. A. Kramers and G. H. Wannier, “Statistics of the two-dimensional ferromagnet. part I,” *Physical Review*, vol. 60, no. 3, p. 252, 1941.

156. J. Salas and A. D. Sokal, “Transfer matrices and partition-function zeros for antiferromagnetic Potts models. I. general theory and square-lattice chromatic polynomial,” *Journal of Statistical Physics*, vol. 104, no. 3-4, pp. 609–699, 2001.
157. X. Wang, “Physical examples of phase transition in one-dimensional systems with short range interaction.” (unpublished), 2012.
158. C. M. Fortuin and P. W. Kasteleyn, “On the random-cluster model: I. Introduction and relation to other models,” *Physica*, vol. 57, no. 4, pp. 536–564, 1972.
159. S.-Y. Kim and R. J. Creswick, “Density of states, Potts zeros, and fisher zeros of the q -state Potts model for continuous q ,” *Physical Review E*, vol. 63, no. 6, p. 066107, 2001.
160. R. Ghulghazaryan and N. Ananikian, “Partition function zeros of the one-dimensional Potts model: the recursive method,” *Journal of Physics A: Mathematical and General*, vol. 36, no. 23, p. 6297, 2003.
161. Z. Glumac and K. Uzelac, “Complex- q zeros of the partition function of the Potts model with long-range interactions,” *Physica A: Statistical Mechanics and its Applications*, vol. 310, no. 1-2, pp. 91–108, 2002.
162. P. Kasteleyn and C. Fortuin, “Phase transitions in lattice systems with random local properties,” *Journal of the Physical Society of Japan Supplement*, vol. 26, p. 11, 1969.
163. J. L. Jacobsen, J. Salas, and A. D. Sokal, “Spanning forests and the q -state Potts model in the limit $q \rightarrow 0$,” *Journal of Statistical Physics*, vol. 119, no. 5-6, pp. 1153–1281, 2005.
164. S. N. Majumdar and D. Dhar, “Equivalence between the abelian sandpile model and the $q \rightarrow 0$ limit of the Potts model,” *Physica A: Statistical Mechanics and its Applications*, vol. 185, no. 1-4, pp. 129–145, 1992.
165. A. B. Harris and T. C. Lubensky, “Potts-model formulation of the random resistor network,” *Physical Review B*, vol. 35, no. 13, p. 6987, 1987.
166. C. Bonati and M. D’Elia, “Three-dimensional, three-state Potts model in a

- negative external field,” *Physical Review D*, vol. 82, no. 11, p. 114515, 2010.
167. D. Dalmazi and F. Sá, “The Yang–Lee edge singularity in spin models on connected and non-connected rings,” *Journal of Physics A: Mathematical and Theoretical*, vol. 41, no. 50, p. 505002, 2008.
168. D. Ruelle, *Statistical mechanics: Rigorous results*. World Scientific, 1999.
169. W. Aiello, F. Chung, and L. Lu, “A random graph model for massive graphs,” in *STOC*, vol. 2000, pp. 1–10, Citeseer, 2000.
170. X. Qian, Y. Deng, and H. W. Blöte, “Dilute Potts model in two dimensions,” *Physical Review E*, vol. 72, no. 5, p. 056132, 2005.
171. J. A. Nelder and R. Mead, “A simplex method for function minimization,” *The Computer Journal*, vol. 7, no. 4, pp. 308–313, 1965.
172. P. Mac Carron, *A network theoretic approach to comparative mythology*. PhD thesis, Coventry University, UK, 2014.
173. B. Putilov, “Bylyny: Collection,” *Sovier writer*, 1986 (in Russian).
174. B. Larin, *Russian-English dictionary-diary of Richard James (1618-1619)*. Leningrad University Press, 1959 (in Russian).
175. K. Danilov, *The Ancient Russian Poems*. Ripol Classic, 1977 (in Russian).
176. V. Avenarius, *Book of Bylyny*. Kushneriov and Co, 1902 (in Russian).
177. V. Shevchuk, *Ukrainian Bylyny: Historical and literary edition of the East Slavic epic*. Veselka, 2003 (in Ukrainian).
178. M. Newman, A.-L. Barabasi, and D. J. Watts, *The structure and dynamics of networks*, vol. 12. Princeton University Press, 2011.
179. L. A. N. Amaral et al., “Classes of small-world networks,” *Proceedings of the National Academy of Sciences*, vol. 97, no. 21, pp. 11149–11152, 2000.
180. M. E. Newman, “The structure of scientific collaboration networks,” *Proceedings of the National Academy of Sciences*, vol. 98, no. 2, pp. 404–409, 2001.
181. S. Dorogovstev and J. Mendes, *Evolution of networks*, Oxford University Press, 2003.
182. R. Albert and A.-L. Barabási, “Statistical mechanics of complex networks,”

- Reviews of Modern Physics*, vol. 74, no. 1, p. 47, 2002.
183. S. N. Dorogovtsev and J. F. Mendes, “Evolution of networks,” *Advances in Physics*, vol. 51, no. 4, pp. 1079–1187, 2002.
184. S. Boccaletti et al., “Complex networks: Structure and dynamics,” *Physics Reports*, vol. 424, no. 4-5, pp. 175–308, 2006.
185. A. Lesne, “Complex networks: from graph theory to biology,” *Letters in Mathematical Physics*, vol. 78, no. 3, pp. 235–262, 2006.
186. D. Watts, *Small worlds*, Princeton University Press 1999.
187. R. Pastor-Satorras and A. Vespignani, *Evolution and structure of the Internet: A statistical physics approach*. Cambridge University Press, 2007.
188. S. Milgram, “The small world problem,” *Psychology Today*, vol. 2, no. 1, pp. 60–67, 1967.
189. M. Gurevitch, *The social structure of acquaintanceship networks*. PhD thesis, Massachusetts Institute of Technology, 1961.
190. P. Erdős and A. Rényi, “On the evolution of random graphs,” *Publ. Math. Inst. Hung. Acad. Sci.*, vol. 5, no. 1, pp. 17–60, 1960.
191. B. Bollobás, “The diameter of random graphs,” *Transactions of the American Mathematical Society*, vol. 267, no. 1, pp. 41–52, 1981.
192. A. Fronczak, P. Fronczak, and J. A. Hołyst, “Average path length in random networks,” *Physical Review E*, vol. 70, no. 5, p. 056110, 2004.
193. G. Sabidussi, “The centrality index of a graph,” *Psychometrika*, vol. 31, no. 4, pp. 581–603, 1966.
194. U. Brandes, “A faster algorithm for betweenness centrality,” *Journal of Mathematical Sociology*, vol. 25, no. 2, pp. 163–177, 2001.
195. M. Grushevskiyi, *History of Ukrainian Literature*, vol. 4. Lybid, 1994 (in Ukrainian).
196. “Mykhailo Potyk on Russian Wikipedia”
https://ru.wikipedia.org/wiki/Михайло_Потык
197. M. E. Newman, “Assortative mixing in networks,” *Physical Review Letters*,

- vol. 89, no. 20, p. 208701, 2002.
198. K. Rohe, “The difference between the transitivity ratio and the clustering coefficient”, unpublished.
 199. J. Yose et al., “A networks-science investigation into the epic poems of Ossian,” *Advances in Complex Systems*, vol. 19, no. 04n05, p. 1650008, 2016.
 200. M. D. Humphries and K. Gurney, “Network ‘small-world-ness’: a quantitative method for determining canonical network equivalence,” *PloS one*, vol. 3, no. 4, p. e0002051, 2008.
 201. P. M. Gleiser, “How to become a superhero,” *Journal of Statistical Mechanics: Theory and Experiment*, vol. 2007, no. 09, p. P09020, 2007.
 202. D. Chyzhevsky, “*Epic Poetry*” in: Internet encyclopedia of Ukraine www.encyclopediaofukraine.com/display.asp?linkpath=pages\E\P\Epicpoetry.htm.
 203. L. Šubelj and M. Bajec, “Clustering assortativity, communities and functional modules in real-world networks,” *arXiv preprint arXiv:1202.3188*, 2012.
 204. J. W. Essam, “Percolation theory,” *Reports on Progress in Physics*, vol. 43, no. 7, p. 833, 1980.
 205. D. Stauffer and A. Aharony, *Introduction to percolation theory*. Taylor & Francis, 2018.
 206. R. Cohen et al., “Resilience of the internet to random breakdowns,” *Physical Review Letters*, vol. 85, no. 21, p. 4626, 2000.
 207. R. Cohen et al., “Breakdown of the internet under intentional attack,” *Physical Review Letters*, vol. 86, no. 16, p. 3682, 2001.
 208. M. E. Newman and M. Girvan, “Finding and evaluating community structure in networks,” *Physical review E*, vol. 69, no. 2, p. 026113, 2004.
 209. F. Harary et al., “On the notion of balance of a signed graph.,” *The Michigan Mathematical Journal*, vol. 2, no. 2, pp. 143–146, 1953.
 210. “Dobrynia Mykytych on Ukrainian Wikipedia” https://uk.wikipedia.org/wiki/Добриня_Микитич